



UNIVERSITY OF
BIRMINGHAM

**FIRST STEP IN THE DESIGN
AND REALISATION OF A
'SMART' SWITCHABLE SURFACE**

by Alice Pranzetti

A Thesis submitted to
The University of Birmingham
for the Degree of MRes in
Nanochemistry and Materials Chemistry

School of Chemistry
The University of Birmingham

2009/2010

UNIVERSITY OF
BIRMINGHAM

University of Birmingham Research Archive

e-theses repository

This unpublished thesis/dissertation is copyright of the author and/or third parties. The intellectual property rights of the author or third parties in respect of this work are as defined by The Copyright Designs and Patents Act 1988 or as modified by any successor legislation.

Any use made of information contained in this thesis/dissertation must be in accordance with that legislation and must be properly acknowledged. Further distribution or reproduction in any format is prohibited without the permission of the copyright holder.

ABSTRACT

This thesis reports the first step in the design and fabrication of a double armed switchable surface that exhibits dynamic changes in its interfacial properties in terms of bio-recognition, in response to an electrical potential (**Figure 1a**). The aim of the work herein is to develop a suitable synthetic strategy to ensure the stability of the desired self-assembled monolayer (**Figure 1b**). In order to obtain a better understanding of the possible chemical interactions involved, different portions of the surface have been studied separately on a simpler system (**Figure 1c**).

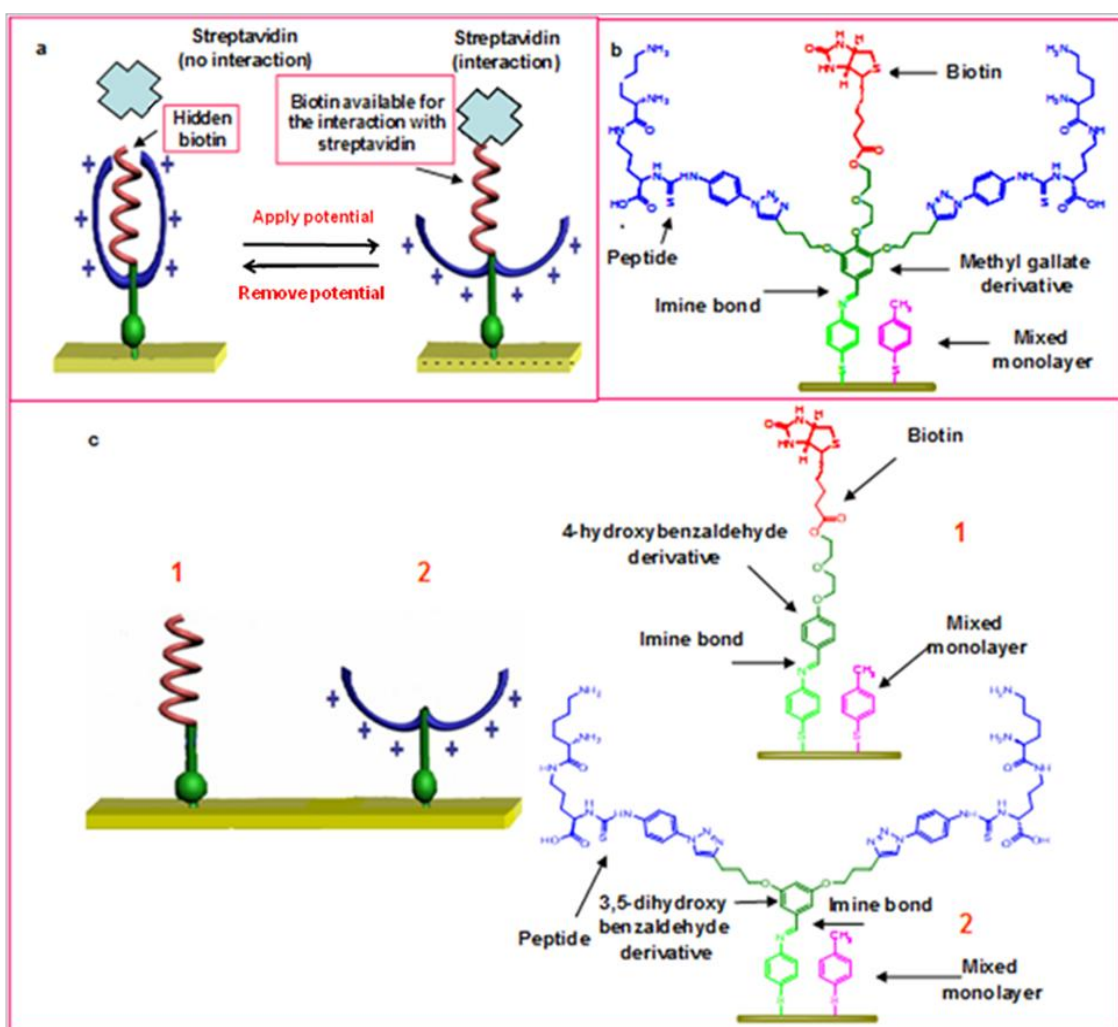


Figure 1 a) Cartoon image showing the opening of the positively charged double armed system when a negative voltage is applied and consequent interaction between biotin and streptavidin, b) chemical structure of the double armed switchable surface, c) scheme and chemical structure of the selected portions examined in the present research.

In particular, this thesis will discuss the successful coupling of biotin (**Figure 1c**) with a 4-hydroxybenzaldehyde derivative and the attempts to obtain a 'double armed' 3,5-dihydroxybenzaldehyde derivative (**Figure 1c**) *via* a Huisgen reaction. The last section of this work will focus on the fabrication and characterisation of pure and mixed aromatic monolayers of 4-aminothiophenol and 4-methylbenzenethiol.

ACKNOWLEDGMENT

Firstly, I would like to say “thank you” to my two supervisors, Dr. P. M. Mendes and Prof. J. A. Preece, who have given me extraordinary support throughout this project, helping me with precious advice and a lot of patience.

Secondly, I would like to thank my family, Romolo, Lorian and Michela and my boyfriend, Max, for their support and encouragement during my studies.

Thanks must also go to the members of both the Preece and Mendes group past and present, namely Dr. Parvez Iqbal, Dr. Mayaandithevar Manickam, Dr. Christopher Hamlett, Dr. James Bowen, Scott Charlesworth, Dr. Simon Leigh, Cheng Yeung, Akash Beri, Vivek Davda, Cait Costello, Marzena Allan, Minhaj Lashkor and Rachel Allen.

I would also like to thank the many students, researchers, academics and many more people besides who have given me so much support and confidence throughout the duration of this project. These include Alex Cremonesi, Christelle Detti-Mambo, Renate Gleixner, Nicolas Martin, Marcus Main, Parmjit Heer, Marilena Ragoussi, Zara Locke and Andreas Bergman.

In particular I would like to thank (almost) Dr. Matt Sadler and Dr. Peter Jervis for their special friendship and for all the effort in teaching me the English language without (unfortunately) gaining the hoped results.

Thanks must also go to all the staff of “The centre for Chemical and Biochemical Analysis”, in particular to Mr P. R. Ashton, Dr. N. Spencer, Mr N. G. May and Mr G. D. Burns. Finally I would like to thank my friend Jessie Mercedes Venegas Garcia for her irreplaceable company and Ajay Gupta for his precious help and care.

TABLE OF CONTENTS

1.0 INTRODUCTION	1
<i>1.1.Thin films: organic and metallic</i>	<i>1</i>
1.1.1 Metallic thin films	1
1.1.2 Organic thin films	2
<i>1.2 Self-assembled monolayer: static SAMs</i>	<i>2</i>
1.2.1 Single component self-assembled monolayers	2
1.2.1.1 Surfactant	3
1.2.1.2 Substrate	4
1.2.1.3 SAM formation	6
1.2.1.4 SAM structure/Intermolecular packing	9
1.2.1.4.1 Influence of the backbone nature: alkyl and aromatic backbones	9
1.2.1.5 Multicomponent SAMs: aromatic and alkyl moieties	11
<i>1.3 Switchable SAMs</i>	<i>13</i>
1.3.1 SAMs surface modification	13
1.3.1.1 Suitable characteristics for a conformational switch: low density SAMs	13
1.3.1.2 Switchable biological surfaces	14
1.3.1.3 Switchable surfaces and click chemistry	15
<i>1.4 Concluding remarks</i>	<i>18</i>
	<i>20</i>
2.0 CHARACTERISATION OF SUBSTRATES BY DIFFERENT METHODS	22
<i>2.1 Contact angle measurements</i>	<i>22</i>
<i>2.2 Ellipsometry for thin-film and surface analysis</i>	<i>22</i>
<i>2.3 X-ray photoelectron spectroscopy (XPS)</i>	<i>25</i>
	<i>26</i>
3.0 PROJECT OVERVIEW	28
<i>3.1 Hypothesis</i>	<i>28</i>
<i>3.2 Aims</i>	<i>29</i>
4.0 RESULTS AND DISCUSSION	36
<i>4.1 Synthesis</i>	<i>36</i>
4.1.1 Synthesis of biotin-derivative 5	36
4.1.2 Synthesis the double arms moiety (14)	39
4.1.2.1 Huisgen reaction	41
4.1.2.2 Click chemistry: 4-AA	42
4.1.2.3 Click chemistry: 4-MA	43
<i>4.2 Surface work</i>	<i>46</i>
4.2.1 Introduction	46
4.2.2 Fabrication of single component SAMs	48
4.2.2.1 Concentration and kinetic studies	49
4.2.2.1.1 Concentration study	49
4.2.2.1.2 Kinetic study	53
4.2.3 Fabrication of double component SAMs	59

4.2.4 Reaction on SAMs: imine bond formation	63
4.3 <i>Imine bond: control study</i>	65
4.3.1 Synthesis of the disulfide 18	66
4.3.2 Surface work	68
5.0 CONCLUSION	72
6.0 FUTURE WORK	75
7.0 EXPERIMENTAL METHODS	78
7.1 <i>General Experimental</i>	78
7.2 <i>Synthesis</i>	80
7.2.1 Ether 3	80
7.2.2 Ester 5	81
7.2.3 Diether 8	82
7.2.4 Imine 11	83
7.2.5 Imine 15	84
7.2.6 Disulfide 16	85
7.2.7 Diimine 18	86
7.3 <i>Surface work</i>	87
7.3.1 Materials	87
7.3.2 Cleaning of glassware	87
7.3.3 General procedure for the preparation of SAMs	88
7.3.4 Characterisation of SAMs	89
7.3.5 SAMs formation	91
7.3.5.1 4-ATP, BT SAMs formation: concentration studies	91
7.3.5.2 4-ATP, BT, 4-MBT, 4-NBT SAMs formation: kinetic studies	91
7.3.5.3 Mixed 4-ATP/4-MBT SAMs formation	92
7.3.5.4 Imine bond formation on 4-ATP SAMs	92
7.3.5.5 16' SAMs formation from disulfide 16	93
7.3.5.6 18' SAMs formation from disulfide 18	93
7.0 REFERENCES	94

1.0 INTRODUCTION

1.1 Thin films: organic and metallic

Thin films are classified as either *metallic* or *organic* and *inorganic* and are employed in the creation of chemically modified surfaces. Thin films can be deposited using either physical or chemical methods.¹ Physical methods are based on physical vapour deposition (PVD) which include evaporation (thermal, laser ablation, electron beam) and sputtering (Radiofrequency, Diode-Cathode, magnetron), while chemical methods include chemical vapour deposition (CVD), plating (electroplating and electroless) and solution methods.²

1.1.1 Metallic thin films

Thin films of conducting materials, such as metals and alloys are currently in use in many areas of technology, particularly in modern integrated circuit microelectronics. Commonly deposited metallic thin films include Au, Al, Cu and Mo, and the choice of substrate material used (*i.e.* glass, Si/SiO₂) depends on the application of the film (*i.e.* circuitry).^{3,4} The metallic thin film employed for this work, and therefore, further discussed in this thesis is Au, which is normally deposited onto a glass substrate.

1.1.2 Organic thin films

Thin crystalline films of organic molecules on inorganic substrates have attracted considerable attention. These structures are potentially useful for new applications, such as coating technology, optoelectronics, sensors, and bio-medical devices.⁵ The main characteristic of organic thin films is the possibility of obtaining the desired properties by attaching the appropriate tail functional groups. Due to their versatility, organic thin films have been studied and used in the fabrication of electronic devices such as organic light emitting devices (OLEDs) and organic thin-film transistors (OTFTs).^{6,7}

1.2 Self-assembled monolayer: static SAMs

The most common methods for forming supported organic thin films are the *Langmuir-Blodgett method*⁸ and the *self-assembly techniques*.⁹ The main difference between the two methods is the ability to produce physisorbed and chemisorbed monolayers, respectively. The second technique will be discussed in the next paragraph.

1.2.1 Single component self-assembled monolayers

Self-assembled monolayers (SAMs) are 2D-molecular assemblies that are formed spontaneously by the immersion of an appropriate substrate into a solution of an active surfactant.⁸

1.2.1.1 Surfactant

From an energetic viewpoint, a self-assembling surfactant molecule can be divided into three parts (**Figure 2**).^{9,10}

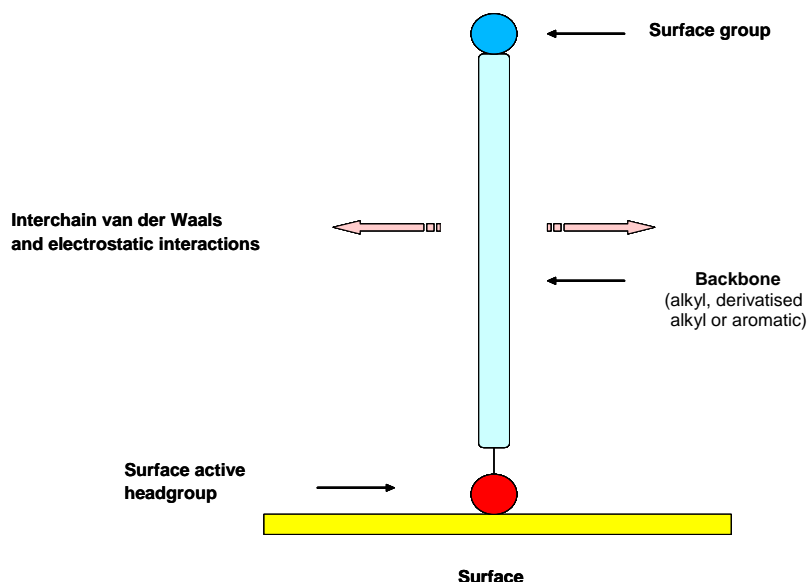


Figure 2 General scheme of the structure of SAMs and their relative interaction forces.

The first part is the *head group*, which provides the most exothermic process: the chemisorption on the substrate surface. The very strong molecule-substrate interactions result in an apparent pinning of the head group to a specific site on the surface through a chemical bond. This can be a covalent Si-O bond in the case of alkyltrichlorosilanes on hydroxylated surfaces;¹¹ a covalent, slightly polar, Au-S bond in the case of alkanethiols on gold;¹² or an ionic $\text{-CO}_2^-\text{Ag}^+$ bond in the case of carboxylic acids on AgO/Ag surfaces.¹³ As a result of the exothermic head group-substrate interactions, molecules try to occupy every available binding site on the surface. In this process, the molecules reorganise leading to the formation of quasi-crystalline molecular assemblies.^{9,10}

The second molecular part is the *backbone*, which can be either hydrophobic/hydrophilic¹⁴ or alkylic/aromatic.¹⁵ The nature of the backbone depends upon the target SAM and its application. Most of the alkylic backbones sit at a tilt angle normal to the plane of the substrate. Further to this tilt there is a twist along the axis of the backbone.⁹ The length of the backbone chain is an important factor in molecular ordering. Fourier transform infra-red and electron diffraction studies suggest that alkanethiols on Au have crystal-like periodicity, provided the backbone has a chain length ≥ 12 carbon units.¹⁶ This crystal-like intermolecular order is a manifestation of exothermic intermolecular forces acting between the surfactant backbones. Van der Waals forces are typically the most common and most important of these intermolecular interactions. Other intermolecular forces (electrostatics, π - π interactions), may be present, depending on the nature of the backbone.⁹ Ordering can also be influenced by heating of the monolayer.¹⁰

The third part is the *terminal functionality*, which, in the case of a simple alkyl chain, is a methyl (CH₃) group. This domain of the surfactant provides a SAM with its surface properties for different applications such as wettability,¹⁷ corrosion susceptibility, friction/lubrication¹⁸ and bio-molecule immobilisation.¹⁹

1.2.1.2 Substrate

There are several types of SAMs depending on the headgroup and substrate used. These include organosilanes on hydroxylated surfaces (SiO₂, Al₂O₃, glass, etc.); alkanethiols on gold, silver and copper;¹² dialkyl sulfides on gold;²⁰ alcohols and amines on platinum;²¹ carboxylic acids on aluminium oxide,²² silver and indium tin

oxide (ITO).²³ Below are described the three most important headgroup-substrate SAM systems:

- *Thiol-gold*: Even though sulphur compounds have been found to bind strongly to Au, Ag, Cu and Pt substrates, Au has received the most attention since SAMs on Au are highly organised, easy to prepare and analyse. In addition, oxide layers can form on the other metal substrates, thus complicating SAM preparation on non-gold surfaces. Furthermore, smooth surfaces can be easily prepared on gold substrates, allowing a vast number of analytical techniques to be used that will not be complicated by roughness.²⁴
- *Silane-SiO₂*: Silane compounds form a strong bond with hydroxylated surfaces. The most widely studied system is silanes on SiO₂, due to two main reasons. Firstly, a vast amount of literature already exists on organosilanes reacting with silica, much more so than other hydroxylated surfaces. Secondly, SiO₂ is the base material of the microelectronics industry, a major driving force of early SAM research. Silane SAMs on SiO₂ are less ordered than thiols on Au. Despite this loss of order, silane SAMs on SiO₂ are more chemically, thermally and mechanically stable (except in presence of an aqueous base).²⁵ Increased stability allows for extensive synthetic modification post SAM formation.²⁶ Despite the increased stability of silane SAMs, their formation is complicated by the inherent instability of silanes. Silanes are much more reactive than sulphur compounds. This increased reactivity limits the nature of the surfactant end group/functionality. Furthermore, (trihydrolyisable) silanes are prone to water induced polymerisation, thus making the preparation of silane SAMs

harder than thiol SAMs. In fact, while loosely packed monolayers are formed in the absence of water, excess water results in polymerisation of silanes.^{27,28}

- *Silane-TCO*: Recently, transparent conducting oxides (TCOs) have been identified as silane SAM substrates. Interest in TCOs as SAM substrates is due mainly to their electrical conductivity and transparency.²⁹ The TCO indium tin oxide (ITO) is the most widely studied. Despite our knowledge of the bulk structure, the surface chemistry is poorly understood. The systematic study of functionalised ITO surfaces is complicated by the large variation in the topology of commercially available substrates from batch to batch, independent of supplier. However, ITO has found many applications as a SAM substrate, namely on organic opto-electronic devices, biosensors, solar cells, electrochromic windows, flat panel displays, photovoltaic and probing cell-substrate interactions.^{30,31}

For the purpose of this thesis, only thiol-gold SAMs will be further discussed.

1.2.1.3 SAM formation

Self-assembly is initiated by the absorption of surfactants onto the substrates surface from either solution or vapour phase. Formation involves a four steps process (**Figure 3**).⁹

1. *Physisorption* of surfactants from either solution or vapour. The surfactant molecules now lie parallel to the substrate's surface due to attractive physical forces.
2. *Chemisorption* occurs as the surfactant's head group forms a chemical bond (covalent) with the substrate. As a result, the surfactants now lie more normal to the surface (generally at a certain tilt angle).
3. *Initial molecular ordering* occurs. The fraction of chemisorbed surfactants increases so that their proximity to one another also increases. The increased proximity between chemisorbed surfactants allows intermolecular forces to act between the backbone chains of the surfactants. These exothermic intermolecular forces provide the SAM with quasi-crystalline order.²⁹
4. *Definitive molecular ordering*. After the initial formation of the SAM more ordering may take place after a few hours to 24 hours even though some literature shows that increased order could be achieved after 48 hours or a few days.¹⁰

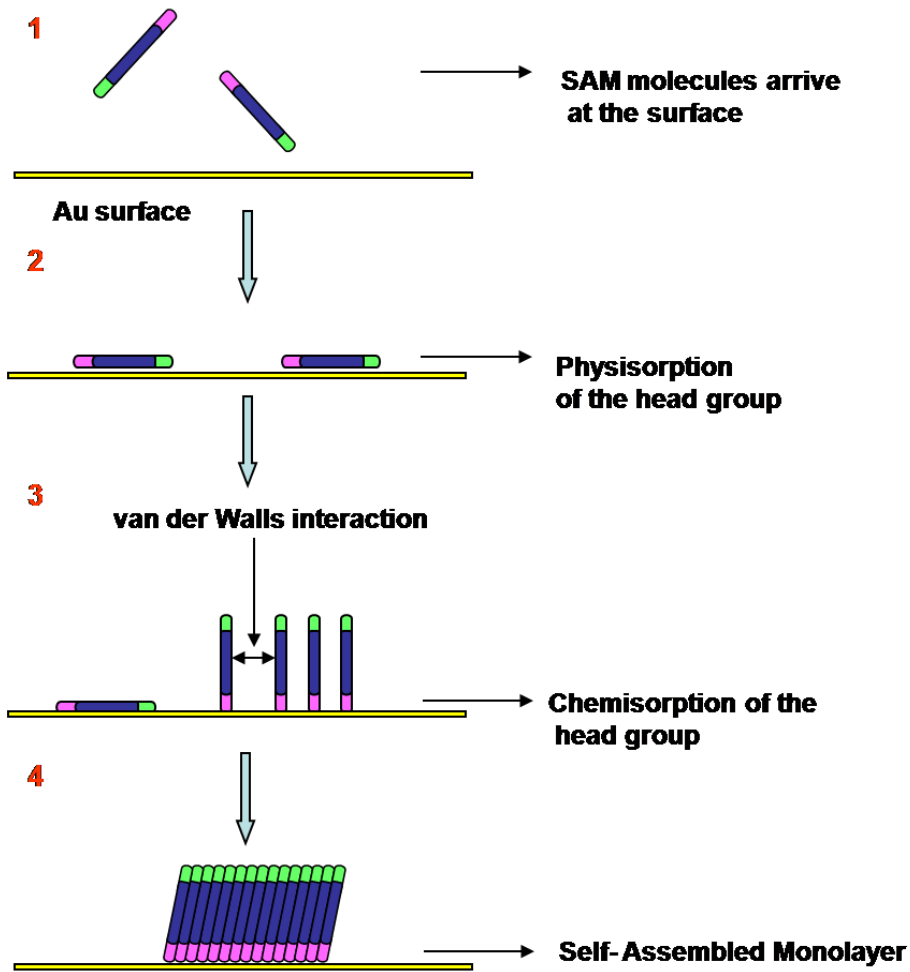


Figure 3 Schematic of SAM formation.

During the SAM formation process several energies are involved as shown in **Figure 4**.³¹

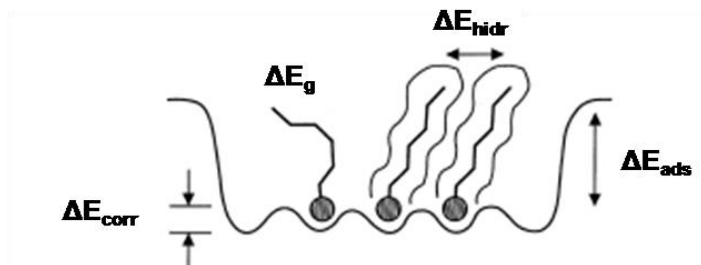


Figure 4 Schematic of the energies involved in SAMs formation.

In particular, the molecule assembly on the surface is influenced by the adsorption energy (ΔE_{ads}), which involves the interaction between the substrate and the head group, the substrate corrugation energy (ΔE_{corr}), which is related to the surface characteristics, the van der Waals interaction between the backbone (ΔE_{hyd}) and (ΔE_{g}), the gauche defect energy, which represents any variation from the stretched conformation of the backbone.³⁰

1.2.1.4 SAM structure/Intermolecular packing

The following paragraph will briefly present the crystal lattice of SAMs with alkyl and aromatic backbones and their alignment on the gold surface.

1.2.1.4.1 Influence of the backbone nature: alkyl and aromatic backbones

Scanning Tunneling Microscopy (STM) studies have shown that there is a degree of ordering of aromatic and alkyl moieties on gold surfaces.³¹ Recent STM studies have highlighted that aromatic compounds present two kind of organisation on the surface **(Figure 5a)**:^{32,33}

(A) *Parallel stripes* separated by a distance of 1.19 ± 0.13 nm, **(Figure 5a-b)**.

(B) Agglomerates of disordered molecules called *islands* **(Figure 5a)**.

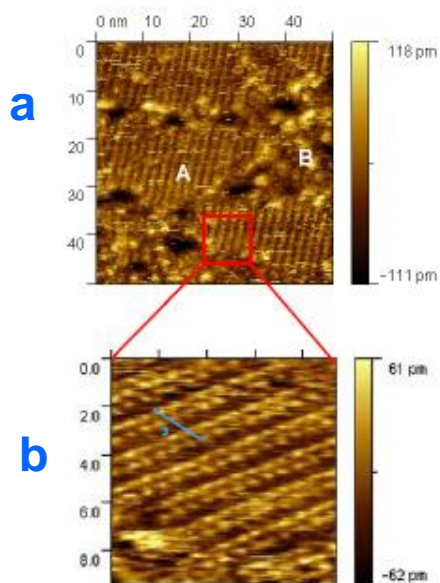


Figure 5 a) STM topographic image of thiophenol SAMs (toluene, 72h); zone A highlights the parallel alignment of the molecules while zone B shows the presence of disordered agglomerates (islands). b) Higher resolution image showing only zone A.³³

In (A) each stripe is constituted by a pair of rows at a distance of 0.50 ± 0.01 nm where the molecules are aligned perpendicularly to each other (**Figure 6**).

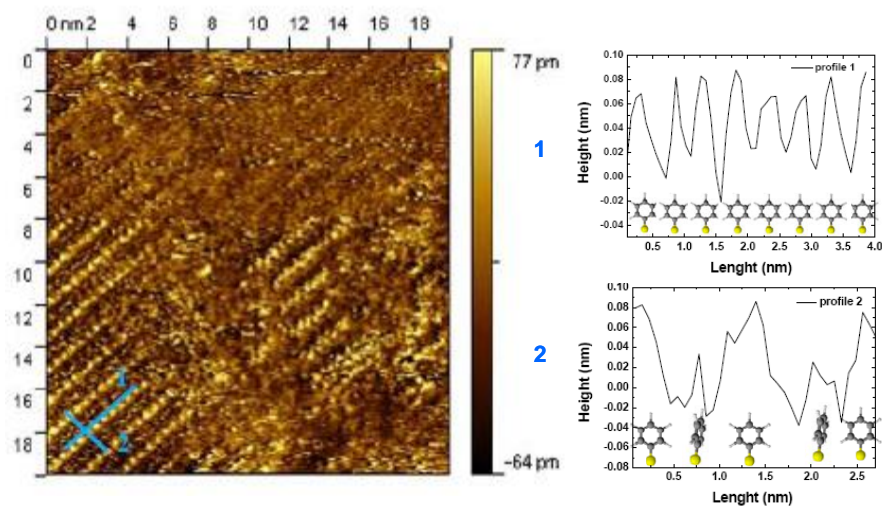


Figure 6 On the left: STM topographic image of thiophenol SAMs (toluene, 24h) with (in blue) the two cross-section 1 and 2 in which zone A (**Figure 5**) has been divided. On the right: cross-section of the profile 1 and 2 showing the parallel and perpendicular alignment of the molecules in zone A.³³

In dodecanethiol SAMs, each stripe is composed by only one row of dodecanethiol molecules separated by 1.92 ± 0.01 (nm). Furthermore, the coverage of a dodecanethiol

SAM is lower in agreement with the stronger interaction between aromatic thiols and gold. (Figure 7).³³

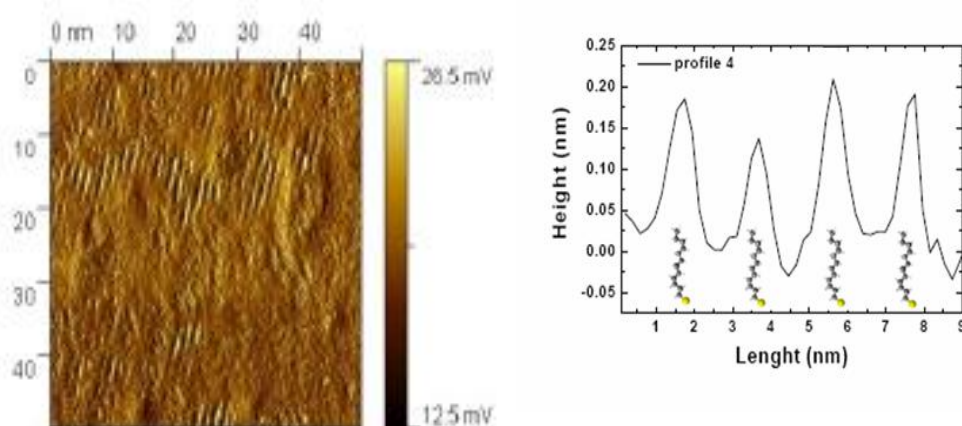


Figure 7 On the left: AFM topographic image of dodecanethiol SAMs (toluene, 24h) which shows its organisation in parallel rows. On the right: cross-section of the same surface showing the alignment of the molecules.³³

1.2.1.5 Multicomponent SAMs: aromatic and alkyl moieties

Formation of multicomponent SAMs is more complicated than single component SAMs. Multicomponent SAMs can be formed by either selectively changing the end group functionality, after the SAM formation using a number of different patterning methods (*i.e.*, UV photolithography,^{34,35} electron beam bombardment³⁶ and micro-contact printing),³⁷ or by co-adsorbing two or more species onto the substrate during SAM formation.^{38,39} Co-adsorption of two or more species is the route generally employed. The composition of co-adsorbed SAMs does not reflect the relative surfactant concentrations in solution. Rather the composition of mixed SAMs depends on both adsorbate–solvent and backbone interactions that occur during SAM formation.⁴⁰ The next paragraph reports some examples of multicomponent SAMs where the interaction between biotin and streptavidin is utilised.^{41,42} These examples

were chosen because we aim to use the same molecular recognition mechanism in the research reported here.

Mixed SAMs of biotin-terminated thiols and oligoethylene glycol thiols on gold have been shown to work as substrates for specific streptavidin immobilisation while retaining its native structure.^{43,44} Pérez-Luna *et al.*, for instance, examined the binding of wild-type streptavidin and streptavidin mutants to a mixed biotin-terminated SAM as a model of biomolecular recognition at the solid-liquid interface. In their study they highlighted the importance of the preparation, the order and the structure of the monolayer for the molecular recognition process to occur.⁴⁵

Tokuhisa *et al.* reported an elegant example of how to fabricate well-defined and optimally spaced mixed monolayers using dendrons. An anchor molecule (*i.e.*, thioctic acid), of which the end group is a dendron is adsorbed on Au substrate (**Figure 8a**). The removal of the dendron end group to expose a carboxylic moiety and the co-adsorption of mercaptohexanol lead to the attainment of a mixed monolayer with a homogeneous distribution of the two thiol molecules (**Figure 8b**). The selective reaction of the amino terminated biotin to the exposed carboxylic moieties afforded a biotinylated surface where the biotin probe density is controlled (**Figure 8c**).⁴⁶

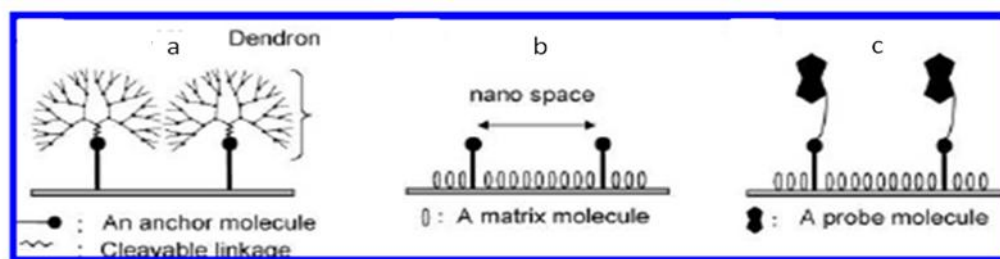


Figure 8 a) Fabrication of a dendrimer monolayer. b) Removal of dendron spacers and introduction of a matrix molecule - 6-hydroxy-1-hexanethiol. c) Modification of the mixed SAM with a probe molecule-biotin.⁴⁶

1.3 Switchable SAMs

Recently, SAMs have been developed with switchable/dynamic end groups. These dynamic end groups can be switched “on” and “off” by applying external stimuli.^{47,48}

Dynamic switching may be achieved by either changing the molecular ordering of the end group or by changing its chemical nature.⁴⁷

1.3.1 SAMs surface modification

There have been many attempts at controlling the surfaces properties of SAMs, most often by using a photochemical, electrical, solvent, temperature or pH stimulus as shown in **Figure 9**.⁴⁹ Here, the discussion will focus mainly on the range of switchable surfaces which undergo a conformational change in response to an external stimulus.

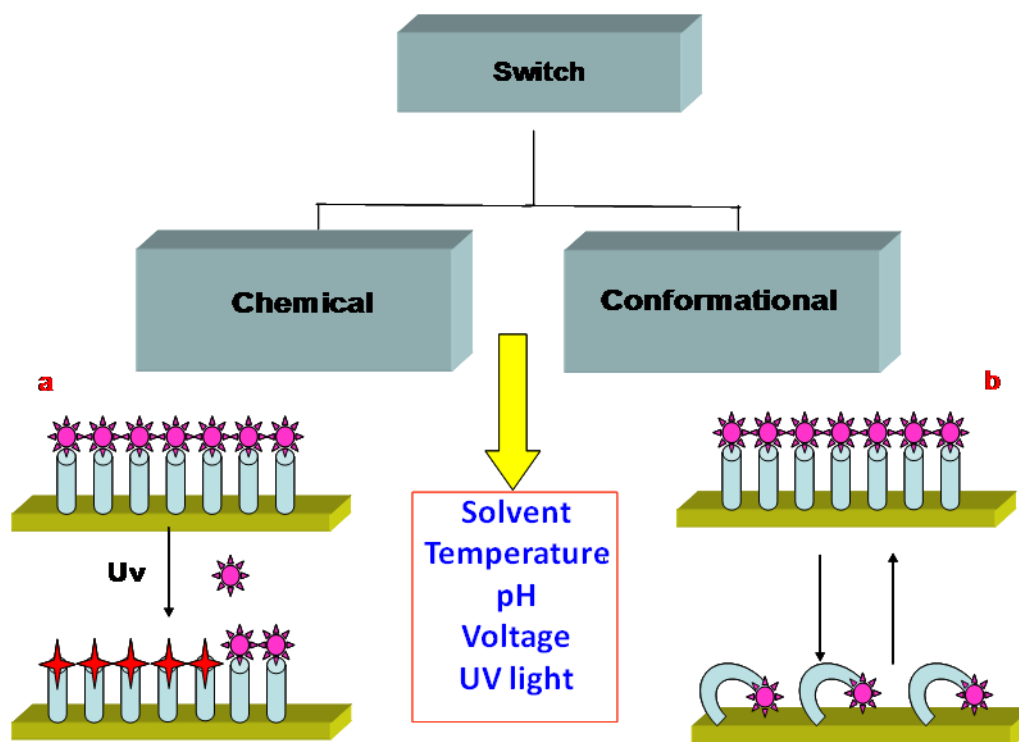


Figure 9 a) *Chemical switch: the structure of the monolayer changes after an external stimulus is applied. (i.e., UV light).* b) *Conformational switch: the chemical structure of the monolayer is still the same while its conformation has changed allowing the exposure on the surface of moieties different from the terminal functionality.*

1.3.1.1 Suitable characteristics for a conformational switch: low density SAMs

Conventional SAMs are too dense to allow conformational transitions and consequently no switching can occur on such high density SAMs. In order to explore SAMs as a model system for switching, sufficient spatial freedom must be established for each molecule.⁵⁰ Once a low density SAM (LD-SAM) is created, preferential exposure of either hydrophobic or hydrophilic moieties of the SAM to the surrounding medium could be exploited for the switching of macroscopic surface properties.^{51,52}

In 2003, Choi *et al.* reported the design of SAM surfaces which exhibit dynamic changes in interfacial properties in response to the application of an electrical potential. Thus, without altering the chemical identity of the SAMs, reversible switching surfaces

can be prepared (**Figure 10**).⁴⁷ In this work carboxyl-terminated LD-SAMs, such as mercaptohexadecanoic acid (MHA) monolayers, are fabricated through the use of a bulky group (precursor) as end group, which acts as a spacer and allows the correct distribution of the molecules on the surface. The subsequent hydrolysis of the precursor leads to a hydrophilic monolayer exposing a charged carboxylate moiety, which can bend on the gold surface when a positive voltage is applied.

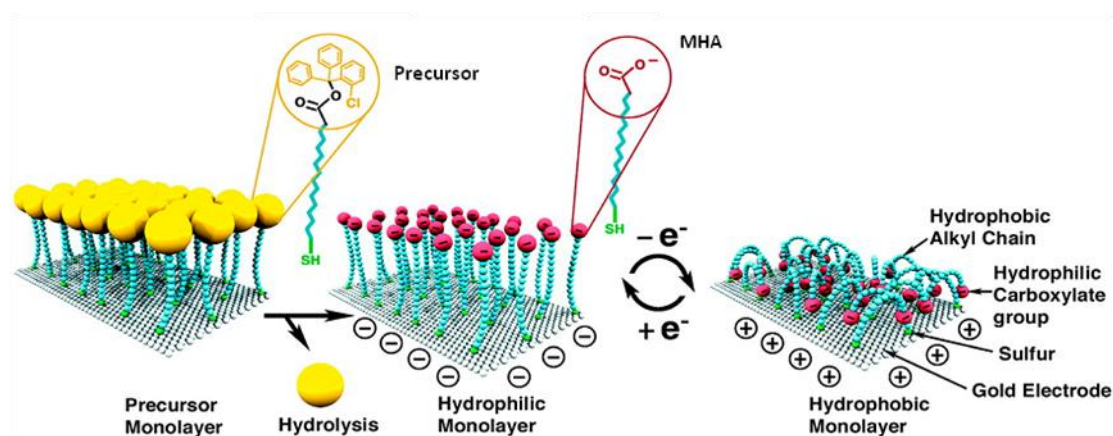


Figure 10 Illustration of the preparation and switching of a low-density self-assembled monolayer of mercaptohexadecanoic acid on gold. The switch is due to a positive voltage being applied on the surface, which leads to a conformational change between straight (hydrophilic) and bent (hydrophobic) molecular conformations.⁴⁷

1.3.1.2 Switchable biological surfaces

One of the aims of the recent research on switchable surfaces includes the control over surface adsorption of biomolecules (i.e. DNA and proteins).^{53,54} In particular, the possibility to control the adsorption of proteins to a synthetic surface would permit to control some important processes such as ligand/receptor or antigen/antibody interactions. There are two main mechanisms by which the interactions between surfaces and biomolecules can be controlled, namely by changing either the interfacial

properties of the surface or the properties of the biomolecules.^{55,56} The following paragraph discusses some switching methods applied to the adsorption/desorption of biological species.

Recently, DNA-based SAMs have been shown to be capable of producing reversible, well-defined nanometre-scale motions. Owing to the strong intrinsic negative charge of DNA, DNA molecules immobilised on a conductive surface could be driven away from, or pulled toward the surface, depending on the electrode potential. At a negative electrical potential, the DNA molecules were shown to stand straight up on the surface, whereas at positive potentials the molecules lay flat. The appropriate surface coverage, in order to prevent steric interactions between neighbouring strands, together with the strength of the electrical potential were key elements to realise electrically switchable surface-tethered DNA (**Figure 11**).^{57,58,59}

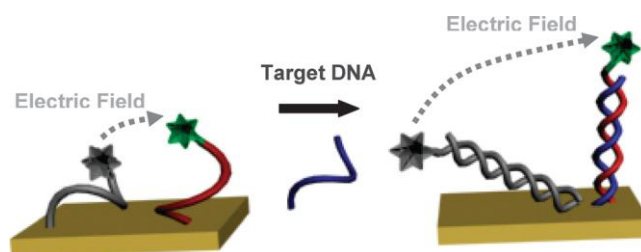


Figure 11 Schematic representation of the electric-field-induced switching amplitude of a single-stranded oligonucleotide immobilised on a gold surface (left) and upon hybridization of the target sequence to the surface confined-single-stranded oligonucleotide (right). The flexible single-stranded oligonucleotide is shown to be only partially aligned by the electric field, whereas the double-stranded oligonucleotide is oriented more efficiently because of its intrinsic rigidity.^{24,57}

Liu *et al.* generated SAMs of a pre-formed inclusion complex cyclodextrin (CD)-wrapped alkanethiolate on gold. Removal of the non covalently bound large CD was a means by which a low density, regular monolayer could be formed. Loosely packed carboxylate-terminated and amino-terminated SAMs were shown to induce dynamic

changes in the surface properties, such as wettability and charge, in response to an electrical potential. In fact, the acid terminated surfaces were negatively charged and hydrophilic under a negative applied potential (straight chains with carboxylate anions exposed at the surface), whereas a positive potential rendered a neutral and hydrophobic surface (bent chains with greasy alkyl chains exposed at the surface). On the other hand, amino-terminated monolayers induced a neutral and hydrophobic surface under a negative potential and a positively charged and hydrophilic surface under a positive potential. These LD-SAMs SAMs have been successfully integrated in microfluidic chips to reversibly control the assembly of two proteins with different isoelectric points (**Figure 12**).⁵⁰

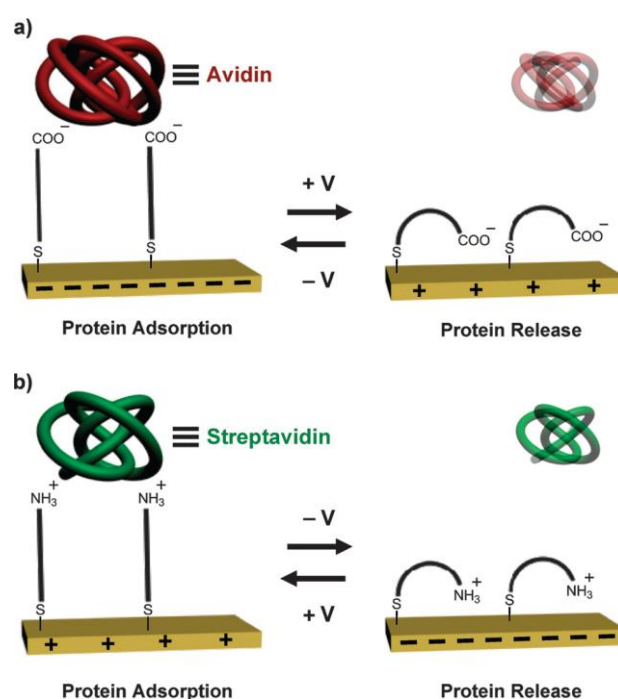


Figure 12 Electrically controlled adsorption of avidin and streptavidin proteins using LD alkanethiolate SAMs on gold surfaces. (a) Carboxylate terminated and (b) amino terminated monolayers have shown reversible switching in conformation under a positive and negative potential.^{25,50}

1.3.1.3 Switchable surfaces and ‘click’ chemistry

‘Click’ chemistry⁶⁰ has recently evolved as a powerful method in organic and biological chemistry, as well as in the field of self-assembled monolayers.^{60,61,62}

The copper(I)-catalysed cycloaddition between the azide and the alkyne proceeds through a stepwise mechanism.⁶³ The mechanism, (**Figure 13**) starts by coordination of alkyne **6** to Cu(I) **5**, displacing one ligand, which then re-coordinates, to give the copper acetylide **7**. In the next step, azide **8** replaces one of the ligands and the copper complex binds to the nitrogen next to the R group, forming intermediate **9**. The attack by the terminal nitrogen in **9** onto C-2 of the acetylide forms the unusual six-membered metallocycle intermediate **10**. Rearrangement of **10** gives the five-membered species **11**, which is transformed to **12** by proteolysis (**Figure 13**).⁶³

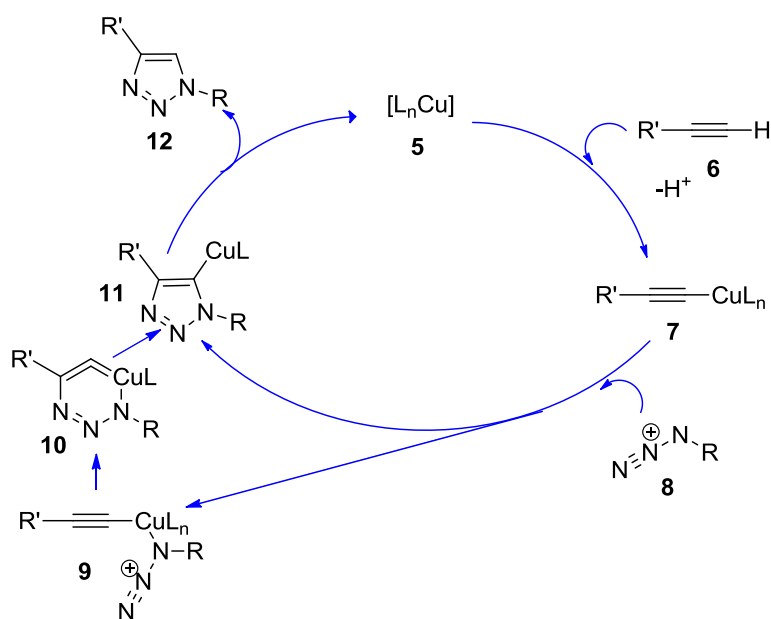


Figure 13 The mechanism of copper(I)-catalysed cycloaddition between the azide and the alkyne.⁶³

Cu(I)-catalysed modification of Huisgen's 1,3-dipolar cycloaddition of alkynes to azides, allows modification of a preformed SAM without the requirement for classical workup or purification procedures.⁶⁴

Such an approach has been described in literature to develop switchable biological surfaces.^{65,66} For instance, Pearson *et al.*⁶⁷ demonstrated the reversible photoswitchable binding of a protease (α -chymotrypsin) to a gold surface attached inhibitor (**Figure 14**). This inhibitor contains an azobenzene switch (core), an ethylene glycol tether (to extend the inhibitor in solution), as well as a terminal alkyne for the attachment to a surface-bound azide via 'click' chemistry.⁶⁷

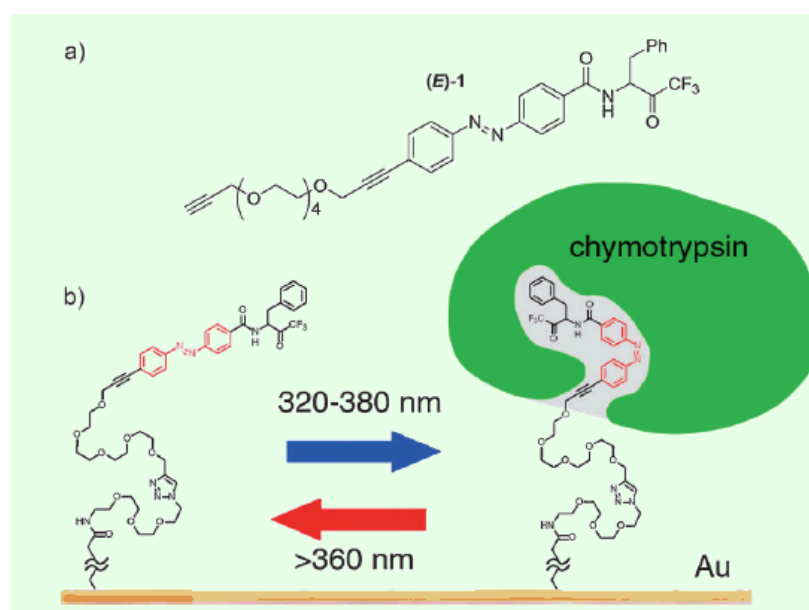


Figure 14 Photoswitch of α -chymotrypsin. a) photoswitch inhibitor (E)-1. b) Schematic of surface photoswitching showing surface-attached (E)-1 and α -chymotrypsin-bound.⁶⁷

In another example Ostaci *et al.*⁶⁸ presented a versatile method for grafting polymer brushes to passivate silicon surfaces based on the Cu(I)-catalysed Huisgen reaction of

azido-terminated polymers and alkynyl-functionalised silicon substrates as shown in **Figure 15**.⁶⁸ The obtained surface can undergo thermo-switching.⁶⁹

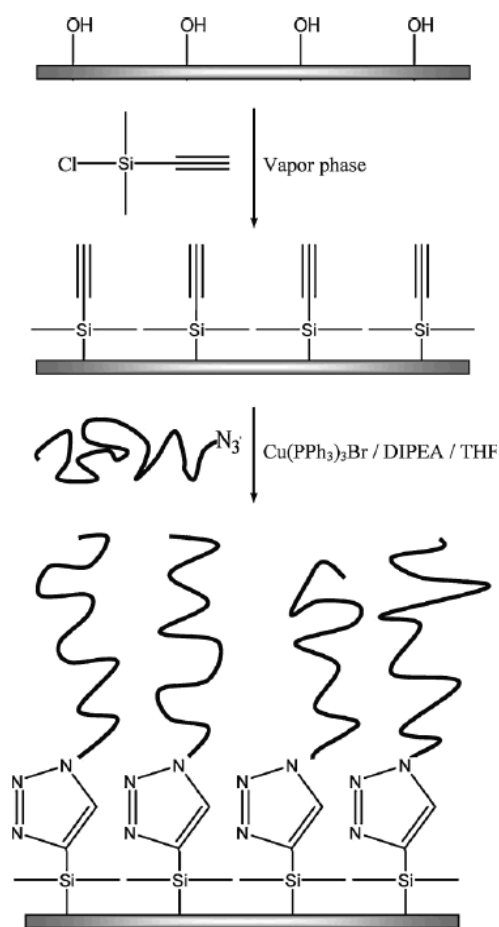


Figure 15 Grafting of polymer brushes to ‘passivated’ silicon substrates using a ‘click’ reaction.⁶⁹

1.4 Concluding remarks

SAMs, which form spontaneously by the adsorption of an active surfactant onto a solid surface, possess important properties of self-organisation and adaptability to a number of technologically relevant surface substrates. In the past decade, important progress on static biological surfaces has been made but current research is focusing on the development of ‘smart’ biological substrates. In particular, a significant number of switchable biological surfaces based on SAMs and polymer films have been described

in recent years. Such surfaces are able to modulate interactions with biomolecules, including peptides, DNA and proteins, and change the response of cells and tissues that come into contact with them. To date, a variety of stimuli, including chemical/biochemical, thermal, electric and optical stimuli have been used to this goal.

The majority of current studies aim to develop a reversible response, in which the properties are switched when stimuli are delivered and then regenerated when the stimuli are removed.

2.0 SURFACE CHARACTERISATION TECHNIQUES

In the field of self-assembly, the structure and bonding of organic molecules adsorbed to metal surfaces may be investigated using different surface sensitive techniques such as Infrared Reflection Absorption Spectroscopy (IRAS), contact angle measurements, Atomic Force Microscopy (AFM), ellipsometry, Surface Plasmon Resonance (SPR), Neutron Reflectivity, and Cyclic Voltammetry (CV).⁷⁰ This chapter briefly describes the techniques used to characterise the SAMs fabricated in this research.

2.1 Contact angle measurements

Contact angle measurements are a very popular methodology for the evaluation of wetting and adhesion properties, calculation of surface energies and the critical surface tension of solids. When a liquid (water, in the example provided below) does not wet a surface completely, it forms an angle θ , the contact angle with the surface. In **Figure 16**, typical hydrophobic and hydrophilic surfaces are shown.⁷¹

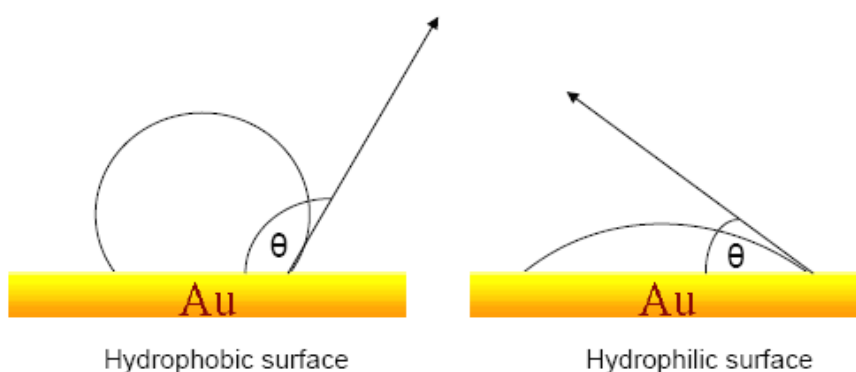


Figure 16 Schematic diagram of the contact angles on hydrophobic and hydrophilic surfaces .

The calculation of the contact angle (θ_c) is based on the *Young-Dupree equation* showed below, where γ is the surface interfacial tension, and VL, VS, and LS refer to vapour-liquid, vapour-solid, and liquid-solid interfaces.

$$\gamma_{VL} \cos\theta_c = \gamma_{VS} - \gamma_{LS}$$

There are three kinds of contact angle experiments that can be performed:

a) Static contact angle measurement: where a droplet of liquid of volume x (V_x) is dropped onto a surface which is in the horizontal plane. The droplet spreads on the surface and the contact angle is measured (V_x remain constant) (**Figure 17**).

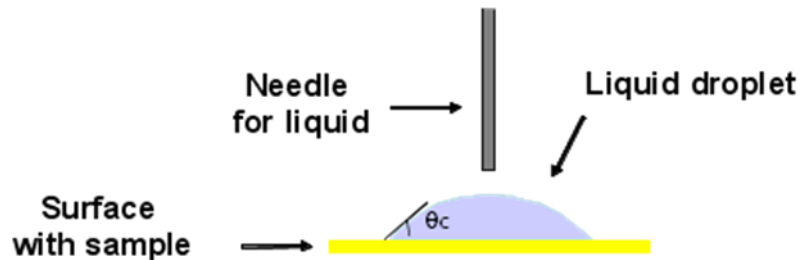


Figure 17 Schematic representation of the measurement of a static contact angle.

b) Dynamic contact angle measurement: where the volume of a droplet of liquid placed onto a horizontal surface is changed during the experiment. V_x is first increased (V_a) and then decreased (V_r) to measure the advancing θ_a and receding angle θ_r , respectively. The difference between the advancing and receding angles ($\theta_a - \theta_r$), gives the contact angle hysteresis (θ_h) (**Figure 18**).

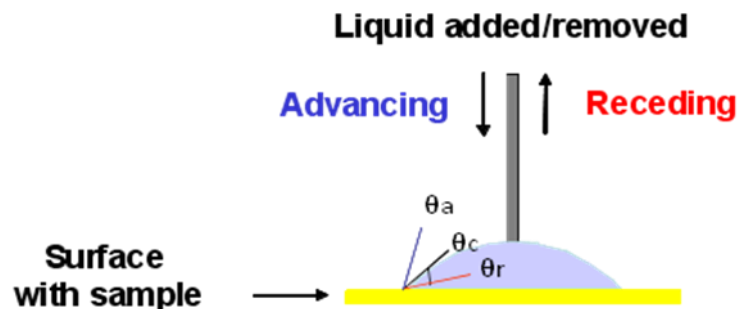


Figure 18 Schematic representation of the measurement of a dynamic contact angle.

c) *Tilting plate contact angle measurement*: where a droplet of liquid of volume x (V_x) is placed on a horizontal surface and the advancing angle θ_a and receding angle θ_r are measured as the surface is tilted up until the drop reaches a point where it almost moves (**Figure 19**).⁷²

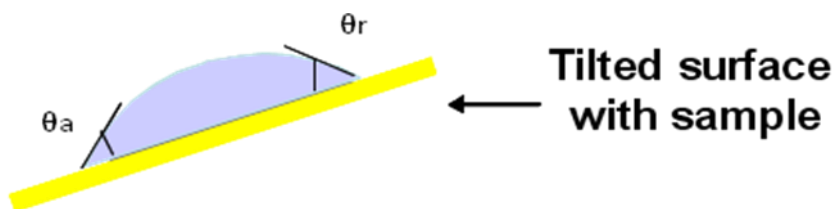


Figure 19 Schematic representation of the measurement of a tilting plate contact angle.

2.2 Ellipsometry

Ellipsometry is an optical technique that uses polarised light to probe the dielectric properties of a sample. The analysis of the light state of polarisation reflected from the sample, through an ellipsometer, can yield information about layers that are thinner than the wavelength of the light itself, down to a single atomic layer or less. Therefore, this technique is useful to study a range of properties including the layer thickness, morphology, or chemical composition. When a polarised light beam reflects from any specular surface, changes occur in both the amplitude and phase of the oscillating parallel (s-polarised) and perpendicular (p-polarised) vector components of the electric field associated with the beam, as shown in **Figure 20**. This phenomenon is used to estimate the thickness of a transition region (e.g. SAM) between the reflective surface and the air. As for contact angle measurements, ellipsometry is a non-destructive technique that it is generally performed under ambient environmental conditions.⁷³

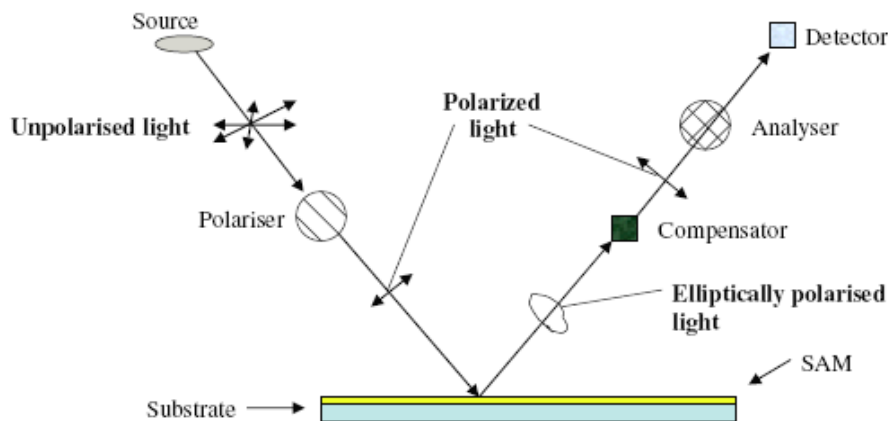


Figure 20 Schematic drawing of an ellipsometer.

2.3 X-ray photoelectron spectroscopy (XPS)

X-ray photoelectron spectroscopy (XPS) is a quantitative spectroscopic technique that measures the elemental composition, empirical formula, chemical state and electronic state of the elements that exist within a material. XPS spectra are obtained by irradiating a material with a beam of X-rays while simultaneously measuring the kinetic energy (KE) and number of electrons that escape from the top 1 to 10 nm of the material being analysed (**Figure 21**). Each element produces a set of XPS peaks at characteristic binding energy values that directly identify each element that exist in or on the surface of the material being analysed. These characteristic peaks correspond to the electron configuration of the electrons within the atoms, e.g., 1s, 2s, 2p, 3s, etc. The number of detected electrons in each of the characteristic peaks is directly related to the amount of the element within the area (volume) irradiated.⁷⁴ XPS must be performed under ultra-high vacuum (UHV) conditions because electron counting detectors in the XPS instruments are typically one meter away from the material irradiated with X-rays. XPS analysis is a destructive technique because it involves the loss of material from the surface. Therefore, once a sample has been analysed it is unsuitable for analysis by other methods.⁷⁵

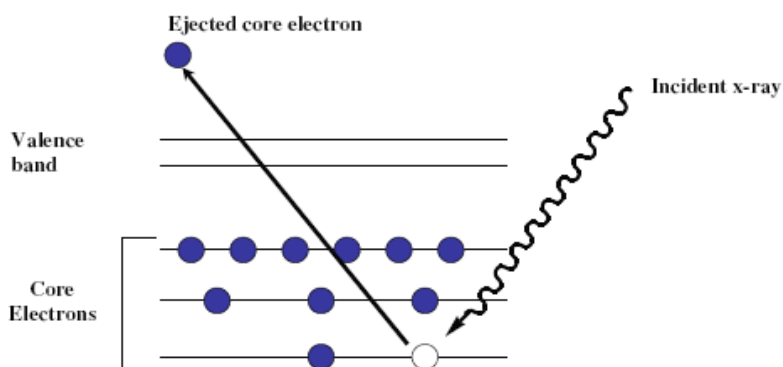


Figure 21 Schematic diagram of the XPS process: The binding energy of the electron released can then be calculated using the following equation;

$$EB = h\nu - EK - W$$

Where, *EB* is the binding energy of the electron, *hν* is the energy of the X-ray, *EK* is the kinetic energy of the emitted electron and *W* is the spectrometer work function.⁷⁶

3.0 PROJECT OVERVIEW

3.1 Hypothesis

The synthesis and characterisation of a double molecular armed system able to undergo on/off bio-switching in response to an electrical potential represents the long term goal of this research (**Figure 22**). The development of such a switchable double armed system, in which multiple cationic or anionic groups are distributed along the molecular arms, offers the opportunity to reversibly control different biomolecules on surfaces (i.e. biotin/streptavidin).^{77, 78}

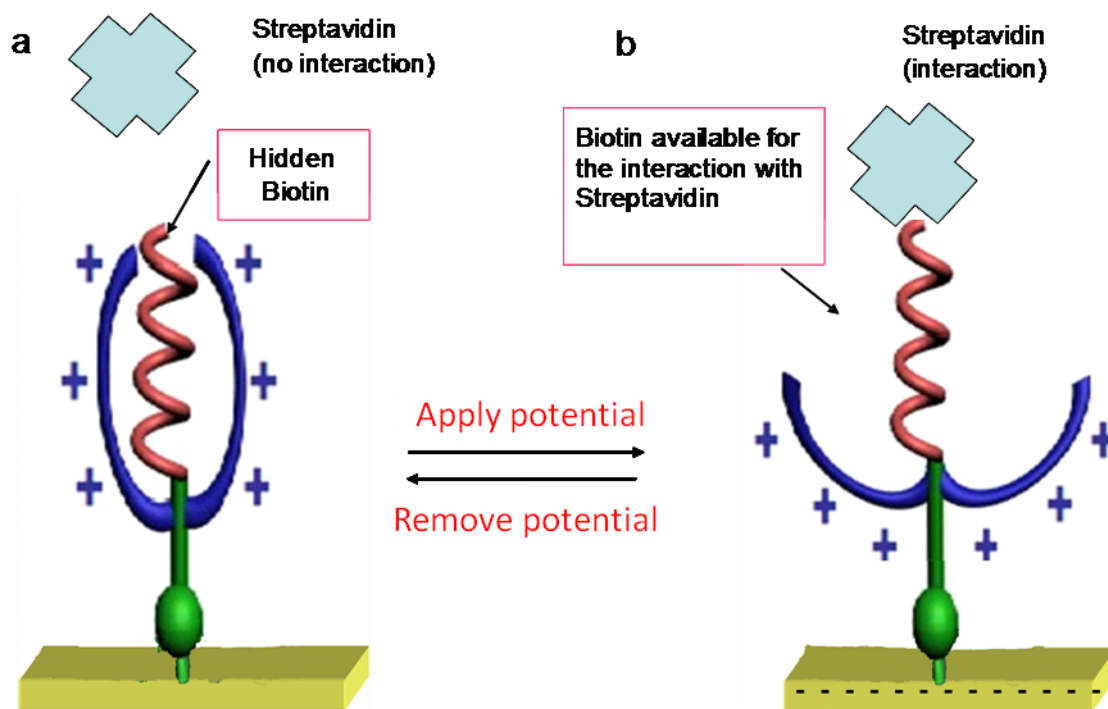


Figure 22 Representation of the double armed electro-switchable biological surface; a) No potential applied: the positively charged molecular arms create a steric hindrance effect which does not allow the interaction between biotin and streptavidin. b) Negative potential applied: the positively charged molecular arms open because they are attracted by the charged surface allowing the interaction between biotin and streptavidin.

3.2 Aims

In order to achieve conformational transitions of surface-confined molecules, monolayers of the addressable molecules must have sufficiently low packing density so that homogenous structural changes can occur across the entire surface without hindrance from intermolecular steric interactions.⁷⁷ Towards this aim, surface substrates will be functionalised⁷⁸ with a two-component, aromatic-mixed SAM formed by 4-methylbenzenthionol (4-MBT) and 4-aminothiophenol (4-ATP). The former compound will act as spacer molecule while the latter will present the amine moiety needed for further reactions on surface (**Figure 23**).

For the synthesis of the double armed system (**Figure 23**), the methyl gallate derivative will be first immobilised on the surface through covalent imine bonding between the aldehyde moiety and the amine group on the SAM surface. Positively charged molecular arms will be developed using oligolysine peptides as they exhibit protonated amines at pH =7. The oligolysine peptides will be immobilised on the surfaces through a Huisgen reaction between the alkyne group on the benzaldehyde derivative and the azide-functionalised oligolysine peptides. It is expected that steric hindrance from the molecular arms will impede the availability of the biotin previously immobilised in *para*-position of the benzaldehyde derivative towards any possible biomolecular interaction. Application of a negative potential to the surface will attract the charged arms to the surface, allowing the biotin to be available for further interaction, without any steric hindrance. The selective detection of biotin in the on/off status will be performed through interaction with a fluorescently labelled streptavidin (**Figure 22**).⁷⁹

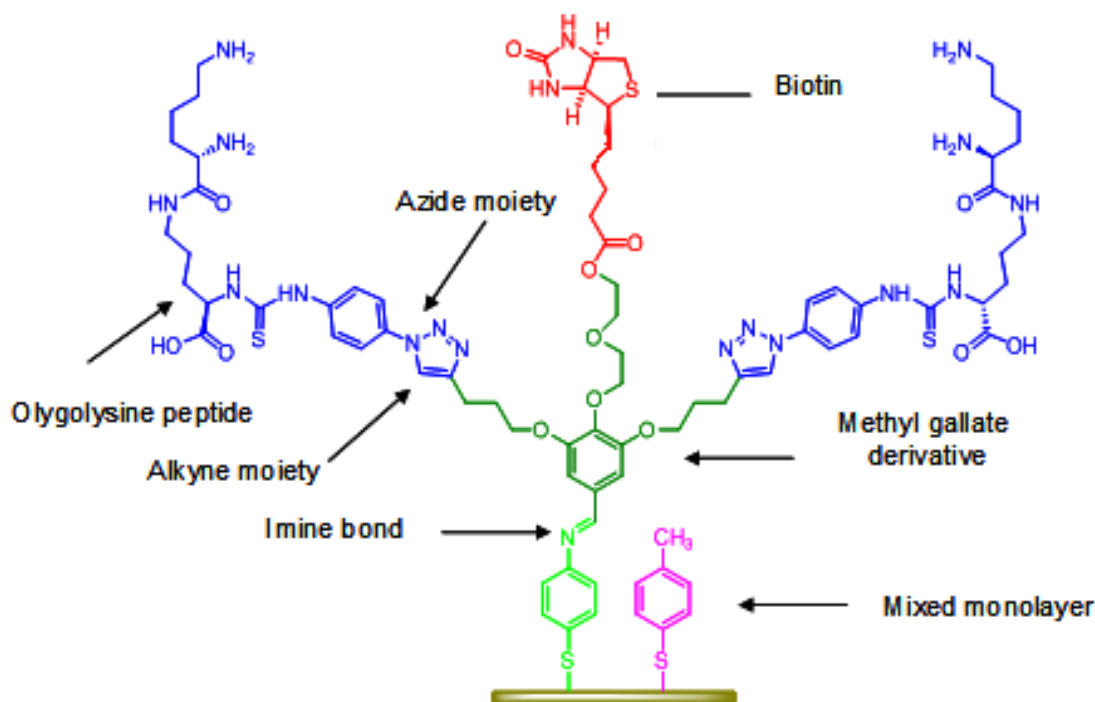


Figure 23 Representation showing the chemical structure of the double armed switchable system: the main moieties are highlighted by using different colours.

In order to gain as much information as possible about the reactivity and the stability of each single molecular portion forming the double armed system, it has been decided to simplify the original model (**Figure 23**), as shown in **Figure 24 a-b**. The synthesis of these SAMs will give a better understanding of the possible interactions which could occur on the surface and will also help in finding the right strategy for the future fabrication of the desired surface (**Figure 23**).

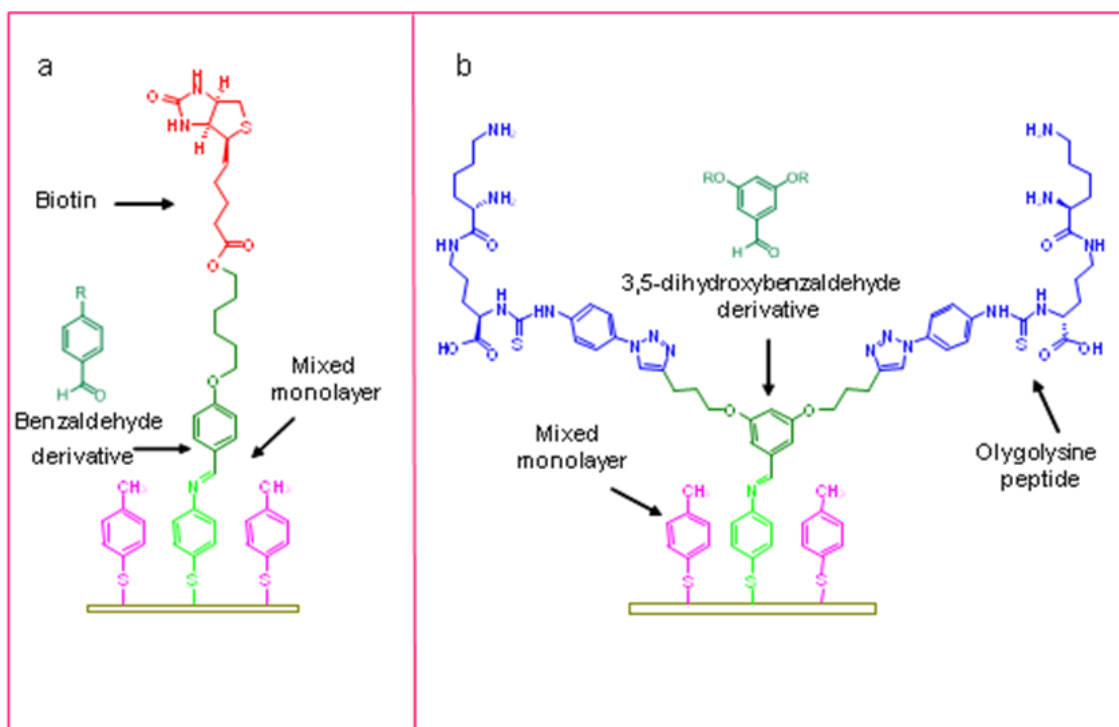


Figure 24 a) Representation of the mixed monolayer containing only the biotin moiety. b) Representation of the mixed monolayer containing only the double arms moiety.

To achieve the surfaces illustrated in **Figures 24a** and **24b**, four main objectives have been identified:

Objective 1:

- a) The coupling of biotin **4** with alcohol **3** through an EDC coupling (**Figure 25**). The two step sequence for the synthesis of **5** will be performed using different coupling reactants and different strategies, which will be discussed along with biotin reactivity issues.

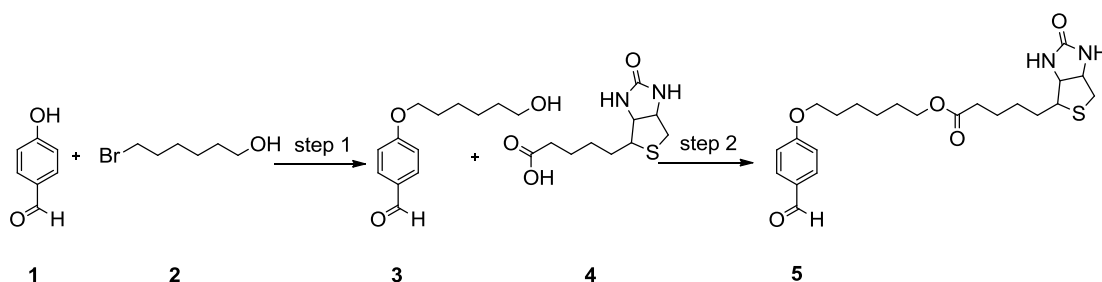


Figure 25 Overall synthesis of biotin derivative **5**.

b) Formation of the triazole ring to immobilise the molecular arms, through a Huisgen reaction in solution. The reaction will be performed using both 4-azido aniline (**12**) and 4-methoxybenzyloxycarbonyl azide (**12'**). The scheme showed in **Figure 26** illustrates the four step sequence that has been followed in order to achieve **14**.

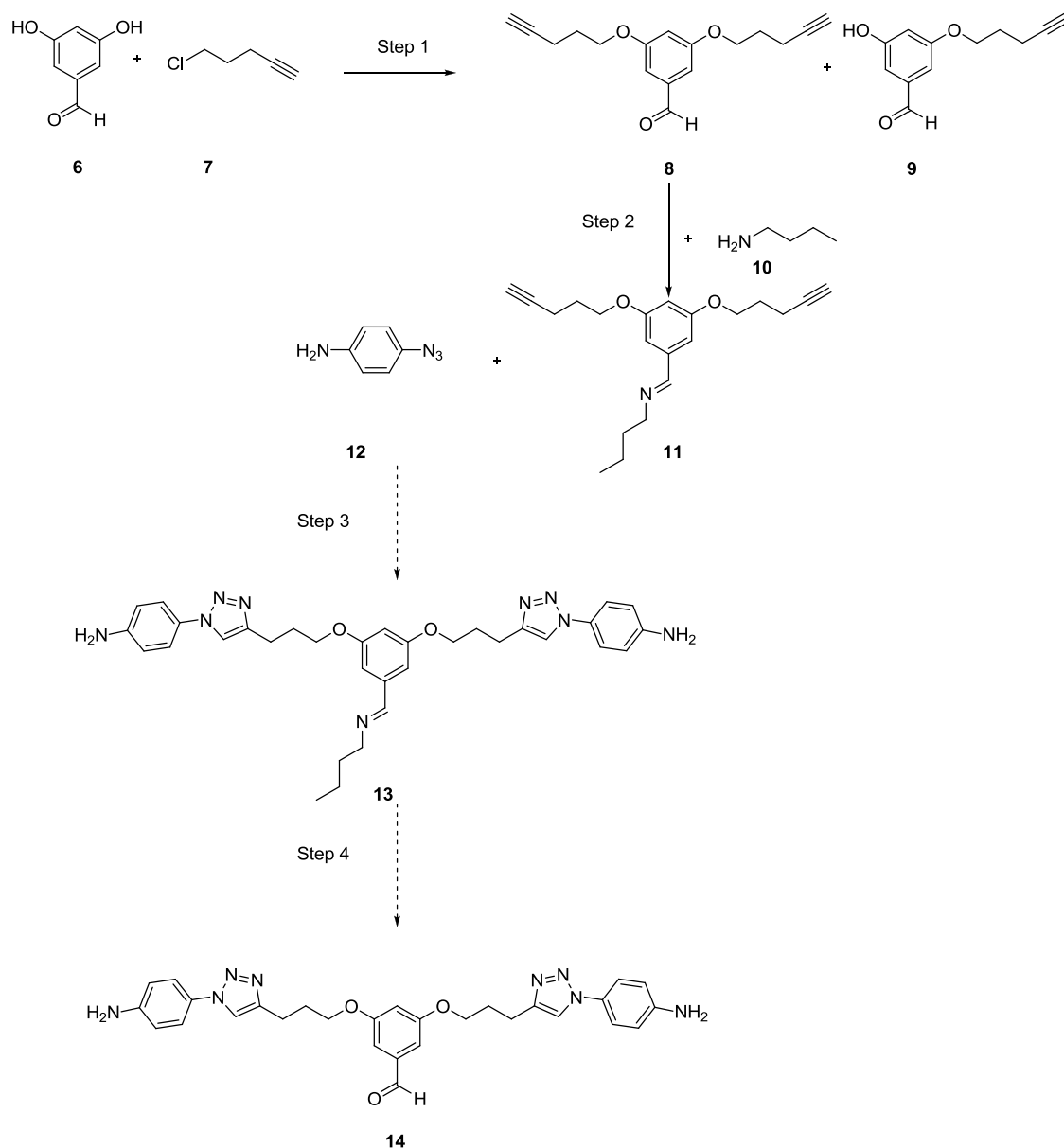


Figure 26 Synthesis of the double armed moiety **14** through a Huisgen reaction. In this case, the azide involved in the reaction is 4-AA.

Both **5** and **14** contain the aldehyde moiety necessary to form an imine bond with the amine moiety present in para position on 4-ATP.

Objective 2:

Creation and characterisation of an aromatic mixed monolayer formed from 4-aminothiophenol (4-ATP) and 4-methylbenzenthionol (4-MBT) (**Figure 27a**). The production of such a monolayer will take into account the following parameters: a) time, b) ratio of the chemicals used and c) solvent influence. The characterisation will be performed by contact angle, ellipsometry and XPS. The results obtained from these studies will be compared with the ones obtained from the analysis of the corresponding single monolayers (**Figure 27b**).

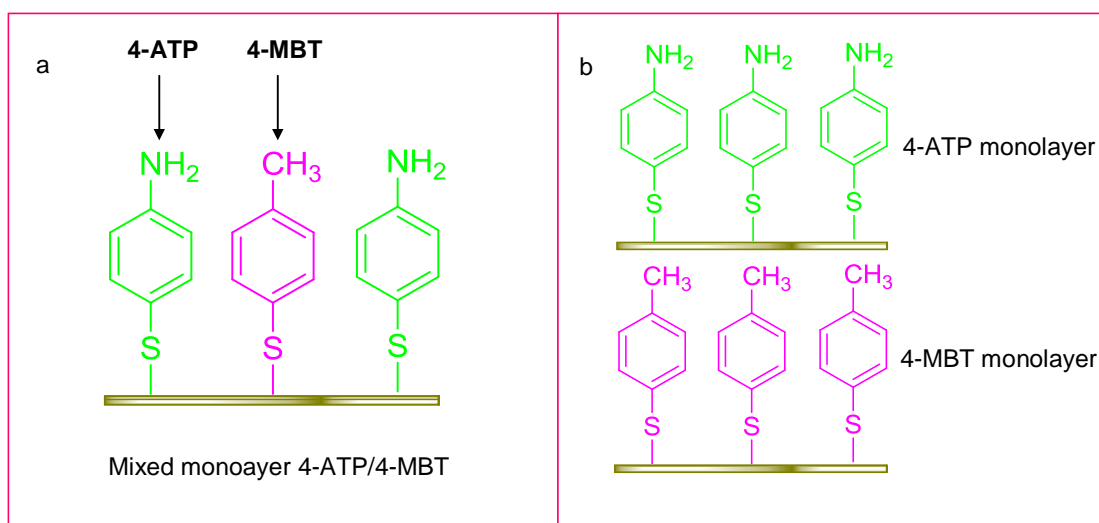


Figure 27 a) Representation of the mixed monolayer of 4-ATP/4-MBT on gold surface. b) Representation of the single monolayer of 4-ATP (green) and 4-MBT (pink) on a gold surface.

Objective 3:

Imine bond formation, between the benzaldehyde derivative and the surface-bound aniline derivative (**Figure 28a**), will be attempted on the surface of SAMs on gold. In this context, the imine bond formation will be investigated using some model compounds as shown in

Figure 28b, in order to test its feasibility. The monolayer obtained will be analysed by ellipsometry and XPS. The results will give information on the stability of this bond and on its feasibility on the surface of SAMs on gold.

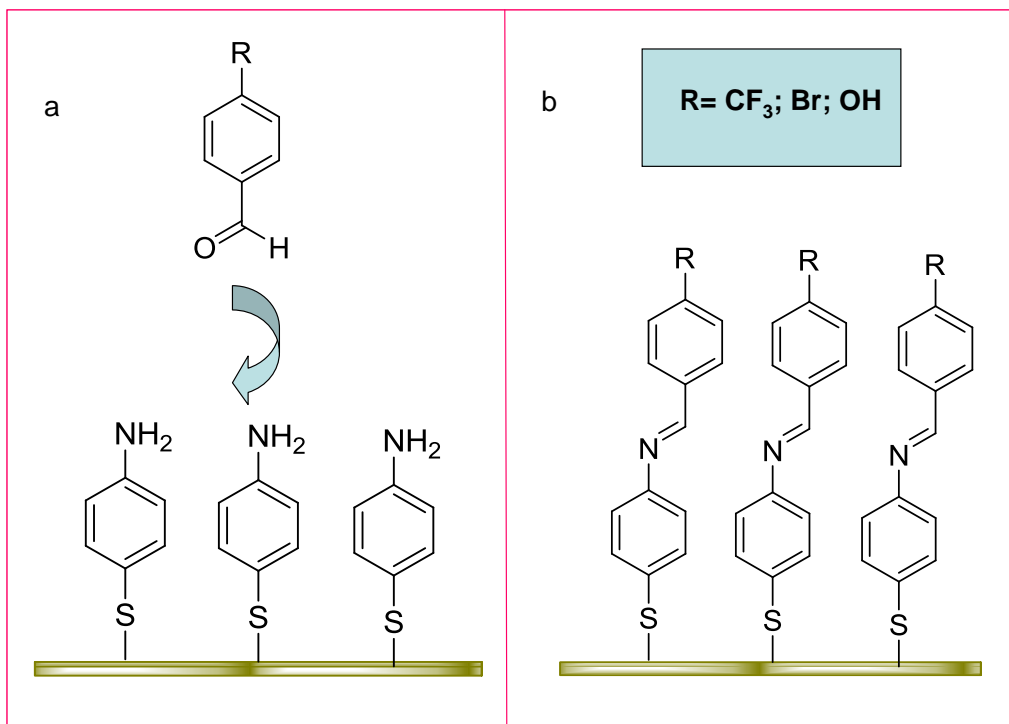


Figure 28 a) Representation of the imine bond formation between the 4-ATP monolayer and the p-substituted aldehyde. b) Representation of the single monolayer after imine bond formation, with the different substituents indicated.

Objective 4:

As a control study, disulfide **18** will be synthesised (the imine bond is formed in solution) (**Figure 29**) and then a single monolayer of **18'** will be formed on the gold surface (**Figure 30**). The characterisation of this surface will be carried out by contact angle, ellipsometry and XPS, and the results will be compared to those achieved in *objective 3* and discussed with reference to the available literature.

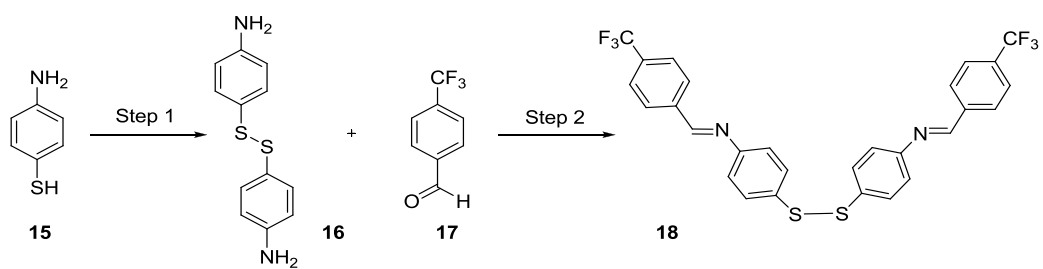


Figure 29 Synthesis of **18** in two steps. **17** has been chosen as the *p*-substituted aldehyde because the fluorine element in the CF_3 moiety provides a strong signal for XPS analysis.

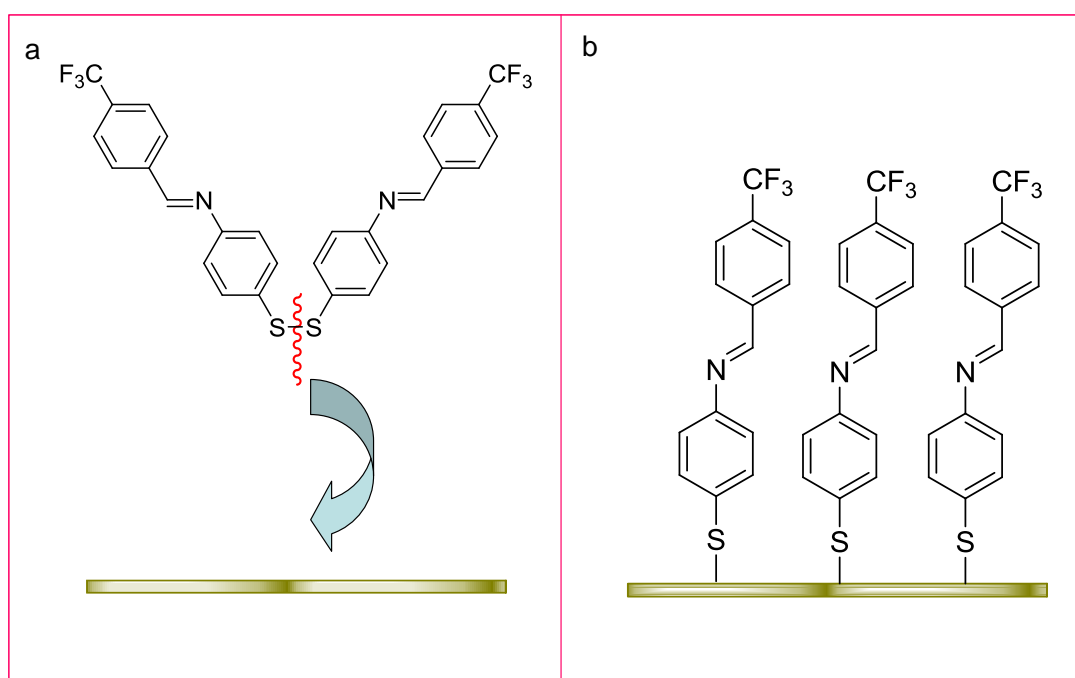


Figure 30 a) Representation of the rupture of disulfide **18** onto a gold surface. b) Representation of the monolayer **18'**, containing an imine bond.

4.0 RESULTS AND DISCUSSION

4.1 Synthesis

4.1.1 Synthesis of biotin-derivative 5

The synthesis of biotin derivative **5** was conducted successfully in 2 steps (**Figure 25**). Each of these steps is discussed below, with analysis of their mechanisms and the alternative routes attempted.

Step 1 (**Figure 31**)⁸⁰

The formation of **3** was achieved by employing K_2CO_3 as a base to deprotonate the hydroxyl proton of **1**. The reaction proceeded *via* an SN_2 pathway, for which the mechanism is shown in **Figure 32**. The phenoxide, formed by deprotonation of **1**, acted as a nucleophile and attacked the σ^* ($C-Br$) orbital of **2** to generate ether **3**.

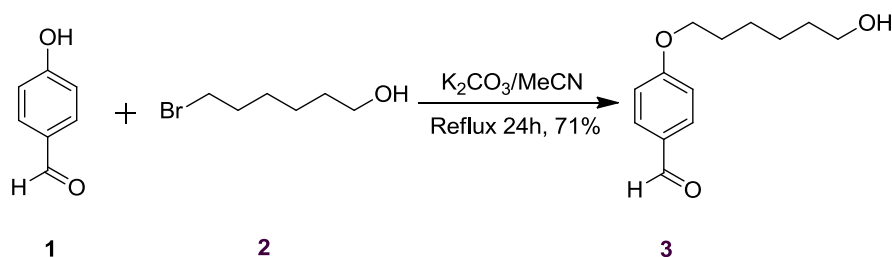


Figure 31 Scheme showing the synthesis of ether **3**.

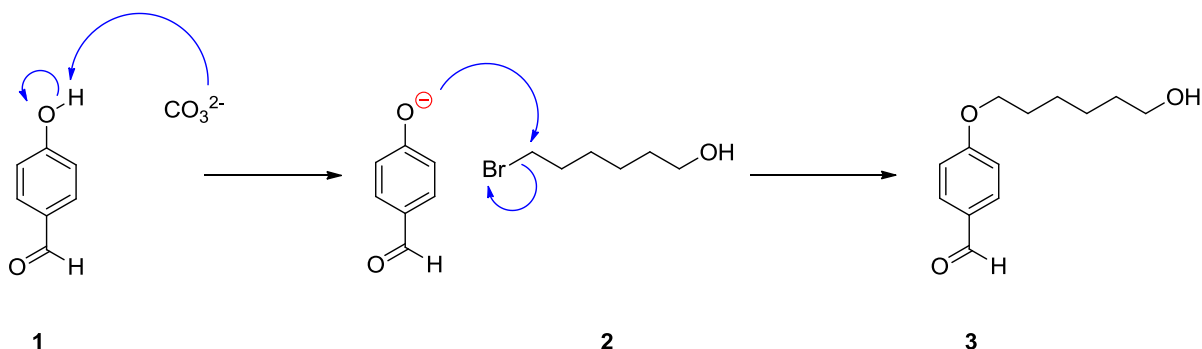


Figure 32 Mechanism for the alkylation of **1**.

Step 2

The formation of **5** was attempted firstly through a Steglich esterification discussed in details below (**Figure 33-34**).^{81,82}

DCC (dicyclohexylcarbodiimide) and carboxylic acid form an *O*-acylisourea intermediate, which offers reactivity similar to the corresponding carboxylic acid anhydride:

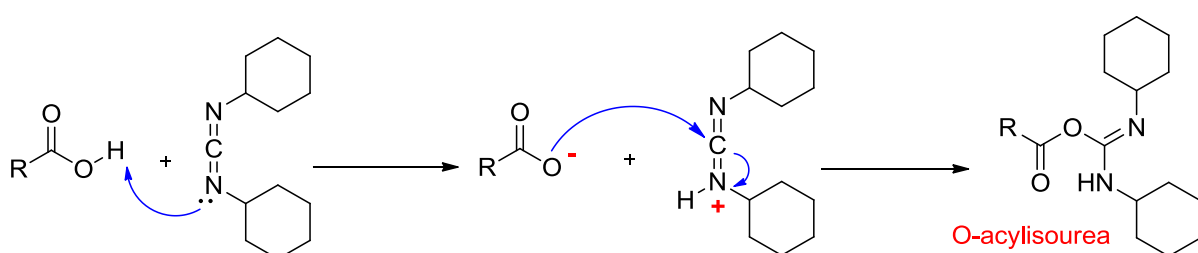


Figure 33 General scheme of *O*-acylisourea formation.

The reaction proceeds with the addition of the alcohol to the activated carboxylic acid to form the stable dicyclohexylurea (DHU) and the desired ester:

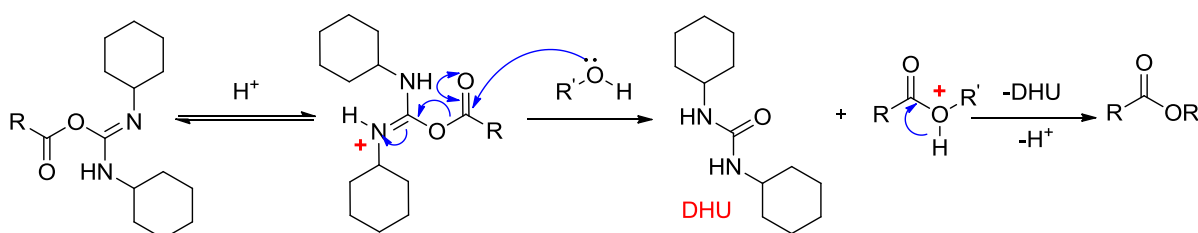


Figure 34 General scheme of ester bond formation.

The addition of approximately 5 mol-% of 4-*N,N*-dimethylaminopyridine (DMAP), (**Figure 35**), is crucial for the efficient formation of esters.

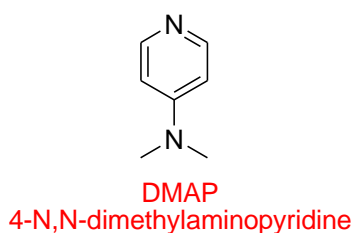


Figure 35 Chemical structure of 4-N,N-dimethylaminopyridine.

A common explanation for this reaction rate acceleration is that DMAP, as a stronger nucleophile than the alcohol, reacts with the *O*-acylisourea leading to a reactive amide ("active ester"). This intermediate cannot form intramolecular side products but reacts rapidly with alcohols. In this way, DMAP acts as an acyl transfer reagent, and subsequent reaction with the alcohol gives the ester (**Figure 36**). This process is known as nucleophilic catalysis.

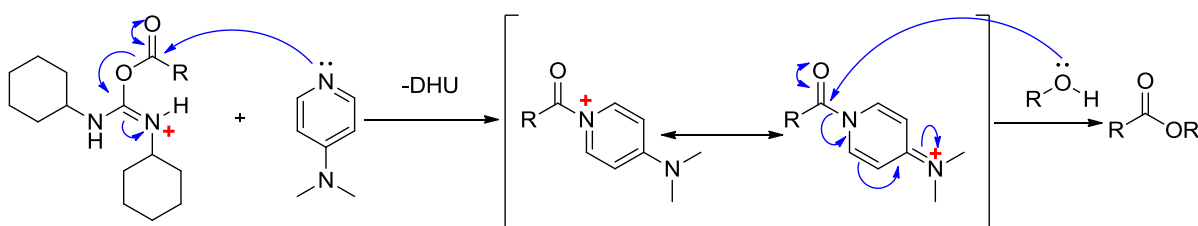


Figure 36 General scheme of the DMAP catalytic mechanism.

Attempted DCC coupling provided a poor yield of the product and showed the formation of by-products. However, the synthesis of **5** (**Figure 37**) was successfully achieved through a 1-ethyl-3-(3-dimethylaminopropyl)-carbodiimide (EDC) coupling reaction. EDC (**Figure 38**) is a water-soluble derivative of carbodiimide.^{83,84}

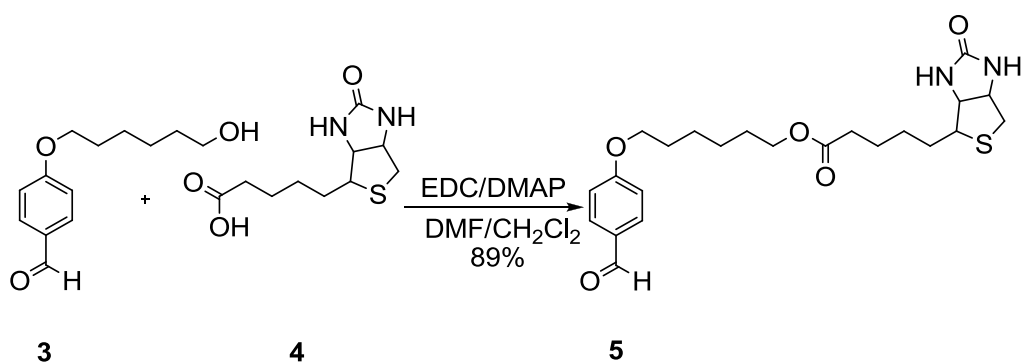


Figure 37 Scheme showing the synthesis of ester **5**.

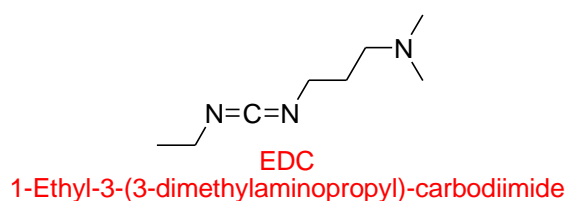


Figure 38 Chemical structure of EDC.

4.1.2 Synthesis of the double arms moiety **14**

Our proposed route to **14** is shown in **Figure 39**. After an initial etherification reaction (*step 1*), ‘click’ chemistry (Huisgen reaction) on diyne **8** was attempted. Performing of ‘click’ chemistry directly on **8** failed (*step 2*), hence the aldehyde moiety of **8** needed to be protected prior to the Huisgen reaction (*step 3*) and then be subsequently deprotected (*step 4*).

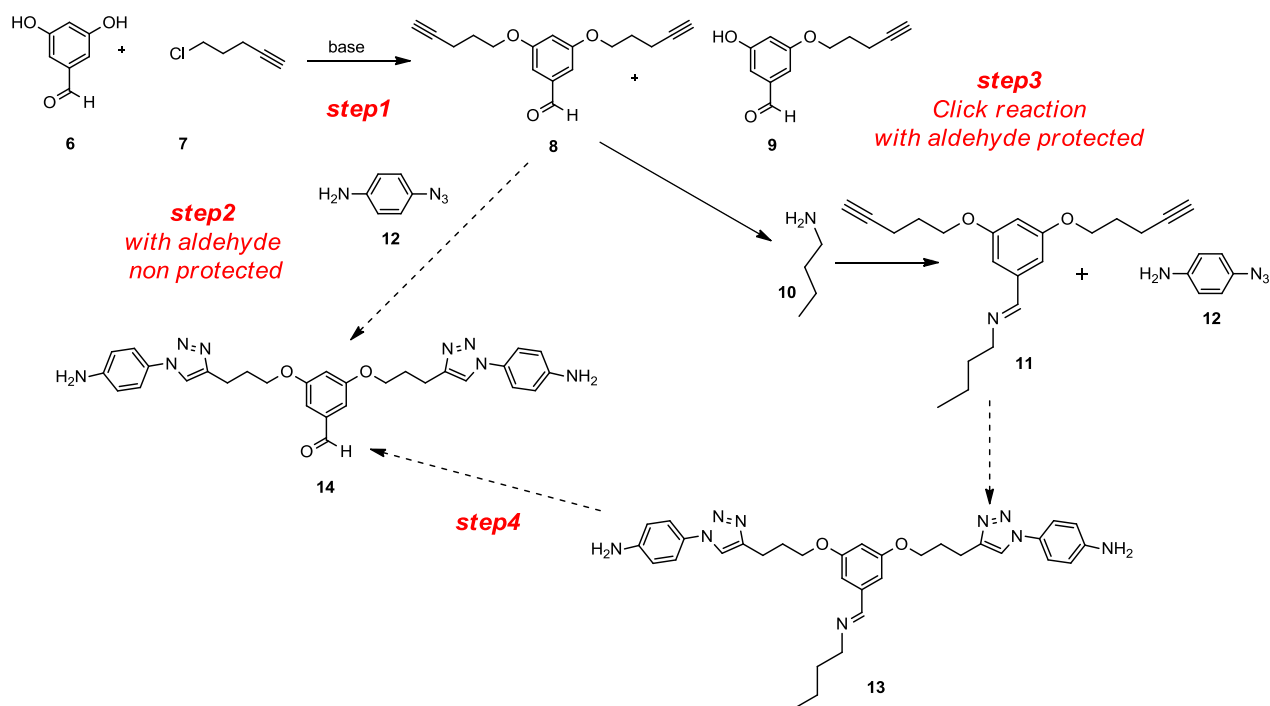


Figure 39 Proposed synthetic pathway to achieve **14**.

Step 1

The formation of **8** from **6** (**Figure 40**) was achieved by employing K_2CO_3 and NaI. The reaction followed a double SN_2 pathway. Compound **7** was activated by halogen exchange with NaI, as this increases the rate of reaction due to the C-I bond being weaker than the C-Cl bond.

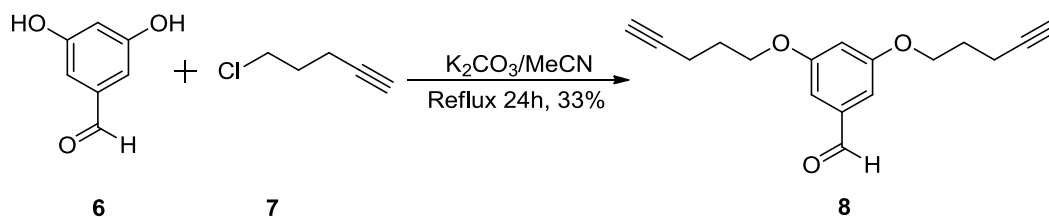


Figure 40 Scheme showing the synthesis of **8**.

Step 2

4.1.2.1 Huisgen reaction

The dialkyne **8** could now be reacted with an azide under ‘click’ condition. The reaction was performed using the following two catalysed alkyne-azide cycloadditions and using combinations of the different solvents and reactants listed below:

Method 1 (M1). *Formation of a Cu^I catalyst by reduction of a Cu^{II} salt:* CuSO₄/DIPEA/sodium ascorbate. In order to avoid the re-oxidation of Cu^I to Cu^{II} a Cu⁰ wire was used.^{85,86}

Experimentally, the azide and the alkyne were dissolved in a solution of H₂O/organic solvent (*t*-BuOH, MeCN, THF) (1:1) and then a solution of CuSO₄/DIPEA and sodium ascorbate in H₂O was added. The reaction was then stirred at room temperature for 48 hours.

Method 2 (M2). *Formation of a Cu^I catalyst by addition of Cu^I salt:* CuI/triethylamine (TEA).^{87,88}

Experimentally, the azide and the alkyne were dissolved in a solution of H₂O/organic solvent (*t*-BuOH, MeCN, THF) (1:1), or in anhydrous toluene, and then CuI/TEA were added. The reaction was then stirred at room temperature for 48 hours.

The formation of **14** was attempted by the employment of a Huisgen reaction, for which the mechanism was previously explained in section 1.3.1.3 (**Figure 13**).

The choice of using azide **12** was due firstly to its similarity with the first portion (highlighted in red) of the oligolysine showed below (**Figure 41**). To achieve **14**, azide **12** was reacted with **8**, using both *M1* and *M2*. This reaction was attempted in both aqueous and anhydrous conditions without protecting the aldehyde moiety of **8**.

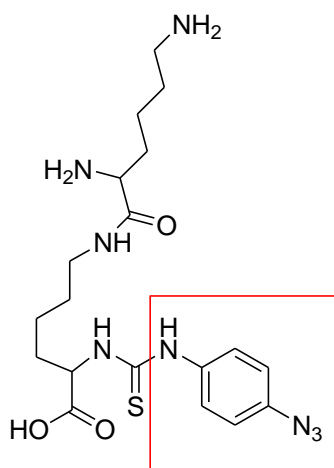


Figure 41 Chemical structure of azide-functionalized oligolysine.

4.1.2.2 ‘Click’ chemistry: **12**⁸⁹

When *M1* was performed, both ¹H NMR and *m/z* suggested that a mixture of products had been obtained. In particular, the ¹H NMR showed the presence of the triazole hydrogen (singlet at 8.30 ppm) which confirmed the formation of the triazole ring. However, the analysis of the integration and the chemical shift showed the presence of different species. The *m/z* analysis confirmed the contemporary presence of **12**, **14'**, **14''** and **14** (**Figure 42**).⁹⁰ Attempts to separate these compounds using HPLC were unsuccessful due to decomposition of the products.

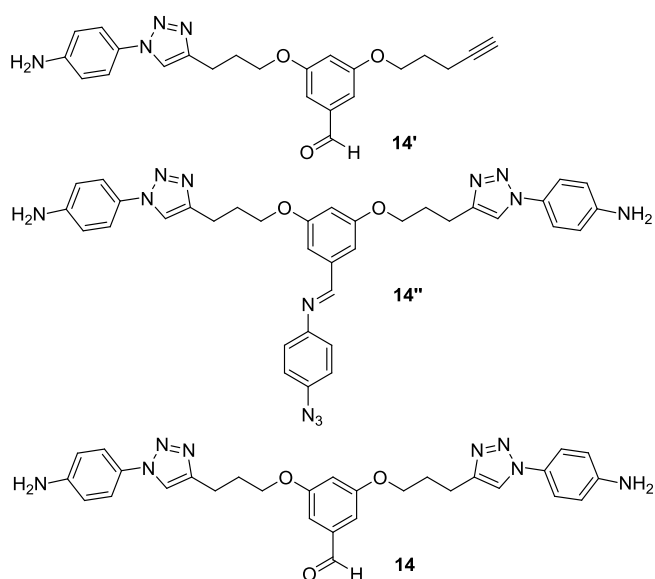


Figure 42 Chemical structure of the “mono” click reaction (**14'**), “double” click reaction with imine bond formation (**14''**) and “double” click reaction (**14**).

When *M2* was performed, surprisingly, the combined analysis (^1H NMR, ^{13}C NMR and MS) of the crude showed the presence of compound **15** (**Figure 43**).

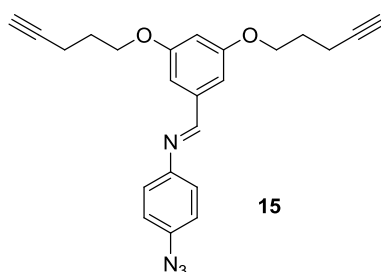


Figure 43 Chemical structure of **15**.

4.1.2.3 ‘Click’ chemistry: **12'**

Previous studies have reported that the amine group could influence the Huisgen reaction promoting a side reaction.^{90,91} For this reason it was decided to attempt *M1* with a different azide, (**12'**) without any amine groups (**Figure 44**).

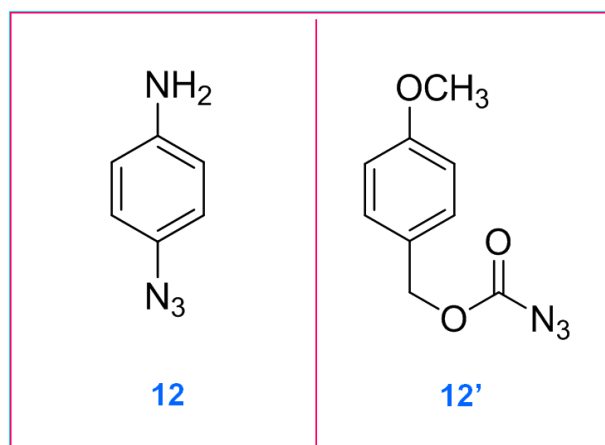


Figure 44 Chemical structure of 4-AA and 4-MA.

The reaction between **8** and **12'** did not give the desired product as the combined analysis of the crude highlighted only the presence of the starting materials.

Step 3

In *step2* we initially attempted 'click' chemistry directly on aldehyde **8** with azide **12**. This provided an inseparable mixture of **14'**, **14''** and **14** (**Figure 42**). Leaving the reaction for longer, as well as adding more copper catalyst, did not allow a full conversion to **14''** (which could then have been cleaved back to aldehyde **14**) and this is believed to be due to steric reasons. It was therefore decided to protect aldehyde **8** as imine **11** by reacting it with 4-butylamine (**10**) (**Figure 45**). Compound **10** was chosen because of its small steric requirement, which would not interfere with the 'click' reaction of **12**. The mechanism for imine bond formation is shown in **Figure 46**.

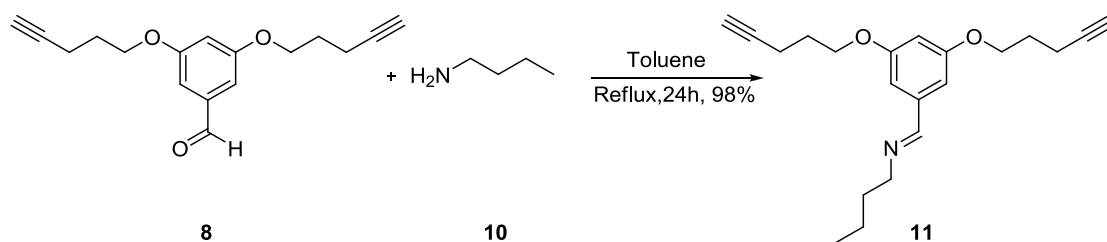


Figure 45 Scheme showing the synthesis of **11**.

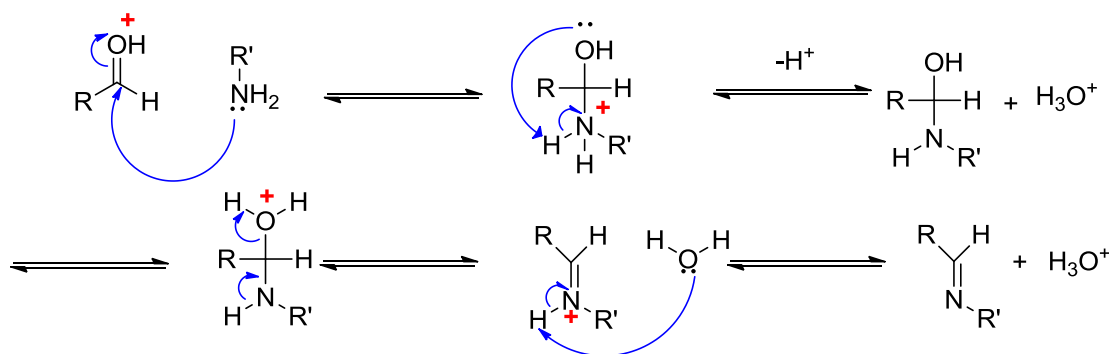


Figure 46 General mechanism of the imine bond formation.

Compound **11** was reacted with **12'** under *M1* and *M2* reaction conditions using anhydrous toluene. In the first case (*M1*), a mixture of the compounds previously mentioned and showed in **Figure 53** was obtained (as proven by ^1H NMR and m/z analysis). The m/z spectra seemed also to indicate a possible polymerisation of **12** and the TLC gave evidence of a number of different spots. It was also found that the imine in **11** was partially cleaved reforming the aldehyde which reacted with the amine moiety of **12**. The aldehyde protection with **10** did not lead to the 'click' reaction.

In the second case (*M2*) the combined analysis of the crude product showed no reaction between **11** and **12** after 48 hours even after heating.

As a result of the unsuccessful reaction pathway, **13** was not achieved and therefore it was not possible to proceed towards *step 4*. Another strategy has to be outlined in order to achieve the final product **14**.

4.2 Surface work

4.2.1 Introduction

In order to allow the double arms system (**Figure 22**) to switch it is necessary to create a mixed SAM. Therefore, this study was aimed at fabricating mixed SAMs which present an amine moiety as a terminal group, which is necessary for the imine bond formation with the aldehyde moiety of **5** and **14**, and an ‘inert’ terminal group such as a methyl group. In order to achieve a rigid and well packed SAM it was decided to use an aromatic backbone for two main reasons:

1) *Phenyl stacking*: the π - π stacking is an interaction between the electronic clouds of aromatic rings oriented face-to-face (**Figure 47**). Previous studies^{92,93} have proven that this orientation stabilises the monolayer and allows to obtain a rigid and well ordered SAM.

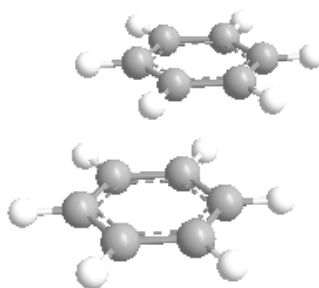


Figure 47 Schematic representation of two aromatic rings in the face to face orientation.

Although the available literature shows that poly-aromatic systems present stronger π - π stacking interactions (**Figure 48**), and therefore form more rigid monolayers, “single ring” molecules have been chosen in this work because of their commercial availability.



				
n	1	2	3	4
Stabilization (Kcal/mole)	-2.62	- 6.81	- 11.46	- 16.33

Figure 48 Schematic representation of the stabilisation energy for mono and poly aromatic systems.⁹³

2) *Molecular conductance charge*: our aim is to apply a voltage to the gold surface in order to allow the switching of the double arms moieties. In this regard, the high conductance of aromatic SAMs would be beneficial to achieve an efficient switching of the double arms.^{94,95}

The molecules selected for the fabrication of the mixed SAMs were 4-aminothiophenol (4-ATP) and 4-methylbenzenthionol (4-MBT) (**Figure 49**). This selection was based on preliminary concentration and kinetic studies carried out with the four thiol molecules shown in **Figure 50**. The studies performed and described in the next paragraphs were useful to understand which two molecules would have been more likely to form a binary SAM.

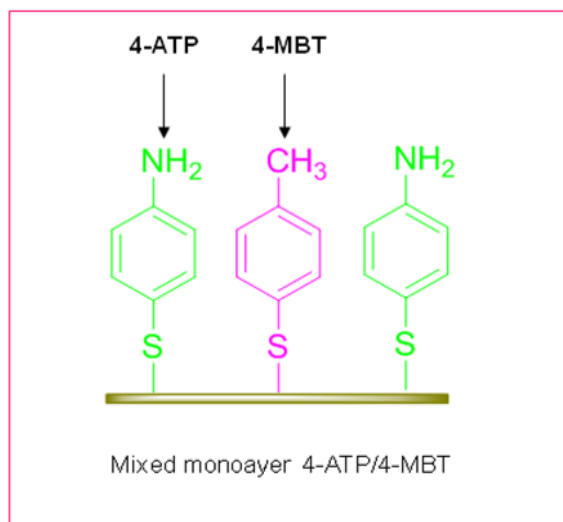


Figure 49 Schematic representation of a mixed monolayer of 4-ATP and 4-MBT.

4.2.2 Fabrication of single component SAMs

In order to determine the most suitable components for the mixed SAMs, four different pure monolayers (4-ATP, 4-MBT, 4-nitrobenzenethiol (4-NBT), and benzenethiol (BT)) were prepared and characterised (**Figure 50**).

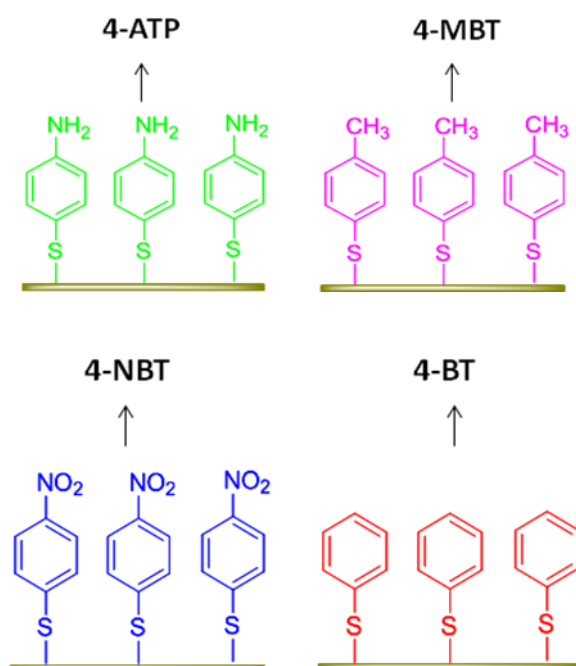


Figure 50 Schematic representation of a single monolayer of 4-ATP, 4-MBT, 4-NBT, and BT.

SAMs of 4-ATP, 4-MBT, 4-NBT and BT were fabricated by immersing freshly cleaned gold surfaces in ethanolic solutions of the above mentioned compounds for 24 hours, (the detailed procedure is described in the *Experimental* section 7.3.5.2). Concentration and kinetic studies were performed to determine the optimal concentration and time relationship to create a well packed monolayer. In particular the formation of SAMs was studied after 2, 4 and 24 hours at different concentrations. The SAMs obtained were characterised by contact angle, ellipsometry and XPS.

4.2.2.1 Concentration and kinetic studies

These studies were designed to understand:

- 1) The suitable concentration for SAMs formation.
- 2) The SAMs formation time.

4.2.2.1.1 Concentration study

In the concentration study only 4-ATP and BT have been investigated. Different solutions of 4-ATP and BT in ethanol were prepared at the following concentrations: 0.1 mM, 0.2 mM, 0.3 mM, 0.4 mM, and 0.5 mM (*Experimental* section 7.3.5.1). A clean gold substrate was immersed in each solution for 24 hours and the thickness of each substrate was measured by ellipsometry analysis. The data shown below are the average of five different measurements. All the ellipsometry results shown in this thesis are those found taking into account the thickness of the clean gold surface (~0.6 nm), which was measured by Atomic Force Microscopy (AFM). Topographic images of the gold surface before and after the cleaning treatment are shown below (**Figure 51**).

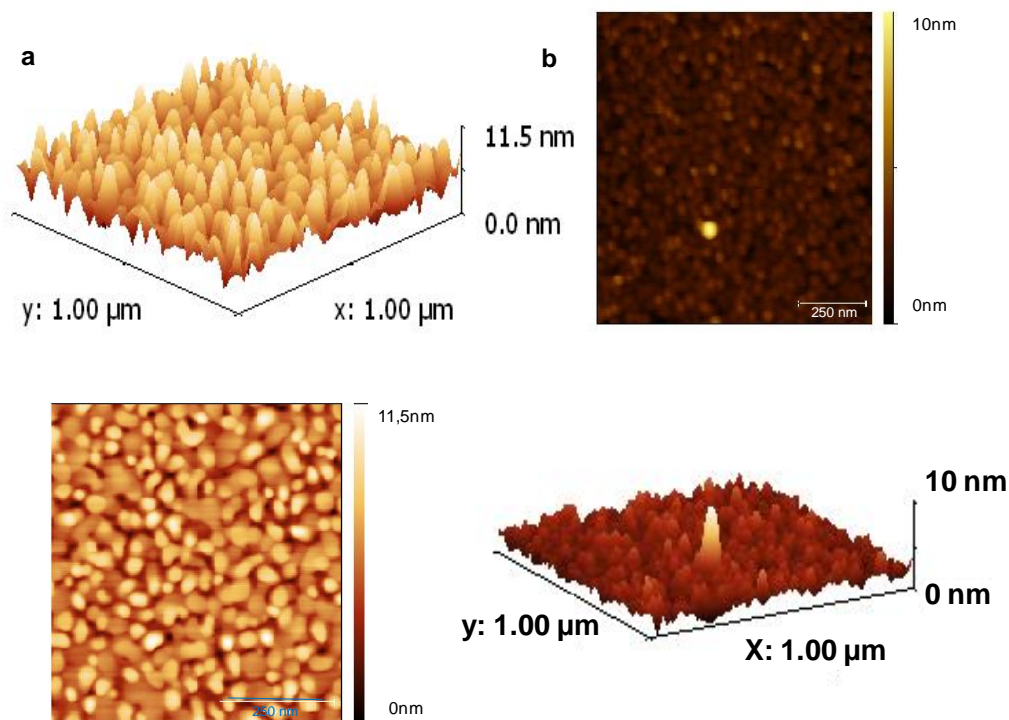


Figure 51 AFM topographic 2D and 3D images of the gold surface used in the fabrication of SAMs in our work before (a) and after (b) the cleaning procedure with piranha solution.

The difference in concentration did not substantially affect the BT-SAMs thickness while marked changes were observed in the 4-ATP-SAMs thickness (**Figure 52**).

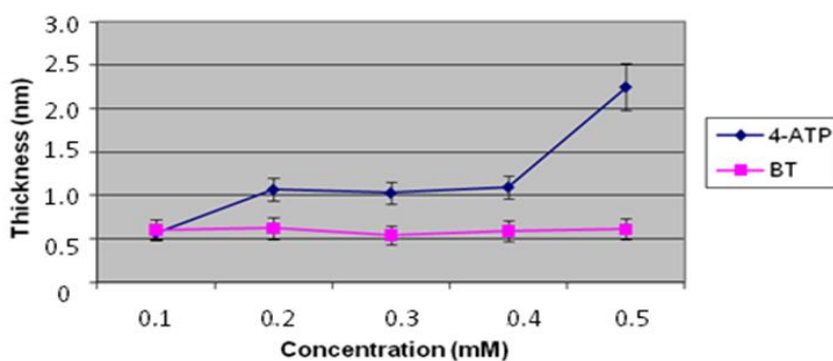


Figure 52 Ellipsometry graph showing the relationship between concentration and thickness for 4-ATP-SAMs and BT-SAMs.

The expected thickness for 4-ATP and BT SAMs was ~0.6 nm. This value has been only found for a 4-ATP concentration of 0.1 mM while for higher concentrations there was an

increase in the thickness values. This result could be explained taking into account the following processes:

1) The absorption of 4-ATP on gold could happen: (i) Through the interaction between the sulphur and the gold atoms, (ii) Through the interaction between the electronic cloud of the aromatic ring and the gold atom (iii) Through the interaction between the nitrogen and the gold atoms (**Figure 53**). The alignment of the 4-ATP molecule due to (ii) and (iii) along with a high concentration of surfactant could induce the formation of a multilayer of molecules kept together by π - π stacking interactions (a) (**Figure 54b**) or the formation of disulfide molecules (b) (**Figure 54a**).⁸⁸

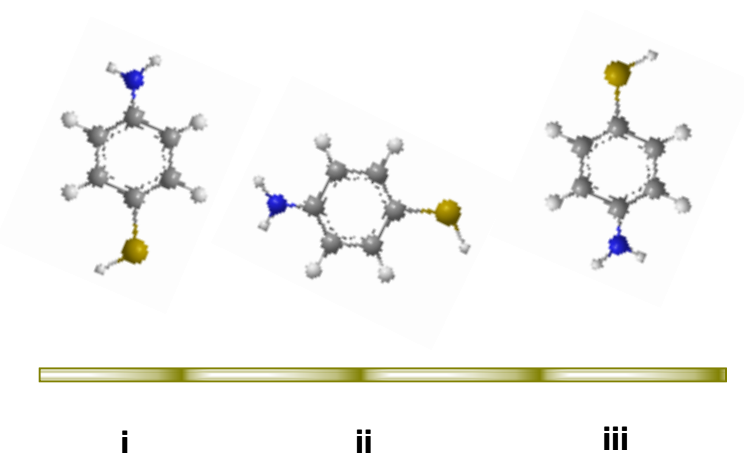


Figure 53 Schematic of the different interaction occurring between 4-ATP and a gold surface.

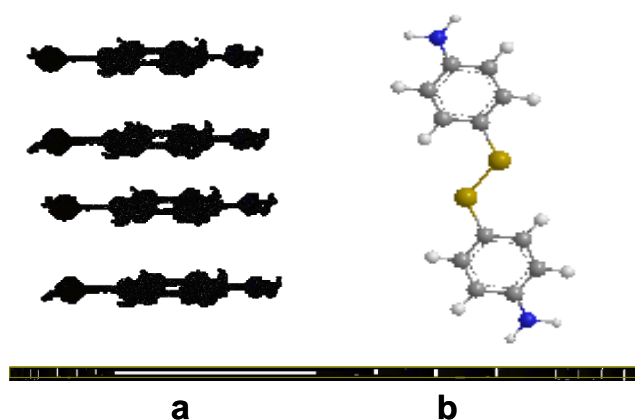


Figure 54 a) A multilayer of 4-ATP molecules. b) A disulfide bond formed between two 4-ATP molecules.

Furthermore, it was found that the average thickness for 4-ATP SAMs (0.55 nm at 0.1 mM) was slightly lower compared to those of BT (0.61 at 0.1 mM). This fact can be due to the solvent influence as shown in **Figure 55**. Recent studies^{96,97} have explained the solvent effects for 4-ATP and BT and other benzenethiol derivatives. 4-ATP has an amino end group which can form hydrogen bonds with polar molecules such as dinitrotoluene (DNT) (**Figure 55a**) and can also form strong π interactions with non polar solvents like toluene (**Figure 55b**). In both cases the result is a compressive stress of the molecules on the gold film and therefore a decrease in the thickness of the monolayer. BT does not present any dipole interaction in polar solvents while it presents both tensile and compressive stress in toluene because of the strong π - π interactions (**Figure 55c-d**).

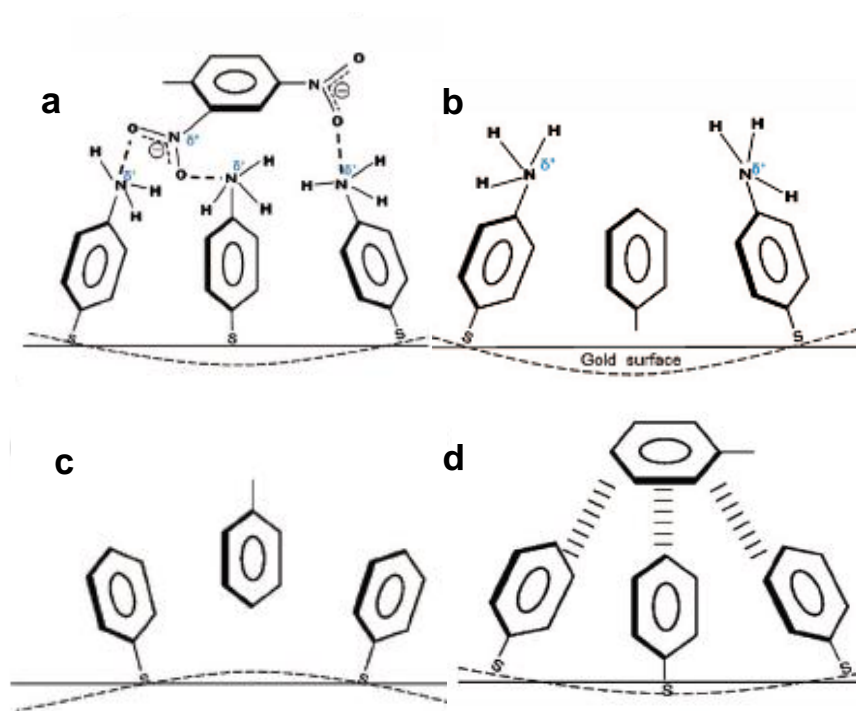


Figure 55 Diagram of possible molecular interactions for a) 4-ATP in dinitrotoluene (DNT), b) 4-ATP in toluene, c) BT in toluene (tensile stress), d) BT in toluene (compressive stress)⁹⁷

In the same study, it was also found that the behaviour of 4-MBT in both polar and non-polar solvents and interestingly, for this thiol molecule, no stress was observed (**Figure 56a-b**).

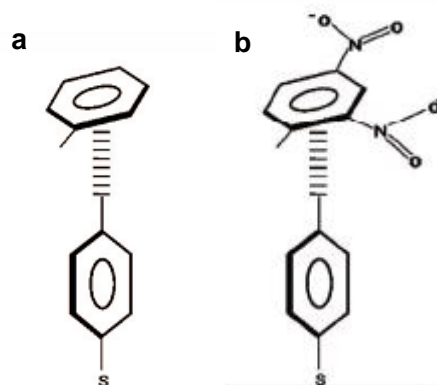


Figure 56 Diagram of possible molecular interaction for a) 4-MBT in toluene b) 4-MBT in DNT.⁹⁷

4.2.2.1.2 Kinetic study

The kinetic studies were performed on the four molecules (4-ATP, BT, 4-MBT, 4-NBT) in order to determine the time of formation of a well packed SAM. The different behaviour of the four molecules when forming a monolayer was also useful to select the two best components to form binary mixed SAMs. SAMs of each compound were prepared at the concentration of 0.1 mM and characterised by contact angle and ellipsometry after 2h, 4h and 24h.

Contact angle

SAMs of the 4-ATP, 4-MBT, 4-NBT and BT were formed (7.3.5.2). The contact angle values obtained for the different monolayers are in agreement with the literature data (**Table 1**).^{98,99,100}

Table 1. Experimental and literature advancing contact angle values for 4-ATP, 4-MBT, 4-NBT and BT after 24 hours of immersion in the surfactant solution.

<i>Contact angle</i>	<i>4-ATP</i>	<i>4-MBT</i>	<i>4-NBT</i>	<i>BT</i>
<i>Experimental advancing values</i>	58°±3	107°±5	63°±3	97°±4
<i>Literature advancing values</i> ^{98,99,100}	55°	110°	64°	92.3°

Figure 57 shows the advancing and receding contact angle values obtained for the four compounds after SAM formation for 2, 4 and 24 hours. The data reported are an average of five different measurements on each surface. SAMs formed from 4-ATP and 4-NBT are more hydrophilic than SAMs formed from 4-MBT and BT; this is due to the presence of polar terminal groups in 4-ATP and 4-NBT. Furthermore, the values found for 4-NBT are higher compared to those found for 4-ATP since the latter presents a more hydrophilic functional group. Contact angle hysteresis ($\theta_a - \theta_r$) is often indicative of disorder and possible reorientation of molecules within SAMs. SAMs of BT and 4-ATP present a higher contact angle hysteresis compared with 4-MBT and 4-NBT. However, the slight decrease in hysteresis over time indicates an improvement in the molecular ordering in all the SAMs formed. **Figure 58** shows the average contact angle (θ_a and θ_r) of the four compounds analysed after SAM formation for 24 hours.

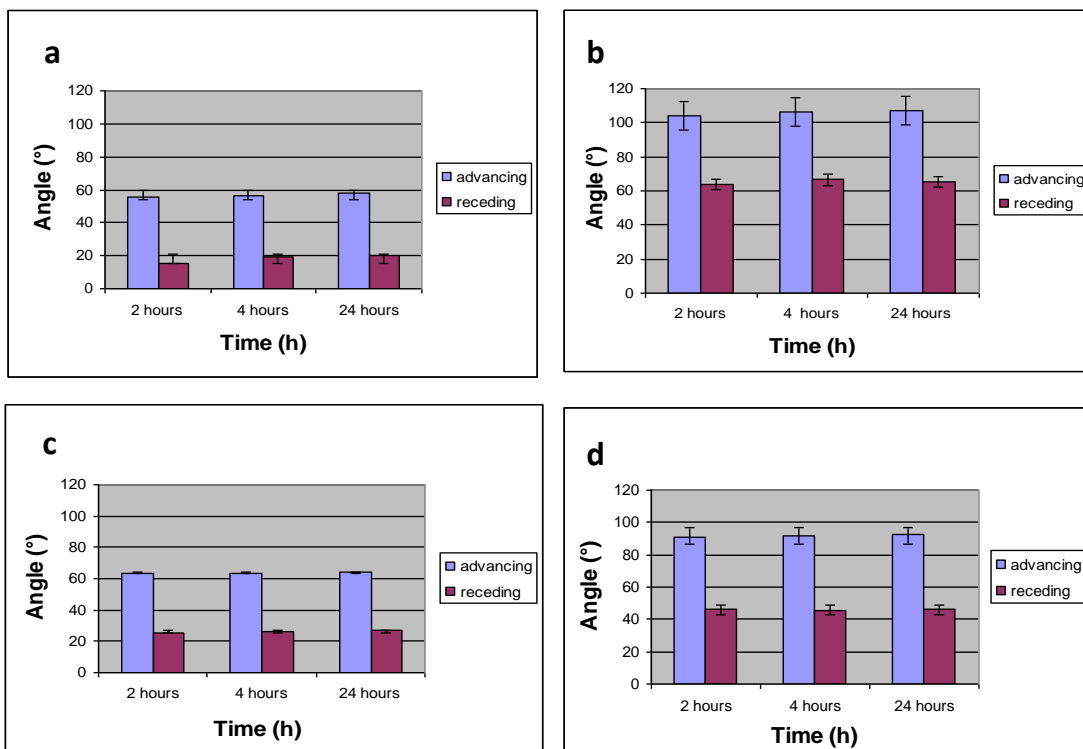


Figure 57 Ellipsometry graphs showing the trend of the advancing and receding contact angle values over time for a) 4-NBT, b) BT, c) 4-ATP and d) 4-MBT.

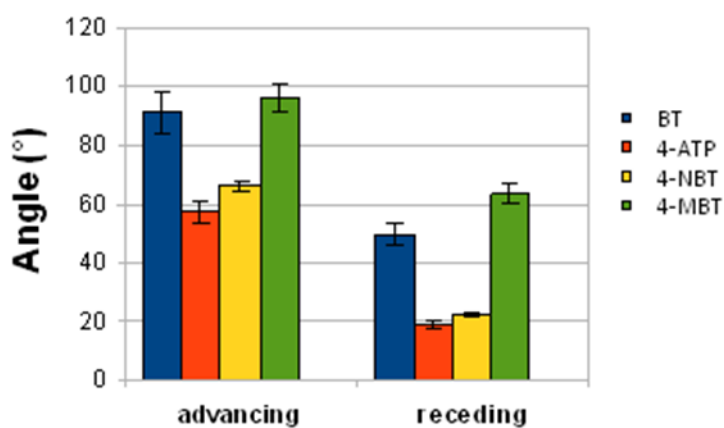


Figure 58 Contact angle Graph showing the average advancing and receding contact angles for BT, 4-ATP, 4-NBT and 4-MBT.

From the analysis of the results obtained through the contact angle studies the suitable compounds for the formation of the binary mixed SAMs were selected. The presence of 4-ATP on the surface is fundamental because of the further interaction that will be attempted

on the amino group. 4-MBT was selected as a ‘spacer’ molecule because it is not as toxic as BT is, it has a lower contact angle hysteresis compared to 4-NBT and BT and it has very different contact angle values from 4-ATP which could provide a simpler contact angle analysis of the mixed 4-ATP/4-MBT SAMs. The following ellipsometry and XPS studies will be assessed only on the surfaces formed from these two compounds.

Ellipsometry

Figure 59 lists the thicknesses for SAMs from 4-ATP and 4-MBT (as described in the *Experimental* section 7.3.5.2) at different times of formation. An estimated thickness for each SAM was obtained by calculating the length of the molecular structures of each compound using Chem3D Ultra (v 11.0, CambridgeSoft) software. The values reported in **Table 2** are an average of five different measurements on three surfaces. The theoretical values were reported to support the results achieved.

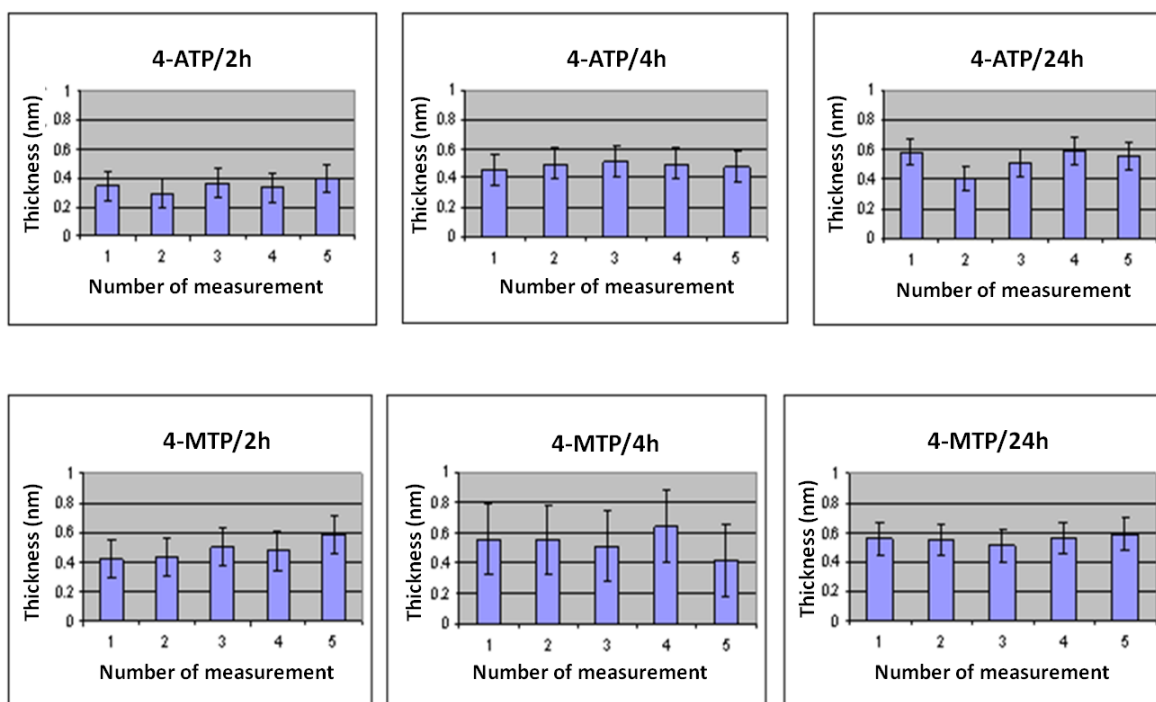


Figure 59 Graphs showing the ellipsometry values obtained from the study of 4-ATP and 4-MBT SAMs analysed after 2, 4 and 24 hours.

Table 2 Table showing the average ellipsometry values for 4-ATP SAMs and 4-MBT SAMs and the theoretical molecular lengths of 4-ATP and 4-MBT.

<i>Ellipsometry</i>	<i>4-ATP</i>	<i>4-MBT</i>
	<i>24 hours SAM formation</i>	<i>24 hours SAM formation</i>
<i>Experimental value</i>	0.52±0.17	0.58±0.10
<i>Theoretical value</i>	0.64	0.61

The results showed that the measured thicknesses of 4-ATP and 4-MBT SAMs are in agreement with the available literature.¹⁰¹

The results obtained also showed that both SAMs are almost formed after 4 hours. In particular, no substantial changes in thickness were observed for 4-MBT SAMs after being formed for 2, 4 and 24 hours while the formation of 4-ATP SAMs seemed to be slower. This could be due to the major effect of the solvent polarity on 4-ATP, but also to its diminished ability to form a stable rigid film as previously highlighted in the contact angle studies.

XPS

For the purpose of this study, the elements we were most interested in analysing were the sulphur and nitrogen. The former was important to confirm the actual binding of the compounds to the gold surface while the latter would have gave us the certainty of the presence of 4-ATP. However, carbon and oxygen binding energy were also measured in order to better understand the monolayer composition. **Figure 60** shows the S2p spectra

for a clean gold surface and 4-ATP SAMs formed after 24 hours of immersion (*Experimental* section 7.3.5.2). The sulphur XPS spectrum for 4-ATP SAMs revealed the characteristic S2p_{3/2} and S2p_{1/2} doublet with components at 161.21 eV and 163.27 eV, indicative of a thiolate bound to a gold surface.^{102,103} The peaks obtained clearly show that formation of an Au-S bond has taken place, indicating the formation of the desired SAMs. The chemisorptions of 4-MBT on the gold surface was also confirmed by XPS, which showed a sulphur doublet at 161.29 eV and 163.27 eV.¹⁰⁴

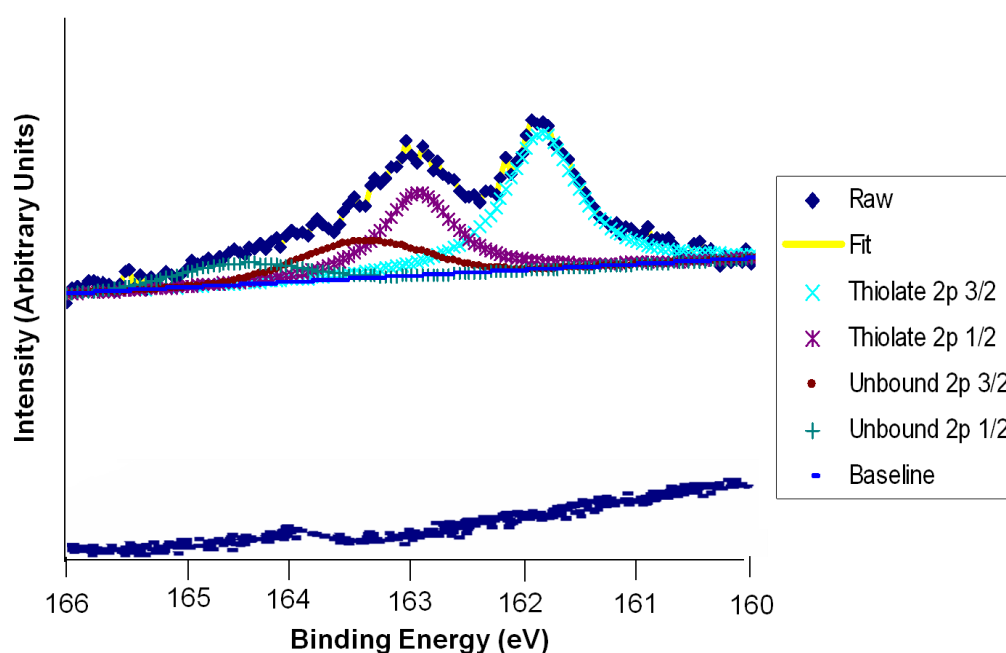


Figure 60 XPS data for sulphur peaks of a) 4-ATP SAMs and b) Clean gold.

As expected XPS analysis of the nitrogen region on both 4-ATP and 4-MBT SAMs revealed as the presence of nitrogen only in the 4-ATP SAMs (**Figure 61**) with a binding energy value of 399.44 eV.¹⁰⁵

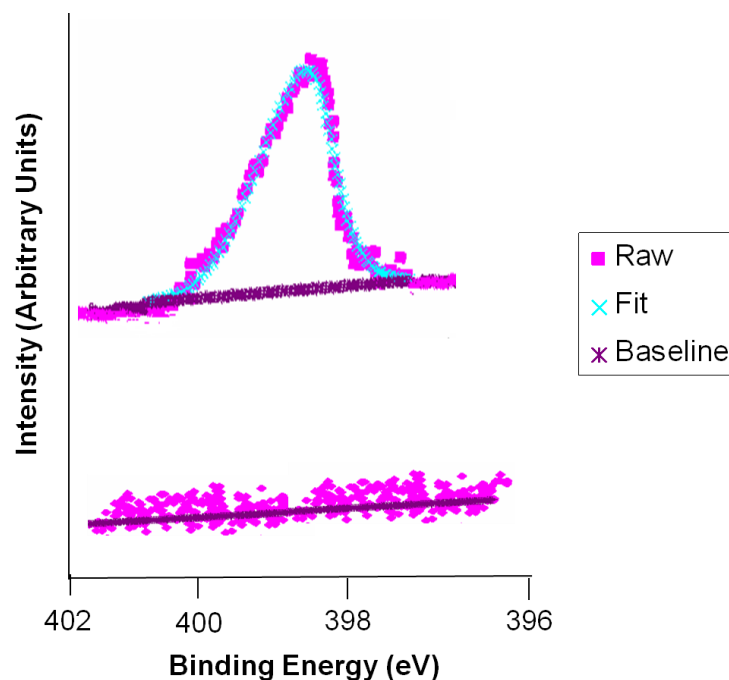


Figure 61 XPS spectra of the N1s peak region of a) 4-ATP SAMs and b) 4-MBT SAMs.

4.2.3 Fabrication of binary mixed SAMs

Mixed SAMs of 4-ATP and 4-MBT were fabricated at the following molar ratios: 4-ATP/4-MBT (1:1) and 4-ATP/4-MBT (2:1) in ethanol. The overall concentration of the compounds in the ethanol solution was 0.1 mM. The two molar ratios were chosen to understand the influence of 4-MBT on the mixed SAMs formation, since it was shown in paragraph 4.2.2.1.2 to self-assemble on the surface faster than 4-ATP. The SAMs obtained were analysed by contact angle, ellipsometry and XPS.

Contact angle

Mixed SAMs of 4-ATP and 4-MBT at a solution ratio of (2:1) 4-ATP/4-MBT were formed (*Experimental* section 7.3.5.3) and the advancing and receding contact angles were

measured. **Table 3** shows the contact angle values obtained for the mixed monolayers as well as the two single-component SAMs.

Table 3 Contact angle values obtained from the study of mixed SAMs of 4-ATP and 4-MBT at a solution ratio of 1:1, 2:1 compared with the single component SAMs.

Contact angle	4-ATP/4-MBT	4-ATP/4-MBT	4-ATP	4-MBT
	(1:1)	(2:1)		
<i>Advancing</i>	103°±4	91°±3	58°±2	107°±3
<i>Receding</i>	66°±4	56°±3	19°±2	63°±3

As we can see from the results achieved for 4-ATP/4-MBT (1:1) SAMs, there were no substantial changes in the contact angle values compared to that of 4-MBT SAMs. The results obtained from the analysis of the 4-ATP/4-MBT (2:1) SAMs showed a drastic decrease of the contact angle values. This results confirmed what was expected; in fact the alignment of 4-ATP on the gold surface in ethanol is slower with respect to 4-MBT. The higher concentration of 4-ATP in 4-ATP/4-MBT (2:1) SAMs, balances this effect allowing the formation of a monolayer in which the two compounds are both present.

Ellipsometry

Figure 62 shows the thicknesses for the double components SAMs formed by 4-ATP/4-MBT (1:1) and 4-ATP/4-MBT (2:1) (*Experimental* section 7.3.5.3). The values reported in **Table 4** are an average of six different measurements made on the same surface. The single component monolayer values are also shown for comparison purposes.

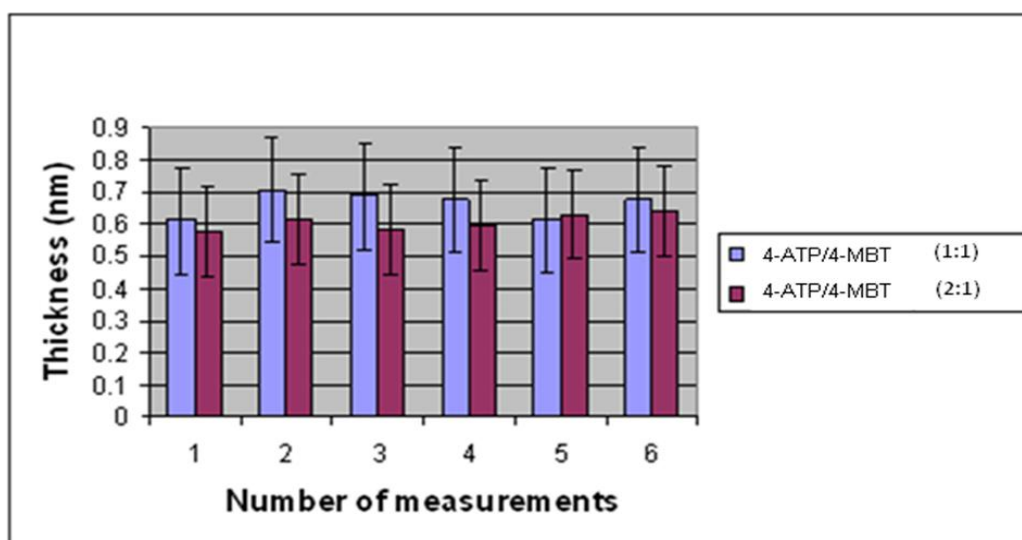


Figure 62 Ellipsometry values obtained from the study of 4-ATP/4-MBT (1:1) SAMs and 4-ATP/4-MBT (2:1) SAMs analysed after 24 hours.

Table 4 Table showing the average thickness of 4-ATP/4-MBT (1:1) SAMs, 4-ATP/4-MBT (2:1) SAMs, 4-ATP SAMs, 4-MBT SAMs.

<i>Thickness (nm)</i>	<i>4-ATP/4-MBT (1:1)</i>	<i>4-ATP/4-MBT (2:1)</i>	<i>4-ATP</i>	<i>4-MBT</i>
<i>Average value</i>	0.66±0.17	0.61±0.14	0.53±0.17	0.59±0.10

The average thickness found for the mixed 4-ATP/4-MBT (1:1) SAMs was slightly higher compared with that of 4-ATP/4-MBT (2:1) SAMs. This result could be due to the prevalence of 4-MBT on the surface which present a higher thickness. However, taken into account that the thickness error values, for 4-ATP and 4-MBT, are very similar it was not possible to gain a consistent difference between the two SAMs from the ellipsometry studies on these surfaces.

XPS

4-ATP/4-MBT (2:1) SAMs were also analysed because of the contact angle results achieved (section 4.2.3) obtained which suggested a similar ratio of 4-ATP and 4-MBT on the surface. The sulphur binding energy for 4-ATP/4-MBT (2:1) SAMs formed after 24 hours of immersion in ethanol (*Experimental* section 7.3.5.3) was detected. The sulphur XPS spectrum revealed the characteristic S2p3/2 and S2p1/2 doublet with components at 162.04 eV and 163.26 eV, indicative of a thiolate bound to a gold surface.^{102,103} When compared to the values obtained for the 4-ATP SAM, as expected the mixed SAMs show a decrease in the nitrogen peak (**Figure 63**) and an increase in the carbon peak.

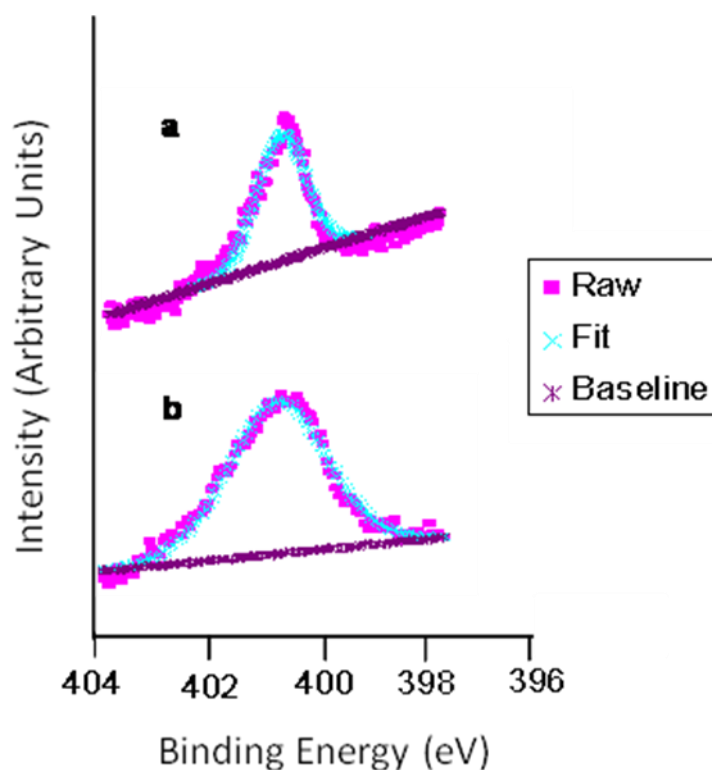


Figure 63 XPS data for the nitrogen peaks of a) 4-ATP/4-MBT(70-30%) SAMs and b) 4-ATP SAMs.

The carbon XPS spectrum revealed more carbon environments, compared to those of 4-ATP SAMs, which are due to the benzene ring, to the $-C-NH_2$ bond and to the $-CH_3$ group

with the respective binding energy values: 284.92 (C₆H₅), 283.93 (-CH₃), 286.27 (-C-NH₂), (Figure 64).¹⁰⁶

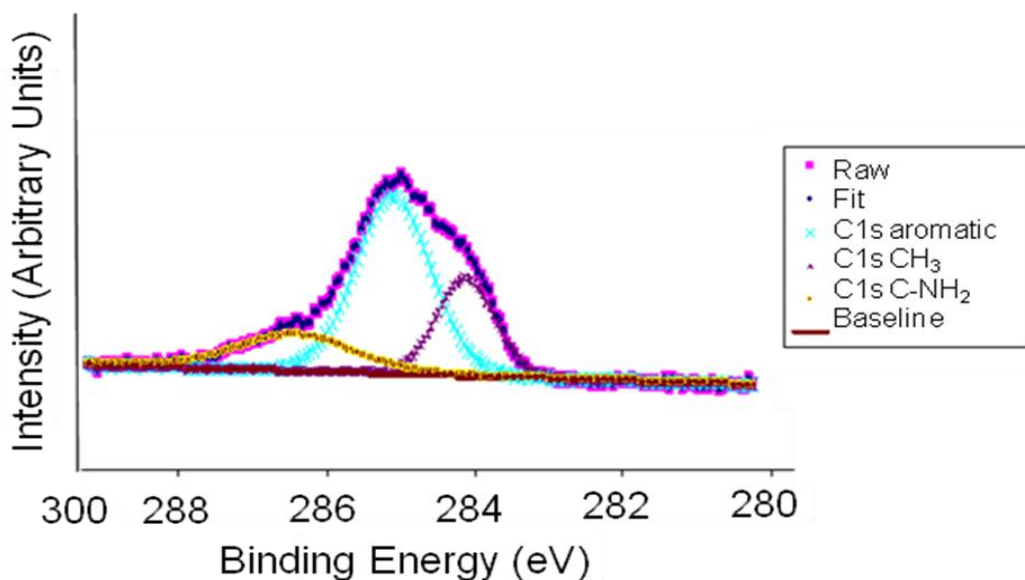


Figure 64 XPS data for carbon peak of 4-ATP/4-MBT (2:1).

4.2.4 Reactions on SAMs: imine bond formation

An imine bond between the amine moieties of a 4-ATP SAM and the aldehyde moieties of some ‘test’ molecules was attempted at the surface. This study was performed to check the feasibility and the stability of this link on the surface in order to successively perform the reaction using molecule **5** and **14** (Figure 25, 30). The model compounds used were the following: 4-hydroxybenzaldehyde (4-HBA), 4-bromobenzaldehyde (4-BBA), 4-trifluorobenzaldehyde (4-TBA). The choice of these 3 compounds, presenting different solubilities due to their different substituents in the *para* position of the aromatic ring, was made to study the influence of different solvents in the achievement of the imine bond. Furthermore, as will be discussed below, certain functional groups (i.e.-CF₃) show a very particular signal in the XPS analysis, which would help to better interpret the data.

Experimentally, 4-ATP SAMs (*Experimental* section 7.3.5.4) were immersed in 10 ml anhydrous 0.1 mM ethanolic solution of the benzaldehyde derivative (4-HBA, 4-BBA, 4-TBA) and trimethylorthoformate (volume ratio = 1:1) for 48 hours. Trimethylorthoformate was added as dehydrating agent and triethylamine (TEA) was further added as a base to neutralise the formation of formic acid.¹⁰⁵ Since the imine bond hydrolyses in presence of water, the water contact angle was not performed and the SAMs fabricated were analysed by ellipsometry and XPS.

Ellipsometry

Thickness measurements performed after 24 hours immersion did not lead to the expected results which would have been ~1 nm (**Table 5**). The thickness obtained was much higher than the theoretical value and this result may lie on the precipitation of 4-BBA and 4-TBA on the surface because of their low solubility in ethanol. However the experiment was repeated in anhydrous toluene and the thickness measured after 24 hours immersion was still high (**Table 5**).

Table 5 Average thickness values for 4-ATP SAMs, 4-HBA SAMs, 4-BBA SAMs and 4-TBA SAMs in ethanol and in toluene.

Thickness (nm)	<i>4-ATP SAMs</i>	<i>4-HBA SAMs</i>	<i>4-BBA SAMs</i>	<i>4-TBA SAMs</i>
<i>Experimental value in Ethanol</i>	0.52±0.17	3.46±0.25	2.88±0.29	3.27±0.24
<i>Experimental value in toluene</i>	0.62±0.14	3.25±0.22	3.11±0.21	3.23±0.19
<i>Theoretical value</i>	0.640	1.214	1.255	1.216

XPS

The XPS analysis confirmed that the imine bond was not formed. The oxygen peak did not increase in its intensity due to the presence of the hydroxyl group in the 4-HBA SAMs. The peaks of the bromine and fluorine were not observed suggesting the absence of the respective compounds 4-BBA and 4-TBA on the surface. Nevertheless, it was difficult to analyse the XPS data obtained from 4-HBA and 4-BBA modified surfaces. Even though the only source of oxygen would have been the 4-HBA, it has been proven that the atmospheric oxygen contaminates the gold surface. In this regard, an oxygen peak was observed in all samples analysed. With respect to 4-BBA, being the XPS source an aluminium source and the aluminium peak very close to the bromide peak, the data obtained for 4-BBA modified surfaces was inconclusive. For these reasons the control study, which will be discussed in the next section, will be based only on 4-TBA modified surfaces which present the fluorine peak.

4.3 Imine bond: control study

Since the imine bond formation was not successful in the previous described strategy, a different synthetic route was investigated. It is known from the literature that the S-Au bond is stronger than the S-S bond therefore the disulfide bond can be broken onto a gold surface as shown in **Figure 65**. It was decided to synthesise molecule **18**, break the S-S bond upon self-assembly on the gold surface to obtain a **18'** SAMs.¹⁰⁷ The monolayer obtained was analysed by ellipsometry and XPS and compared with the previous results discussed in section 4.2.3.

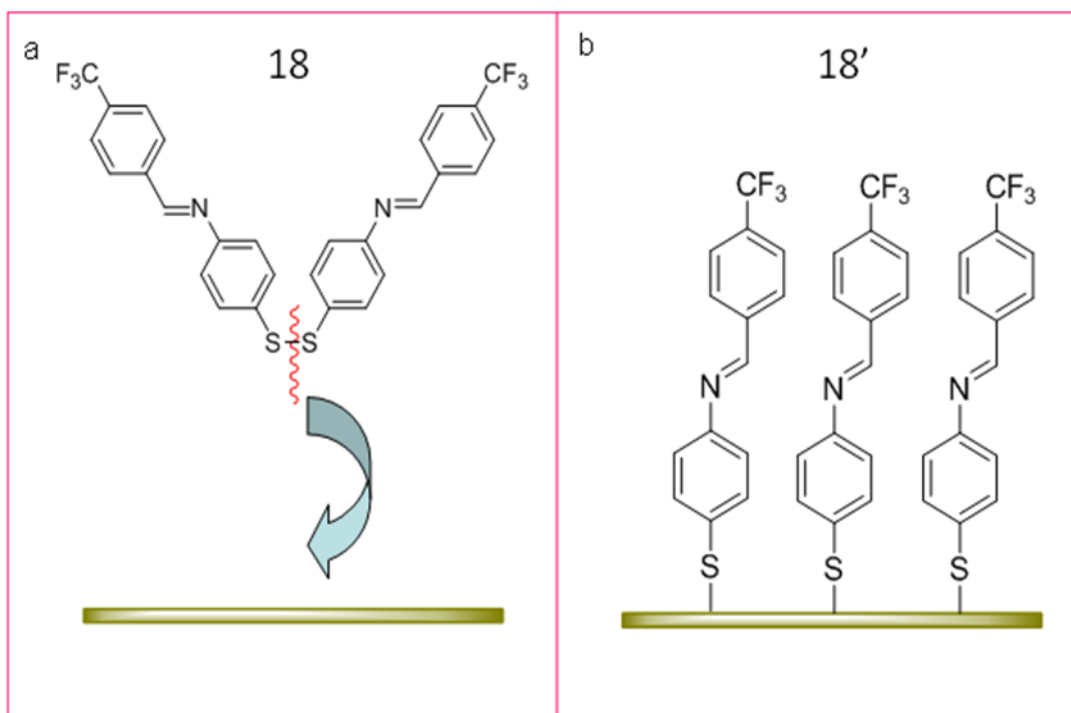


Figure 65 Breaking of the disulfide bond upon self-assembly on the gold surface.

4.3.1 Synthesis of the disulfide **18**

The synthesis of **18** was conducted successfully in two steps (**Figure 66**). Each step is discussed below, with their respective mechanisms.

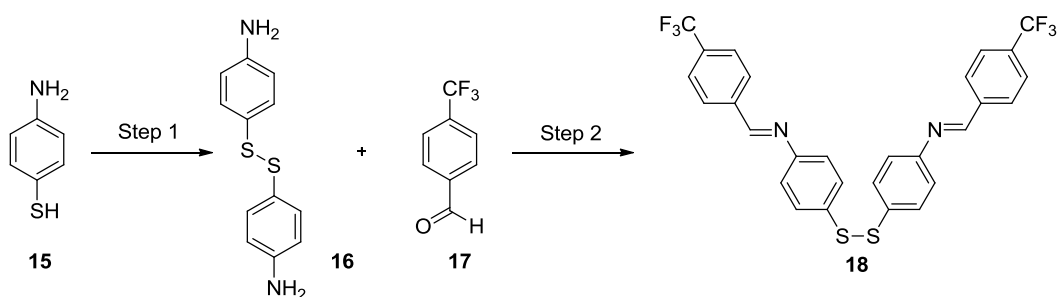


Figure 66 Synthesis pathway followed to achieve **18**.

Step 1¹⁰⁸

The formation of **16** was achieved by employing I₂ as an oxidant of the sulfhydryl (-SH) groups of 4-ATP as shown in **Figure 67**.

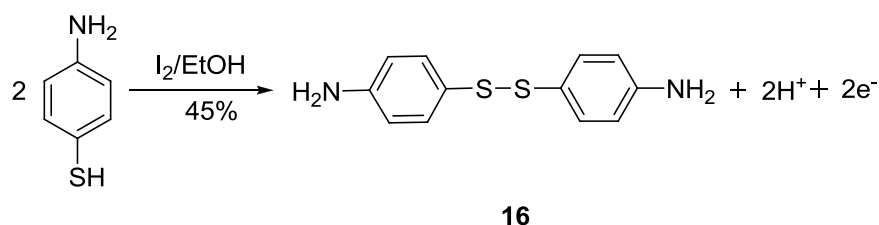


Figure 67 Synthesis pathway followed to achieve **16**.

This reaction is thought to proceed *via* sulfenic acid intermediates (**Figure 68**).

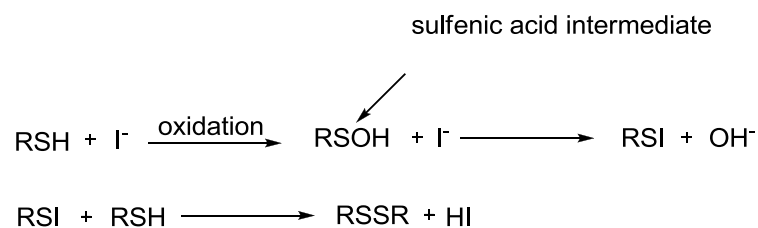


Figure 68 General mechanism of oxidation of a sulfhydryl group with the production of sulfenic acid intermediates.

Step 2

The formation of **18** was achieved through an imine bond formation between the amine moieties of **16** and the aldehyde moiety of **17** (**Figure 69**) of which mechanism has been described previously in section 4.1.2.4.

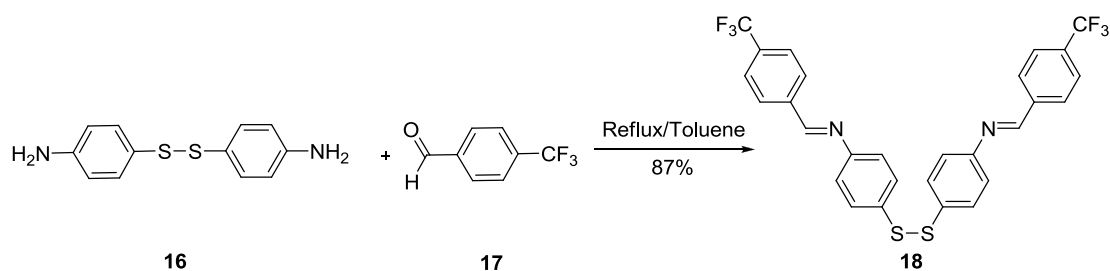


Figure 69 Synthesis pathway followed to achieve **18**.

4.3.2 Surface work

Clean gold substrates were immersed in a 0.1 mM solution of **18** in anhydrous toluene for 24 hours (*Experimental* section 7.3.5.6). Anhydrous toluene was used as a solvent in order to avoid the cleavage of the imine bond. Following an analogous procedure (*Experimental* section 7.3.5.5), clean gold substrates were immersed in a 0.1 mM solution of **16** in anhydrous toluene for 24 hours. After SAM formation, the surfaces were analysed by ellipsometry and XPS.

Ellipsometry

Table 6 shows the thicknesses obtained for 4-ATP SAMs, 4-TBA SAMs, **16'** SAMs and **18'** SAMs as well as the theoretical values calculated using Chem3D Ultra (v 11.0, CambridgeSoft) software (**Figure 70**).

Table 6 Average thickness values for 4-ATP SAMs, 4-TBA SAMs, 16' SAMs and 18' SAMs.

Thickness (nm)	4-ATP SAMs	4-TBA SAMs	16' SAMs	18' SAMs
Experimental value	0.62±0.14	3.23±0.19	0.61±0.20	1.35±0.26
Theoretical value	0.640	1.216	0.640	1.216

The results obtained demonstrated the successful formation of 16' SAMs and 18' SAMs.

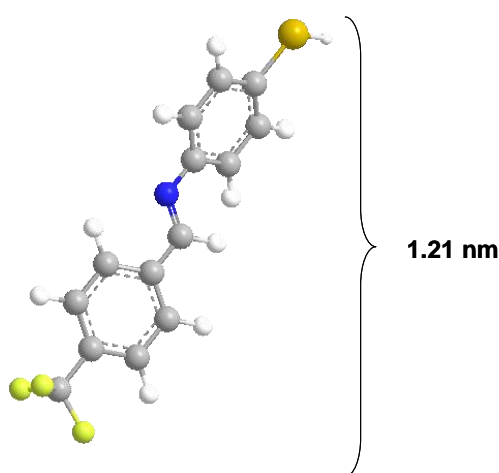


Figure 70 Theoretical thickness value calculated with Chem3D Ultra considering a tilt angle of 15°.

XPS

For the purpose of this study, the elements we were most interested in analysing were sulphur and fluorine. The former was important to confirm the actual binding of the compounds to the gold surface while the latter would give us the certainty of the presence of the imine bond formation and therefore the presence of 4-TBA. However, also the carbon and nitrogen peaks were analysed in order to compare their binding energy with the 4-ATP SAMs. **Figure 71** shows the sulphur binding energy spectra for 18' SAMs and 16' SAMs after 24 hours of immersion. The sulphur XPS spectrum revealed the characteristic

S2p_{3/2} and S2p_{1/2} doublet with components at 161.9 eV and 163.7eV, indicative of a thiolate bound to a gold surface and formation of the desired SAMs.^{102,103}

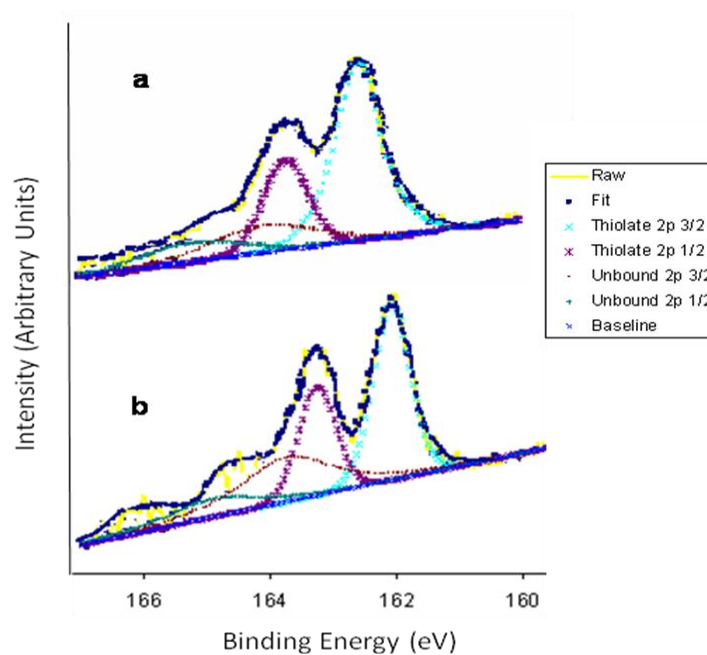


Figure 71 XPS spectra of the 2p peak regions of a) 16' SAMs and b) 18' SAMs.

The fluorine peak shown in **Figure 72** was detected as expected in the 18' SAMs while it was not present in the 16' SAMs. The binding energy found for the F 1s peak was 688.04 eV in accordance with the literature value (688 eV).¹⁰⁹

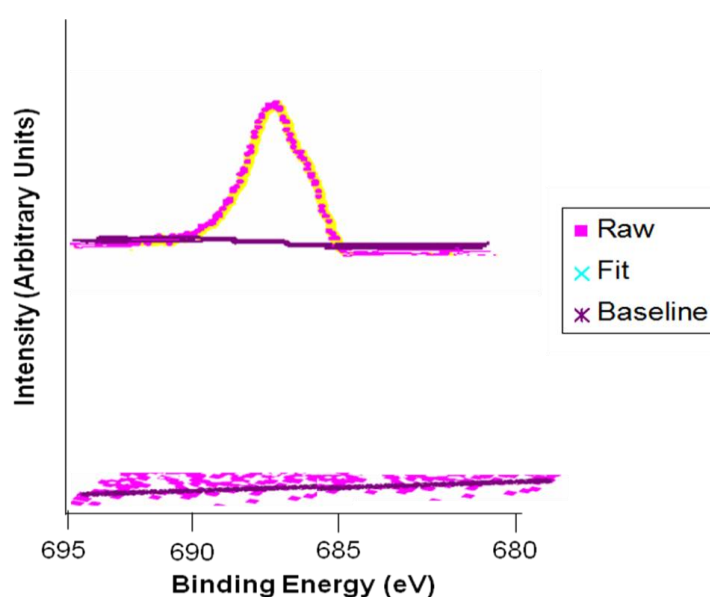


Figure 72 XPS spectra of the F 1s peak regions of (a) 18' SAMs and (b) 16' SAMs.

Building on the successful formation of the **18'** SAMs, synthesis of disulfide **19** was attempted, (**Figure 73**) but as suggested from the ^1H NMR analysis, a mixture of the starting material and **19** was obtained. Purification by HPLC of the mixture was not successful probably because of the instability of the imine bond and the scarce yield.

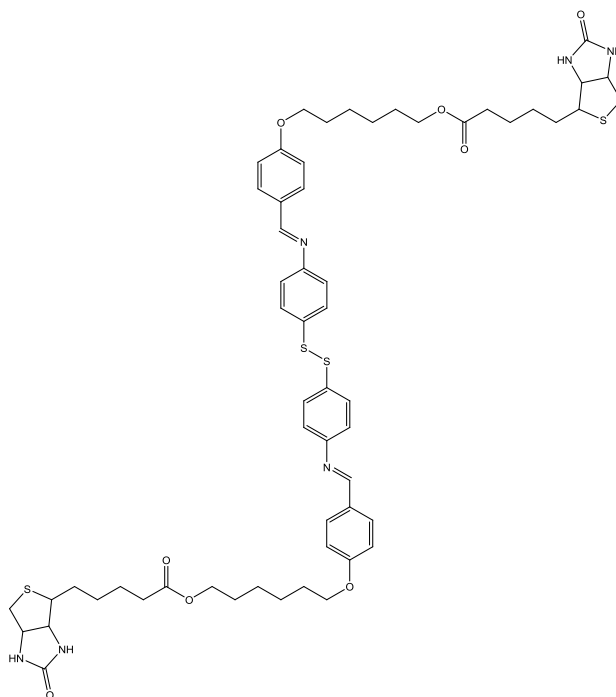


Figure 73 Chemical structure of **19**.

For these reasons it was not possible to proceed with the formation of SAMs of **19'** on the gold surfaces.

5.0 CONCLUSION

Objective 1:

a) Synthesis of compound **5** (Figure 74a) was achieved successfully over two step synthesis. Each step provided relatively good yields when compared to that obtained in the literature. The success of these two steps allowed the synthesis of the disulfide **19** (Figure 73) to be performed but this led to an inseparable mixture of the left over starting material and the product as was highlighted by $^1\text{H-NMR}$ analysis.

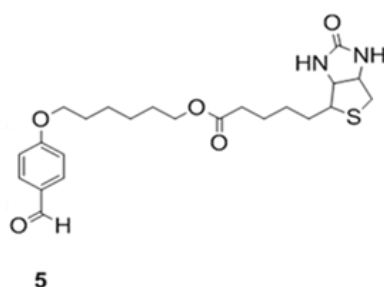


Figure 74 Chemical structure of compound **5**.

b) The route towards the synthesis of compound **14** was only partially completed (Figure 75). The unsuccessful attempts of ‘click’ chemistry between **8**, 4-AA and 4-MA were analysed and discussed.

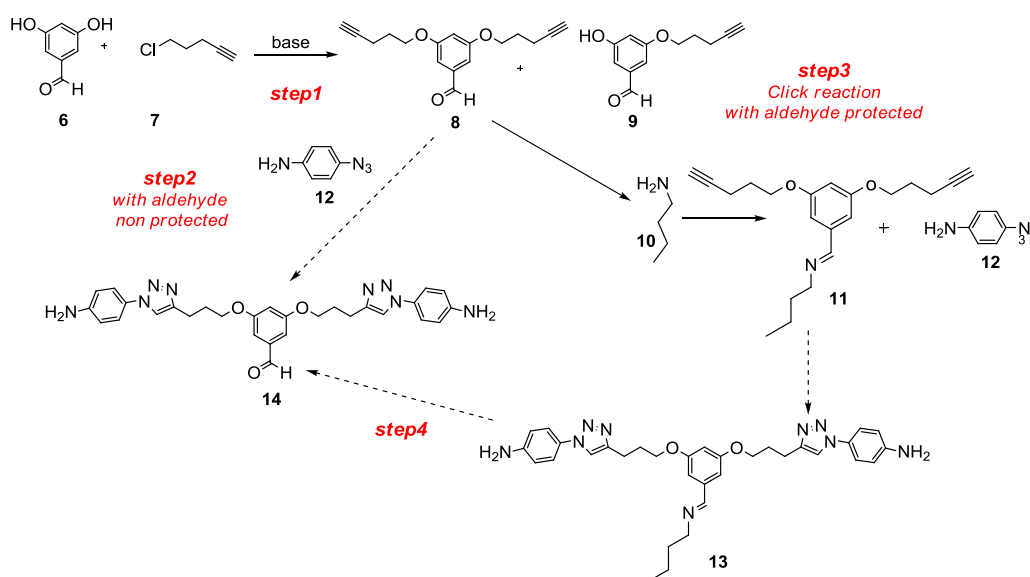


Figure 75 Synthetic pathway followed to achieve **14**.

Objective 2:

Formation of double component 4-ATP/4-MBT monolayers was achieved successfully (**Figure 76**). Due to the different kinetic adsorption of the two surfactants, two different ratios (1:1 and 2:1) were used in order to understand the correspondence between the concentration in solution and the effective adsorption on the surface. The fabricated SAMs were analysed by contact angle, ellipsometry and XPS.

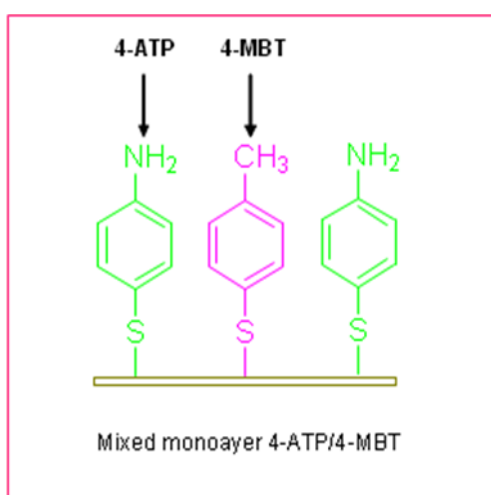


Figure 76 Schematic representation of a mixed monolayer of 4-ATP and 4-MBT.

Objective 3:

Imine bond on 4-ATP SAMs was attempted using three different benzaldehyde derivatives (4-HBA, 4-BBA, 4-TBA) (**Figure 77**). The reaction on the surface was not successful as proven by both ellipsometry and XPS analysis performed.

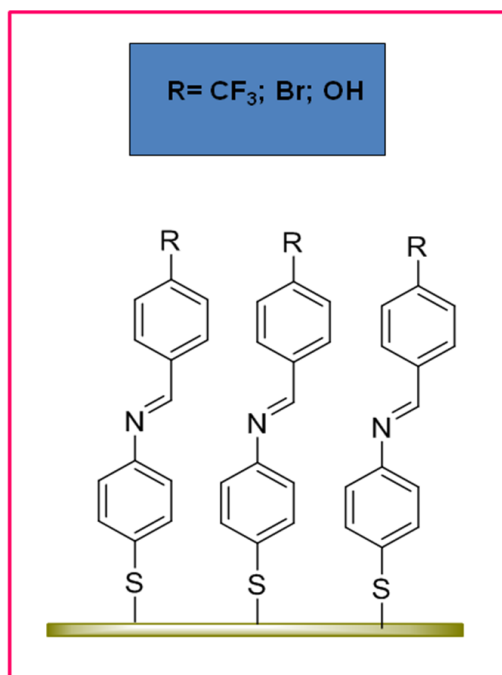


Figure 77 Schematic representation of an imine monolayer with highlighted the different benzaldehyde derivatives used.

Objective 4:

As a control study, disulfide **16** and **18**, imine bond contained, were synthesised. **16'** and **18'** SAMs were fabricated and analysed by ellipsometry and XPS. The results confirmed the obtainment of **18'** SAM and **16'** SAMs as a consequence of the disulfide bond rupture on the gold surface (**Figure 78**).

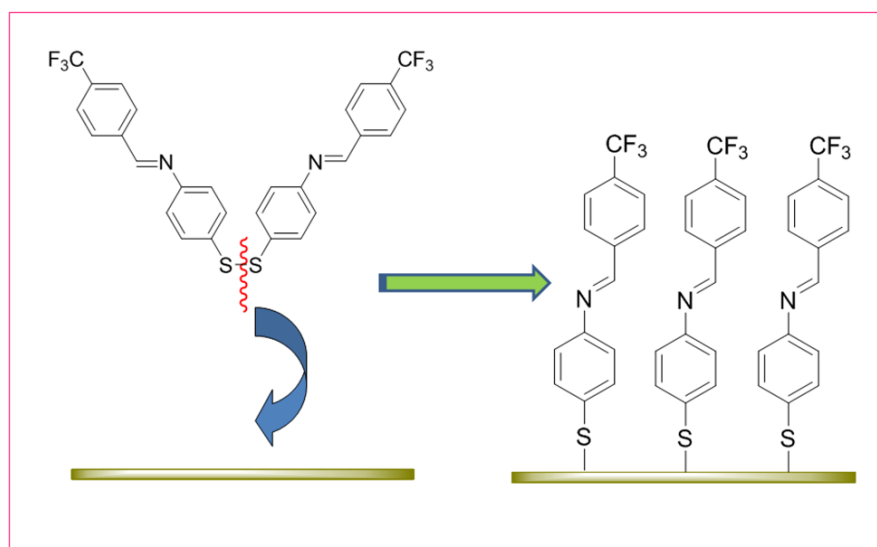


Figure 78 Breaking of the disulfide bond upon self-assembly on the gold surface.

6.0 FUTURE WORK

1. The aldehyde moiety of **5** could be reacted with the amine moiety of 4-ATP in the formation of an imine bond both on surface (**Figure 79a**) and in solution (**Figure 79b-c**) to verify the feasibility of **19**. The surfaces so obtained could be analysed and compared. Two kinds of disulfide **5** contained could be synthesised (**Figure 79b-c**) allowing the fabrication of single component monolayer **19'** (**Figure 80a**), coming from a symmetrical disulfide and double component monolayer **19''** (**Figure 80b**), coming from an unsymmetrical disulfide.^{110,111}

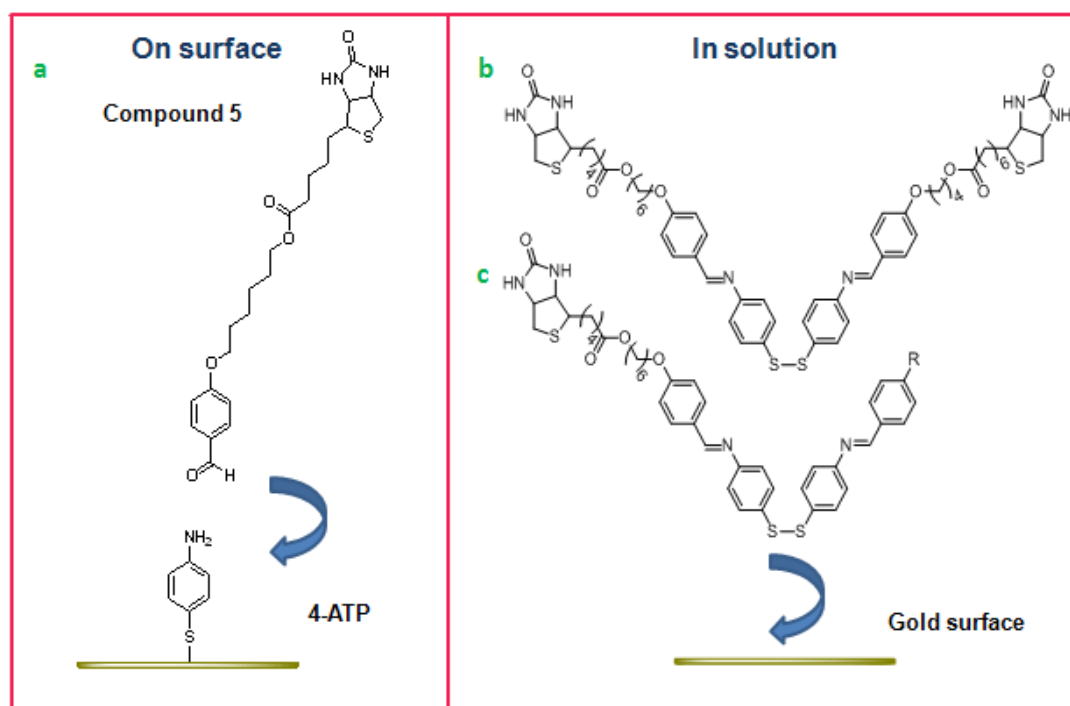


Figure 79 Cartoon image showing the formation of a SAM imine contained. a) The imine bond is formed directly on the surface, b) the imine bond is formed in solution and then compound b or c can be cleaved on the surface to give the corresponding SAMs.

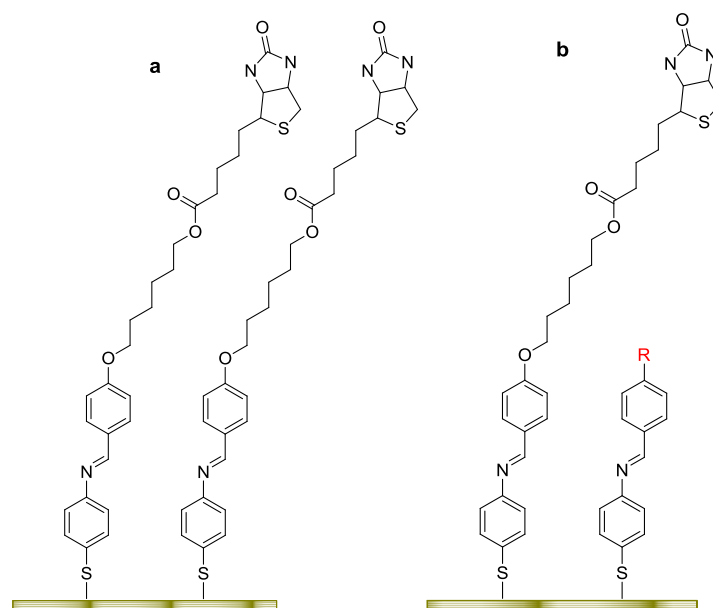


Figure 80 Schematic representations of a) 19' SAM and b) 19'' SAM.

Bio-recognition experiments using the affinity between biotin and streptavidin could be performed on these surfaces and analysed by SPR.

2. Alternative strategies to synthesise compound **14** (**Figure 81**) could be attempted using 'click' chemistry reactions. For instance, since the final aim of the project is the obtainment of a biological switchable surface, the use of copper free 'click' chemistry would be advisable along with the use of the microwave which would permit to reduce dramatically the reaction time.¹¹²

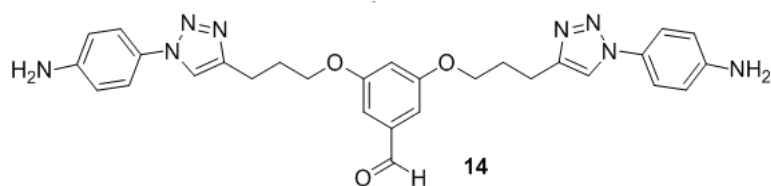


Figure 91 Chemical structure of Compound **14**.

3. Single and double component SAMs could be fabricated using purpose-made biphenyl thiol molecules which have been proven to form well ordered SAMs (**Figure 82**). Concerning the analysis of such surfaces, the use of fluorescent labelled molecules and the

use of AFM microscope could help in analysing the distribution of the molecules adsorbed on the gold surface.

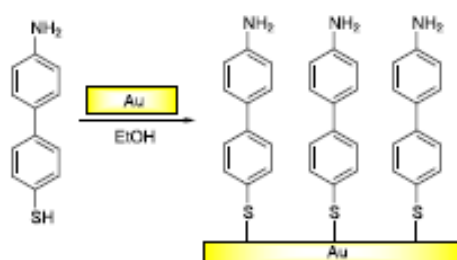


Figure 82 Formation of a biphenyl-thiol SAM.

4. The synthesis of the gallate derivative molecule shown below **Figure 83** could be planned and performed using different synthetic strategies.

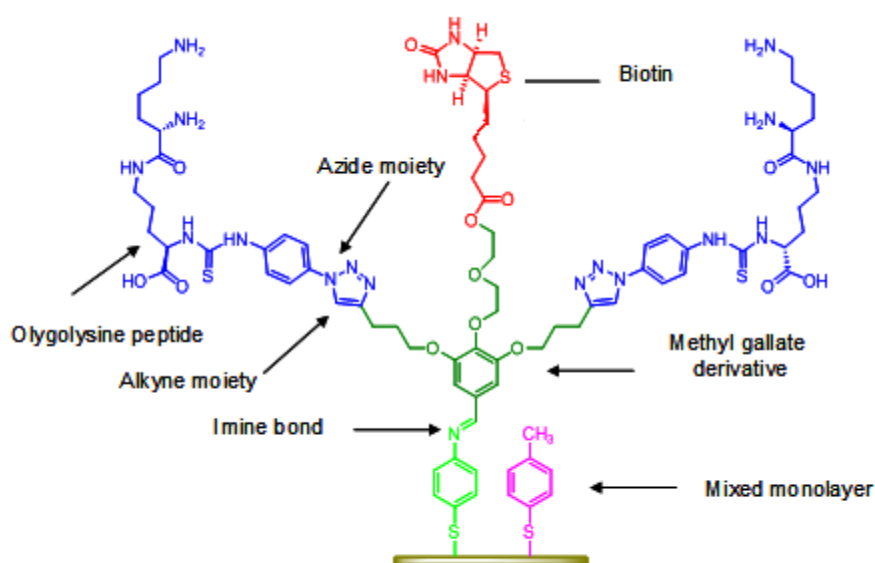


Fig.83 Chemical structure of the double armed switchable system.

7.0 EXPERIMENTAL METHODS

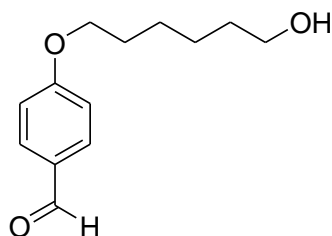
7.1 General Experimental

Thin layer chromatography (TLC): Macherey Nagel silica gel 60F₂₅₄ analytical plates (aluminium support) which were developed using standard visualising agents: UV fluorescence (254 and 366 nm), phosphomolybdic acid/ Δ , and potassium permanganate / Δ . Column chromatographic separations were performed using silica gel 120 (ICN Chrom 32-63, 60 Å). HPLC separations were performed on a Dionex Summit HPLC system with Chromeleon software using a Summit P580P high pressure binary gradient pump with built-in vacuum design and a Summit UVD 170s UV/Vis multi-channel detector with a prep and analytical flow cell. The following method of separation was used: from 0 to 100% of MeOH in water in 60 minutes. MS and HRMS (EI): VG ProSpec or VG-ZabSpec at 70 eV. High resolution EI spectra were measured using perfluorokerosene (PFK) as an internal calibrant. MS and HRMS (ES): Micromass LCT using a methanol mobile phase. HRMS was obtained using a lock-mass to adjust the calibrated mass scale. MS data are reported as m/z (relative intensity). Commercially available compounds were purchased from Aldrich, Fluka, Acros, Strem, Alfa Aesar and used without further purification. All reactions were carried out under N₂ in flame-dried glassware. The solvents used were purified by distillation over the drying agents indicated and were transferred under N₂: THF (Na benzophenone ketyl), Et₂O (Na benzophenone ketyl), CH₂Cl₂ (CaH₂), Et₃N (CaH₂), toluene (Na). Asynt DrySin heating blocks on stirrer hotplates were employed for reactions with temperature controlled *via* external probe. NMR: Spectra were recorded on Bruker AC300 (¹H = 300 MHz, ¹³C = 75.5 MHz), Bruker AV300 (¹H = 300 MHz, ¹³C = 75.5 MHz), and Bruker AV400 (¹H = 400 MHz, ¹³C = 101 MHz) in the solvents indicated; Chemical shifts (δ) are given in ppm relative to TMS. The solvent signals were used as

references and the chemical shifts converted to the TMS scale (CDCl_3 : $\delta_{\text{C}} \equiv 77.0$ ppm; residual CHCl_3 in CDCl_3 : $\delta_{\text{H}} \equiv 7.26$ ppm; $\text{DMSO}-d_6$: $\delta_{\text{C}} \equiv 39.52$ ppm; residual $\text{DMSO}-d_5$ in $\text{DMSO}-d_6$: $\delta_{\text{H}} \equiv 2.50$ ppm). Coupling constants (J) are reported in Hz. Multiplicity is denoted in ^1H NMR by: s (singlet), d (doublet), t (triplet), q (quadruplet), m (multiplet). 1D ^{13}C NMR spectra were recorded using the PENDANT pulse sequence from the Bruker standard pulse program library.

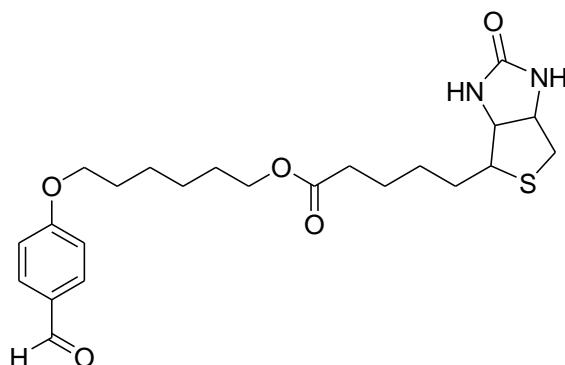
7.2 Synthesis

7.2.1 Ether 3⁸⁰



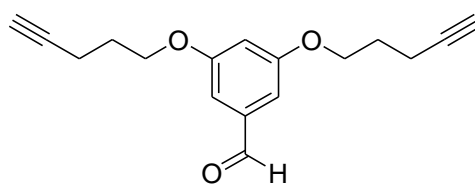
To a solution of 4-hydroxybenzaldehyde (1.50 g, 12 mmol), and K_2CO_3 (3.69 g, 26.0 mmol) in acetonitrile (50ml), heated under reflux for 3 hours, 6-bromo-1-hexanol (2.30 ml, 19.0 mmol) was added dropwise. The solution was further heated under reflux for 12 hours. The residue obtained after evaporation *in vacuo* of the solvent was purified through column chromatography on silica gel with hexane/ethyl acetate (75/25) as eluent, affording white needles after evaporation of the solvent (1.90 g, 71%). Mp: 59-61°C; 1H NMR (300 MHz $CDCl_3$); 9.91 (s, 1H), 7.87 (d, 2H, $J=8.8$ Hz), 7.01 (d, 2H $J=8.8$ Hz), 4.08 (t, 2H $J=6.9$ Hz), 3.7 (t, 2H $J=6.5$ Hz), 2.07 (s, 1H), 1.8-1.4 (m, 8H). ^{13}C NMR (75 MHz $CDCl_3$); 190.80, 163.3, 132.0, 129.8, 114.7, 68.2, 62.8, 32.6, 29.0, 25.8, 25.5. m/z ESMS 245 $[M+Na]^+$: m/z (HRMS) found: 245.1147; calculated mass for $C_{13}H_{18}O_3Na$: 245.1154.

7.2.2 Ester 5



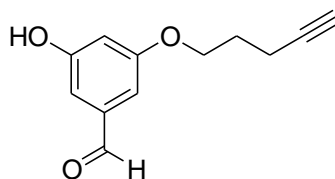
To a N₂ purged reaction flask a solution of D-(+)-Biotin (200 mg, 0.81 mmol) and EDC (232 mg, 1.22 mmol), dissolved in 2 ml of dry DMF, DMAP (20 mg, 0.16 mmol) was added at room temperature. Stirring was continuing for 30 minutes after which a solution of compound **3** (179 mg, 0.81 mmol) in dry CH₂Cl₂ (2 ml) was added. The solution was stirred under N₂ for 48 hours and then poured into water (10 ml) and extracted with CH₂Cl₂ (3 x 10 ml). The organic layer was dried (MgSO₄) and concentrated *in vacuo*. The residue was purified through HPLC (method described in the General experimental section) to give a white powder (324 mg, 89.3%). Mp: 72-75°C; ¹H NMR (300 MHz CDCl₃); 9.81(s, 1H), 7.76 (d, 2H *J*=8.7 Hz), 6.92 (d, 2H *J*=8.7 Hz), 5.55 (s, 1H), 5.17 (s, 1H), 4.44 (m, 1H), 4.24 (m, 1H), 4.02 (t, 2H, *J*= 5.4 Hz), 3.98 (t, 2H, *J*= 5.1 Hz), 3.08 (m, 2H), 2.85 (q, 1H, *J*= 5.9 Hz), 2.26 (t, 2H, *J*= 7.4 Hz), 1.75 (q, 2H, *J*= 6.9 Hz), 1.60 (m, 6H), 1.40 (m, 6H). ¹³C NMR (75 MHz CDCl₃); 190.8, 173.7, 164.2, 163.3, 132.0, 129.8, 114.7, 68.2, 64.3, 61.9, 60.1, 55.4, 40.5, 33.9, 28.9, 28.6, 28.3, 25.9, 25.7, 24.8. *m/z* ESMS: 471.5 [M+Na]⁺; *m/z* (HRMS) found: 471.1945; calculated mass for C₂₃H₃₂N₂O₅NaS: 471.1930.

7.2.3 Diether 8



To a suspension of 3,5-dihydroxybenzaldehyde (1.0 g, 7.24 mmol) and potassium carbonate (3.00 g, 21.0 mmol) in acetonitrile (50 ml), 1-chloropentyne (2.15 g, 21.0 mmol) and sodium iodide (3.14 g, 21.0 mmol) were added, followed by heating under reflux for 24 hours. The cooled mixture was poured in water (30 ml) and extracted with ethyl acetate (3 x 30 ml). The combined extracts was dried (MgSO_4) and filtered. The solvent was removed and solid was purified by column chromatography on silica gel with hexane/ethyl acetate (4:1) as eluent, affording a bright yellow oil after concentration of the solvent *in vacuo* (0.64 g, 33%). ^1H NMR, (300 MHz CDCl_3); 9.92 (s, 1H), 7.04 (d, 2H $J=2.2$), 6.75 (t, 1H $J=2.2$), 4.14 (t, 4H $J=6.0$ Hz), 2.40-2.44 (m, 4H), 2.00-1.99 (m, 6H). ^{13}C -NMR (75 MHz CDCl_3); 192.0, 160.5, 138.4, 108.1, 107.8, 83.2, 71.3, 66.6, 28.0, 15.1. m/z ESMS 270 $[\text{M}+\text{Na}]^+$: m/z (HRMS) found: 293.1249; calculated mass for $\text{C}_{17}\text{H}_{18}\text{O}_3\text{Na}$: 293.1153.

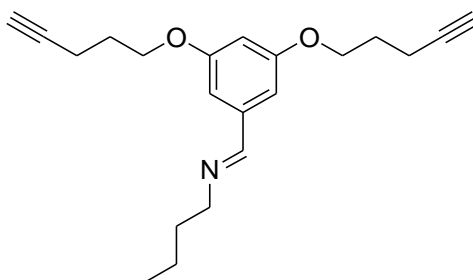
A major by-product was also isolated through column chromatography as brown oil in a yield of 15% (0.22g).



^1H NMR, (300 MHz CDCl_3); 9.80 (s, 1H), 6.92-6.95 (m, 1H), 6.87 (q, 1H, $J=2.3$ Hz), 6.61 (t, 1H $J=2.3$ Hz), 5.38 (s, 1H), 4.04 (t, 2H, $J=5.9$ Hz), 2.30-2.37 (m, 2H), 1.91-1.98 (m, 3H). ^{13}C NMR (75 MHz CDCl_3); 192.0, 159.5, 159.3, 138.9, 107.4, 107.0, 106.3, 84.3,

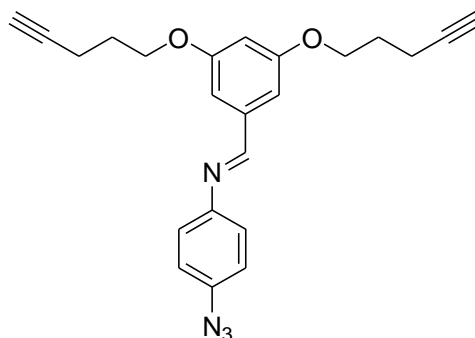
72.3, 66.8, 28.3, 15.7. m/z EIMS 204.1 [M^+], m/z (HRMS) found: 204.0786; calculated mass for $C_{12}H_{12}O_3$: 204.0786.

7.2.4 Imine 11



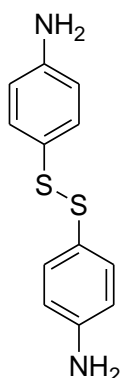
A solution of **8** (280 mg, 1.04 mmol) and 4-butylamine (80 mg, 1.04 mmol) in anhydrous toluene (10ml) was heated under reflux for 12 hours under nitrogen. The cooled mixture was concentrated *in vacuo* affording a yellow oil (333 mg, 98.8%). 1H NMR, (300 MHz $CDCl_3$), 7.98 (s, 1H), 7.09 (d, 2H, $J=2.3$), 6.55 (t, 1H, $J=2.3$), 3.66 (t, 4H, $J=6.0$), 3.49 (m, 2H), 2.07 (m, 4H), 1.73 (t, 2H $J=2.7$), 1.61-1.67 (m, 6H), 1.31-1.39 (m, 2H), 0.85-0.91 (m, 3H). ^{13}C NMR (75 MHz $CDCl_3$); 159.4, 158.9, 137.9, 105.6, 103.1, 82.0, 68.0, 64.9, 60.1, 32.1, 27.1, 19.5, 13.9, 12.7. m/z EIMS 325.2 [M^+].

7.2.5 Imine 15



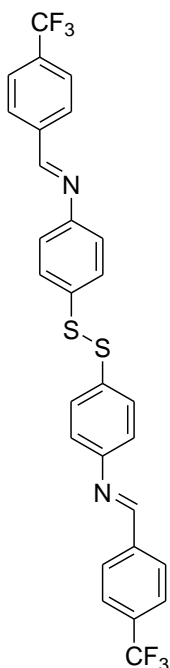
To a solution of **8** (100 mg, 0.37 mmol) and 4-azidoaniline (130 mg, 0.76 mmol) in acetonitrile/H₂O (6.00 ml, 2:1), CuI (18.0 mg, 0.09 mmol) and triethylamine (82 mg, 0.81 mmol) were added. After stirring for 48 hours at room temperature the suspension obtained was filtered and the solution was extracted into CH₂Cl₂ (3 x 5 ml). The solvent was removed *in vacuo* to give the product as a brown oil (135 mg, 95%). ¹H NMR, (300 MHz CDCl₃); 8.26 (s, 1H), 7.15-7.12 (m, 2H), 6.96 (d, 2H, *J*=5.6 Hz), 6.95 (d, 2H, *J*=5.6), 6.51 (t, 1H, *J*=2.3), 4.03 (t, 4H, *J*=6.0), 2.36-2.30 (m, 4H), 1.95-1.90 (m, 6H). ¹³C NMR (75 MHz CDCl₃); 160.5, 159.9, 148.7, 138.4, 137.8, 122.5, 119.8, 107.8, 83.4, 66.4, 28.1, 15.2. *m/z* EIMS 386[M⁺].

7.2.6 Disulfide 16¹⁰⁸



To a solution of 4-ATP (500 mg, 4 mmol) in ethanol (50 ml) heated under reflux, a solution of iodine (500 mg, 2 mmol) in ethanol (20 ml) was added. Heating was continued for 12 hours after which the reaction was allowed to cool to room temperature and washed with a saturated solution of $\text{Na}_2\text{S}_2\text{O}_3$ (20 ml). The products were extracted into CH_2Cl_2 (3 x 20 ml) and the extracts dried (MgSO_4). After filtering off the MgSO_4 , the solvent was removed *in vacuo* and the residue purified by recrystallisation from CH_2Cl_2 /hexane (2:1) to give yellow crystals (225 mg, 45%). Mp: 102-105°C; ^1H NMR, (300 MHz DMSO); 7.17 (d, 4H, $J=8.1$), 6.49 (d, 4H, $J=8.1$), 3.7 (s, 4H). ^{13}C NMR (75 MHz DMSO); 145.4, 130.1, 126.3. m/z EIMS 248 [M^+]: m/z (HRMS) found: 248.0437; calculated mass for $\text{C}_{12}\text{H}_{12}\text{N}_2$: 248.0441.

7.2.7 Diimine **18**



In a N₂ purged reaction flask, a solution of **15** (50 mg, 0.2 mmol) and trifluoromethylbenzaldehyde (70 mg, 0.4 mmol) in dry toluene (10 ml) were heated at reflux for 24 hrs. The solvent was then removed *in vacuo* to give a yellow powder (97 mg, 87%). Mp: 112-115°C; ¹H NMR, (300 MHz CDCl₃); 8.79 (s, 2H), 8.16 (d, 4H, *J*=8.2), 7.89 (d, 4H, *J*=8.2), 7.61 (d, 4H, *J*=8.5), 7.30 (d, 4H *J*=8.5), ¹³C NMR (75 MHz CDCl₃); 160.1, 150.7, 137.4, 134.8, 133.3, 130.5, 129.7, 125.8, 124.1, 122.2. ¹⁹F-NMR (300 MHz, CDCl₃), 63.2 (6F). *m/z* EIMS 560 [M⁺]; calculated mass for C₂₈H₁₈N₂S₂F₆: 560.08.

7.3 Surface work

7.3.1 Materials

Gold

100 nm gold slides were purchased from a company based in Germany called Georg Albert Physikal Vapor Disposition (PVD).

Ultra High Quality Water (UHQ H₂O)

The UHQ H₂O water with a resistivity of 18 MΩ.cm was supplied by a Millipore system.

7.3.2 Cleaning of glassware

All organic contaminants were removed from the glassware prior to use via a standard cleaning procedure. All glassware used in SAM formation was immersed in piranha solution (70% H₂SO₄, 30% H₂O₂) at room temperature for 30 minutes, rinsed and then sonicated in UHQ H₂O followed by drying in an oven at 127 °C for 30 minutes. Piranha solution is a very strong oxidising agent and has been known to detonate spontaneously upon contact with organic material. Therefore, eye protection (Fisher Scientific) and nitrile gloves (Bodyguards) were worn at all times, and as a precaution H₂O ice was used as a quenching agent. Finally the glassware was rinsed, and then sonicated in ethanol for 30 minutes before being dried in the oven for 24 hours prior to use.

7.3.3 General procedure for the preparation of SAMs

Au substrates were cut to a square size approximately 1cm x 1cm using a diamond tipped scriber. The substrates were rinsed with HPLC ethanol to clear the surface of any particles that were produced from the cutting process. The substrates were immersed into piranha solution for 10 minutes and then rinsed vigorously with UHQ H₂O and HPLC ethanol. Self-assembled monolayers were prepared by immersing freshly prepared Cr-primed, Au-coated glass microscope slides in X mM (with $0.1 \leq X \leq 1$ mM) solutions of the SAM compounds, with either ethanol (Sigma Aldrich, HPLC grade or anhydrous) or toluene (Sigma Aldrich, anhydrous) as a solvent. If commercially available, the compound was used as received. After the desired immersion time (usually 24 hours), Au substrates were removed from the SAM solution and rinsed with copious amounts of either ethanol or toluene, depending upon the SAM solution it had been immersed in, before being blown dry using N₂ gas.

7.3.4 Characterisation of SAMs

Contact Angle

Dynamic H₂O contact angles were measured using a home-made stage apparatus, employing a Charge-Coupled Device (CCD) KP-M1E/K camera (Hitachi). FTA Video Analysis software v1.96 (First Ten Angstroms) was used for the analysis of the contact angle of a droplet of UHQ H₂O at the three-phase intersection point. All data was collected at room temperature and pressure under ambient humidity conditions. Mathematical analysis of the contact angle was performed assuming a nonspherical droplet shape, with manual designation of the baseline for each surface analysed. A minimum of five measurements was performed for each sample. All measurements were done on 100 nm gold substrates.

Ellipsometry

Measurements: Ellipsometry measurements were recorded using a Jobin, Yvon UVISEL ellipsometer with Xenon light source. Ellipsometer calibration and alignment of the Polariser and Detector were performed using an Al reference sample, which has a thermally grown Al₂O₃ layer. A wavelength of 280-800nm was used with a fixed angle of incidence of 70°. All measurements were made under ambient conditions of temperature, pressure and humidity. SAM thicknesses are averages of a minimum of five measurements, each made at different non-defective locations on the substrate.

Mathematical modelling: The SAM was modelled using a Cauchy transparent layer, whose initial thickness was varied using a multiguess iterative calculation procedure. The results obtained for each measurement were averaged to give a mean SAM thickness. DeltaPsi software was used to calculate the thickness values using a Cauchy oscillator model. All measurements were done on 100 nm gold substrates.

XPS

XPS spectra were obtained on the Scienta ESCA300 instrument based at the Council for the Central Laboratory of the Research Councils (CCLRC) in The National Centre for Electron Spectroscopy and Surface Analysis (NCESS) facility at Daresbury, UK. XPS experiments were carried out using a monochromatic Al K α X-ray source (1486.7 eV) and a take off angle of 15°. Fitting of XPS peaks was performed using the *Avantage V2.2* processing software. All measurements were done on 100 nm gold substrates.

7.3.5 SAMs formation

7.3.5.1 4-ATP, BT SAMs formation: concentration studies

A 1 mM solution of 4-ATP and BT were prepared by dissolving each compound in 20 ml of HPLC ethanol, which was then diluted using additional solvent in order to achieve the desired concentration of 0.1, 0.2, 0.3, 0.4 and 0.5 mM. Clean gold substrates were immersed in the five solutions for 24 hours. For each concentration two samples were prepared in order to have control data. The samples were then rinsed with HPLC ethanol and dried with N₂. All samples were characterised by ellipsometry.

7.3.5.2 4-ATP, BT, 4-MBT, 4-NBT SAMs formation: kinetic studies

A 1 mM solution of 4-ATP, BT, 4-MBT, 4-NBT were prepared by dissolving each compound in 20 ml of HPLC ethanol, which was then diluted using additional solvent in order to achieve the desired solution (0.1 mM). Clean gold substrates were immersed in the 0.1mM solutions for 2 hours, 4 hours and 24 hours. For each compound two samples were prepared in order to have control data. The samples were then rinsed with HPLC ethanol and dried with N₂. All samples were characterised by contact angle and ellipsometry with the 24 hour sample also being characterised by XPS.

7.3.5.3 Mixed 4-ATP/4-MBT SAM formation

A 1 mM solution of 4-ATP/4-MBT (1:1) and 4-ATP/4-MBT (2:1) were prepared by dissolving each mixture in 20 ml of HPLC ethanol, which was then diluted using additional solvent in order to achieve the desired concentration of 0.1 mM. Clean gold substrates were immersed in the 0.1 mM solutions for 24 hours. For each molar ratio two samples were prepared in order to have control data. The sample were then rinsed with HPLC ethanol and dried with N₂. All samples were characterised by contact angle, ellipsometry and XPS.

7.3.5.4 Imine bond formation on 4-ATP SAMs

A 1 mM solution of aldehyde derivative (4-HBA, 4-BBA, 4-TBA) was prepared by dissolving each compound in 20 ml of anhydrous ethanol or toluene, which was then diluted using additional solvent in order to achieve the desired solution. For each molar ratio two samples were prepared in order to have control data. 4-ATP SAMs (7.2.5.1) were then immersed in the solution for 48 hours. The samples were then rinsed with anhydrous ethanol/toluene and dried with N₂. All samples were characterised by contact angle, ellipsometry and XPS.

7.3.5.5 16' SAMs formation from disulfide 16

A 1 mM solution of **16** was prepared by dissolving the compound in 20 ml of anhydrous toluene, which was then diluted using additional solvent in order to achieve the desired solution. Clean gold substrates were immersed in the 0.1mM solution for 48 hours. For each molar ratio two samples were prepared in order to have control data. The sample were then rinsed with anhydrous toluene and dried with N₂. All samples were characterised by ellipsometry and XPS.

7.3.5.6 18' SAMs formation from disulfide 18

A 1 mM solution of **18** was prepared by dissolving the compound in 20 ml of anhydrous toluene, which was then diluted using additional solvent in order to achieve the desired solution. Clean gold substrates were immersed in the 0.1mM solution for 48 hours. For each molar ratio two samples were prepared in order to have a control data. The sample were then rinsed with anhydrous toluene and dried with N₂. All samples were characterised by ellipsometry and XPS.

8.0 REFERENCES

1. Aicha, A. R. Elshabini-Riad, F.D. Barlow, *Thin Film Technology Handbook*, McGraw-Hill (New York), p 1-1, (1998).
2. Aicha, A. R. Elshabini-Riad, F.D. Barlow, *Thin Film Technology Handbook*, McGraw-Hill (New York), p 1-2, (1998).
3. Aicha A.R. Elshabini-Riad, F.D. Barlow, *Thin Film Technology Handbook*, McGraw-Hill (New York), p 3-4, (1998).
4. D. L. Smith, *Thin Film Deposition: Principles and Practice*, McGraw-Hill (New York), p 2, (1995).
5. C. R. Newman, D. Frisbie, D. A. da Silva Filho, J. L. Brédas, P. C. Ewbank, K. R. Mann, *Chem. Mater.*, **16**, 4436-4451, (2004).
6. S. C. Lima, S. H. Kima, H. Y. Chua, J. H. Leea, J. I. Leea, J. Y. Oha, D. Kimb, *Synthetic Metals* **151**, 3197-201, (2005).
7. C. Yu, T. Lei, J. Liao, J. Yan, and J. Ho, *J. Display Technol.*, **5**, 198-201, (2009).
8. E. Ostuni, G. M. Whitesides, D. E. Ingber, C. S. Chen, *Methods Mol. Biol.*, **522**, 183-94, (2009).
9. A. Ulman, *Chem. Rev.*, **96**, 1533–1554, (1996).
10. A. Ulman, *An Introduction to Organic Thin Films from Langmuir – Blodgett to Self-Assembly*, Academic Press INC, (1991).
11. P. M. Mendes, M. Belloni, M. Ashworth, C. Hardy, K. Niktin, D. Fitzmaurice, K. Critchley, S. Evans, J. A. Preece, *Chem. Phys. Chem.*, **4**, 884-889, (2003).
12. H. Basch, M. A. Ratner, *J. Chem. Phys.*, **120**, 5771-5780, (2004).
13. G. B. Hoflund, Zoltan, F. Hazos, Ghaleb, N. Salaita, *Physical Review B*, **62**, 11126-11133, (1999).
14. Q. Wang, P. Geil, G. Padua, *Journal of Polymers and the Environment*, **12**, 197-202, (2004).
15. G. L. Bowlin, *Encyclopedia of Biomaterials and Biomedical Engineering*, **4**, Second Edition, Informa healthcare, (2008).
16. N. Tillman, A. Ulman, J. S. Schildkraut, T. L. Renner., *J. Am. Chem. Soc.*, **110**, 6136-6144, (1988).

17. J. Lahann, S. Mitragotri, T. N. Tran, H. Kaido, J. Sundaram, I. S. Choi, S. Hoffer, G. A. Somorjai, R. Langer., *Science*, **299**, 371-374, (2003).
18. P. Iqbal, K. Critchley, D. Attwood, D. Tunnicliffe, S. D. Evans, J. A. Preece, *Langmuir*, **24**, 13969-13976, (2008).
19. P. E. Laibiris, G. M. Whiteside, *J. Am. Chem. Soc.*, **114**, 9022-9028, (1992).
20. M W.J. Beulen, B. H. Huisman, P. A. Van der Heijden, F. C. M. Van Veggel, M. G. Simons, M. E. F. Biemond, P. J. De Lange, D. N Reihoudt, *Langmuir*, **12**, 6170-6172, (1996).
21. C. Chen, J. E. Hutchison, T. A. Postlethwaite, J. N. Richardson, R. W. Murray, *Langmuir*, **10**, 3332-3337, (1994).
22. M. Li, M. Dai, Y. J. Chabal, *Langmuir*, **25**, 1911-1914, (2009).
23. H. Hillebrandt, M. Tanaka, *J. Phys. Chem. B*, **105**, 4270-4276, (2001).
24. M. Mrksich, *Chem. Soc. Rev.*, **29**, 267-273, (2000).
25. P. Mendes, *Chem. Soc. Rev.*, **37**, 2512-2529, (2008).
26. C. Chatgililoglu, *Helvetica chimica acta*, **89**, 2387-2398, (2006).
27. C. K. Luscombe, H. W. Li, T. S. Huck, A. B. Holmes, *Langmuir*, **19**, 5273-5278, (2003).
28. A. M. Almanza-Workman, S. Raghavan, P. Deymier, D. J. Monk, R. Roop, *Journal of The Electrochemical Society*, **149**, 6-11, (2002).
29. C. L. Rhodesia, S. H. Brewera, J. Folmera, S. Franzen, *Thin Solis Film*, **516**, 1838-1842, (2006).
30. S. Besbes, H. Ben Ouada, J. Davenas, L. Ponsonnet, N. Jaffrezic, P. Alcouffe, *Materials Science and Engineering: C*, **26**, 505-510, (2006).
31. U. Makal, K. J. Wynne, *Langmuir*, **21**, 3742-3745, (2005).
32. Q. Xu, H. Ma, H. Yip, A. K. Y. Jen, *Nanotechnology*, **19**, 135605-135616, (2008).
33. J. Noh, *Bull. Korean Chem. Soc.*, **27**, 944-946, (2006).
34. F. Schreiber, *Progress in Surface Science*, **65**, 151-256, (2000).
35. E. W. Wollman, C. D. Frisbie, M. S. Wrighton, *Langmuir*, **9**, 1517-1520, (1993).
36. G. P. Lopez, H. A. Biebuyck, G. M. Whitesides, *Langmuir*, **10**, 1498-1511, (1996).
37. G. Gillen, S. Wright, J. Bennett, M. J. Tarlov, *Appl. Phys. Lett.*, **65**, 534-536, (1994).

38. J. L. Tan, Joe Tien, C. S. Chen, *Langmuir*, **18**, 519-523, (2002).
39. C. D. Bain, G. M. Whitesides, *J. Am. Chem. Soc.*, **110**, 3665-3666, (1988).
40. C. D. Bain, G. M. Whitesides, *J. Am. Chem. Soc.*, **111**, 7164-7175, (1989).
41. Y. F. Xing, b, S. F. Y. Lia, A. K. H. Laub, S. J. O'Sheab, *Journal of Electroanalytical Chemistry*, **583**, 124-132, (2005).
42. F. Schreiber, *Journal of Physics: Condensed Matter*, **16**, 881-900, (2004).
43. W. Göpel, P. Heiduschka, *Biosens. Bioelectron.*, **10**, 853-883, (1995).
44. K. Kim, H. Yang, S. Jon, E. Kim, J. Kwak, *J. Am. Chem. Soc.*, **126**, 15368-15369, (2004).
45. V. H. Perez-Luna, M. J. O'Brien, K. A. Opperman, P. D. Hampton, G. P. Lopez, L. A. Klumb, P. S. Stayton, *J. Am. Chem. Soc.*, **121**, 6469-6478, (1999).
46. H. Tokuhisa, J. Liu, K. Omori, M. Kanosato, K. Hiratani, L. A. Baker, *Langmuir*, **25**, 1633-1637, (2009).
47. J. Lahann, S. Mitragotri, T. N. Tran, H. Kaido, J. Sundaram, I. S. Choi, S. Hoffer, G. A. Somorjai, R. Langeret, *Science*, **299**, 371-374, (2003).
48. S. Ferretti, D. A. Russell, *Trends in analytical chemistry*, **19**, (2000).
49. S. Wang, Y. Song, L. Jianga, *Journal of Photochemistry and Photobiology C: Photochemistry Reviews*, **8**, 18-29, (2007).
50. Y. Liu, L. Mu, B. Liu, J. Kong, *Chem. Eur. Journal*, **11**, 2622-2631, (2005).
51. S. L. Gras, T. Mahmud, G. Rosengarten, A. Mitchell, K. Kalantar-Zadeh, *Chem Phys Chem*, **8**, 2036-2050, (2007).
52. J. A. Howarter, J. R. Youngblood, *Adv. Mater.*, **19**, 3838-3843, (2007).
53. C. Alexander, K. M. Shakesheff, A. Kikuchi, T. Okano, *Adv. Mater.*, **18**, 3321-3328, (2006).
54. R. E. Rawsterne, J. E. Gough, F. J. M. Rutten, N. T. Pham, W. C. K. Poon, S. L. Flitsch, *Surf Interface Anal*, **38**, 1505-1511, (2006).
55. R. V. Ulijn, N. Bibi, V. Jayawarna, P.D. Thornton, S.J. Todd, R.J. Mart, *Mater Today*, **10**, 40-48, (2007).
56. J. A. Crowe, J. Genzer, *J. Am. Chem. Soc.*, **127**, 17610-17611, (2005).

57. X. H. Yang, Q. Wang, K. M. Wang, W. H. Tan, J. Yao, H. M. Li, *Langmuir*, **22**, 5654-5659, (2006).
58. S. O. Kelley, J. K. Barton, N. M. Jackson, L. D. McPherson, A. B. Potter, E. M. Spain, M. J. Allen, M. G. Hill, *Langmuir*, **14**, 6781-6784, (1998).
59. U. Rant, K. Arinaga, S. Fujita, N. Yokoyama, G. Abstreiter, M. Tornow, *Org. Biomol. Chem.*, **4**, 3448-3455, (2006).
60. R. Huisgen, *Angew. Chem.*, **2**, 565-598, (1963).
61. V. V. Rostovtsev, L. G. Green, V. V. Fokin and K. B. Sharpless, *Angew. Chem., Int. Ed.*, **41**, 2596-2599, (2002).
62. J. K. Lee, Y. S. Chi, I. S. Choi, *Langmuir*, **20**, 3844-3847, (2004).
63. P. Bertrand, J. P. Gesson, *J. Org. Chem.*, **72**, 3596-3599, (2007).
64. T. Lummerstorfer, H. Hoffmann, *J. Phys. Chem. B*, **108**, 3963-3966, (2004).
65. N. K. Devaraj, G. P. Miller, W. Ebina, B. Kakaradov, J. P. Collman, E. T. Kool, C. E. D. Chidsey, *J. Am. Chem. Soc.*, **127**, 8600-8601, (2005).
66. M. Kleinert, T. Winkler, A. Terfort, T. K. Lindhorst, *Org. Biomol. Chem.*, **6**, 2118-2132, (2008).
67. D. Pearson, A. J. Downard, A. Muscroft-Taylor, A. D. Abell, *J. Am. Chem. Soc.*, **129**, 14862-14863, (2007).
68. R. V. Ostaci, D. Damiron, F. Capponi, G. Vignaud, L. Lager, Y. Grohens, E. Drockenmuller, *Langmuir*, **24**, 2732-2739, (2008).
69. L. Nebhani, C. B. Kowollik, *Adv. Mater.*, **21**, 1-27, (2009).
70. Z. Yang, W. Frey, T. Oliver, A. Chilkoti, *Langmuir*, **16**, 1751-1758, (2000).
71. M. Weisser, J. Käshammer, B. Menges, J. Matsumoto, F. Nakamura, K. Ijio, M. Shimomura, S. Mittler, *J. Am. Chem. Soc.*, **122**, 87-95, (2000).
72. J. Kindersberger, F. Exl, *XIVth International Symposium on High Voltage Engineering*, Tsinghua University, Beijing, China, (2005).
73. F.P. Zamborini, R.M. Crooks, *Langmuir*, **13**, 122-126, (1997).
74. D. Briggs, M.P. Seah, *Practical Surface Analysis Volume 1: Auger and X-ray Photoelectron Spectroscopy*, Second Edition, John Wiley and Sons (Chichester), p 641, (1996).
75. J.F. Moulder, W.F. Stickle, P.E. Sobol, K.D. Bomben, *Handbook of X-Ray Photoelectron Spectroscopy: A Reference Book of Standard Spectra for Identification and*

Interpretation of XPS Data, Perkin-Elmer Corporation Electronics Division (Minnesota), p 61-62, (1972).

76. J. Huang, J. C. Hemminger, *J. Am. Chem. Soc.*, **115**, 3342-3343, (1993).

77. P.M. Mendes, J.A. Preece, *Curr. Opin. Colloid Interface Sci.*, **9**, 236-248, (2004).

78. H. Imahori, M. Kimura, K. Hosomizu, T. Sato, T. K Ahn, S.K Kim, D. Kim, Y. Nishimura, I. Yamazaki, Y. Araki, O. Ito, S. Fukuzumi, *Chem.-Eur. J.*, **10**, 5111-5122, (2004).

79. S.A. Darst, M. Ahlers, P.H. Meller, E.W. Kubalek, R. Blankenburg, H.O. Ribi, H. Ringsdorf, R. D. Kornberg, *Biophys. J.*, **59**, 387-396, (1991).

80. L. Haussling, B. Michel, Helmut Ringsdorf, H. Rohrer, *Angew. Chem. Int. Ed. Engl.*, **30**, 569-572, (1991).

81. M. G. Fritz, D. Seebach, *Helvetica Chimica Acta*, **81**, 2414-2429, (1998).

82. A. I. Haj-Yehia, L. Z. Benet, *Journal of Chromatography A.*, **724**, 107-115, (1996).

83. M. Collot, B. Sendid, A. Fievez, C. Savaux, A. Standaert-Vitse, M. Tabouret, A. Drucbert, P. Danze, D. Poulain, J. Mallet, *J. Med. Chem.*, **51**, 6201-6210, (2008).

84. Y. H. Zhang, Z. X. Gao, C. L. Zhong, H. B. Zhou, L. Chen, W.-M. Wu, X. J. Peng, Z. J. Yao, *Tetrahedron*, **63**, 6813-6821, (2007).

85. B. Sieczkowska, M. Millaruelo, M. Messerschmidt, B. Voit, *Macromolecules*, **40**, 2361-2370 2361, (2007).

86. R. Franke, C. Doll, J. Eichler, *Tetrahedron Letters*, **46**, 4479-4482, (2005).

87. Z. Y. Yan, Y. B. Zhao, M. J. Fan, W. M. Liu, Y. M. Lianga, *Tetrahedron*, **61**, 9331-9337, (2005).

88. C. J. Duxbury, D. Cummins, A. Heise, *Journal of Polymer Science: Part A: Polymer Chemistry*, 3795-3802, (2009).

89. F. Zhang, J. E. Moses, *Org. Lett.*, **7**, 1587-1590, (2009).

90. C. D. Hein, X.-M. Liu, D. Wang, *Pharmaceutical Research*, **25**, 2216-2230, (2008).

91. V.D. Bock, H. Hiemstra, J. Maarseveen, *J. Org. Chem.*, 51-68, (2006).

92. Q. Xu, H. Ma, H. Yip, A. K. Y. Jen, *Nanotechnology*, **19**, 135605-135616, (2008).

93. G. Stefan, *Angew. Chem. Int. Ed.*, **47**, 3430-3434, (2008).

94. Y. Li, D. Lu, G. Galli, *J. Chem. Theory Comput.*, **5**, 881-886, (2009).

95. S. Yasuda, H. Shigekawa, *Jpn. J. Appl. Phys.*, **42**, 4901-4904, (2003).
96. J. Kucera, A. Groß, *Langmuir*, **24**, 13985-13992, (2008).
97. S. Mullegger, I. Salzmann, R. Resel, A. Winkler, *Appl. Phys. Lett.*, **83**, 4536-4538, (2003).
99. L. S. Jiao, L. Niu, J. Shen, T. You, S. Dong, A. Ivaska, *Electrochemistry Communications*, **7**, 219-222, (2005).
99. D. Raorane, S. Hyung, A. Lim, Majumdar, *Nano Letters*, **8**, 2229-2235, (2008).
100. S. Lee, A. Puck, M. Graupe, R. Colorado, Y.-S. Shon, T. R. Lee, S. S. Perry, *Langmuir*, **17**, 7364-7370, (2001).
101. A. Jakubowicz, H. Jia, R. M. Wallace, B. E. Gnade, *Langmuir*, **21**, 950-955, (2005).
102. B. Jäger, H. Schürmann, H. U. Müller, H. J. Himmel, M. Neumann, M. Grunze, C. Wöll, *Z. Phys. Chem*, **202**, 263-272, (1997).
103. D. G. Castner, K. Hinds, D. W. Grainger, *Langmuir*, **12**, 5083-5086, (1996).
104. J. M. Tour, L. Jones II, D. L. Pearson, J. J. S. Lamba, T. P. Burgin, G. M. Whitesides, D. L. Allara, A. N. Parikh, S. Atre, *J. Am. Chem. Soc.*, **117**, 9529-9534, (1995).
105. Y. Luo, M. Piantek, J. Miguel, M. Bernien, W. Kuch, R. Haag, *Appl Phys A*, **93**, 293-301, (2008).
106. B. I Rosario-Castro, E. G. Contès, M. E. Pèrez-Davis, C. R. Cabrera, *Rev. Adv. Mater. Sci.*, **10**, 381-386, (2005).
107. K. Bandyopadhyay, K. Vijayamohanan, M. Venkataramanan, T. Pradeep, *Langmuir*, **15**, 5314-5322, (1999).
108. S. Zhang, F. Lin, M. Hossain, F. Shabanpoor, G. Tregear, J. Wade, *Int. J. Pept. Res. Ther.*, **14**, 301-305, (2008).
109. A. D. Romanshin, L. N. Bui, M. Thompson, N. B. McKeown, P.G. Kalman, *Analyst*, **118**, 463-474, (1993).
110. R. Hunter, M. Caira, N. Stellenboom, *J. Org. Chem*, **71**, 8268-8271, (2006).
111. Witt, D., *Synthesis*, **8**, 2491-2509, (2008).
112. C. R. Becer, R. Hoogenboom, U. S. Schubert, *Angew. Chem. Int. Ed.*, **48**, 2-11, (2009).